5-2015

Carbon Nanotube-Enzyme Conjugates for the Fabrication of Diagnostic Biosensors

Olukayode Adedamola Karunwi
Clemson University

CARBON NANOTUBE-ENZYME CONJUGATES FOR THE FABRICATION OF DIAGNOSTIC BIOSENSORS

A Dissertation
Presented to
the Graduate School of
Clemson University

In Partial Fulfillment
of the Requirements for the Degree
Doctor of Philosophy
Bioengineering

---

by
Olukayode Adedamola Karunwi
May 2015

Accepted by:
Prof. Anthony Guiseppi-Elie, Committee Chair
Prof. Frank Alexis
Prof. Steve Creager
Prof. Delphine Dean
Prof. Yaw Obeng

ABSTRACT

The fabrication of multi-analyte biotransducers continues to be a major technical challenge when the length scales of the individual transducer elements are on the order of microns Generation-3 (Gen-3) biosensors and advanced enzyme biofuel cells will benefit from direct electron transfer to oxidoreductases facilitated by single-walled carbon nanotubes (SWNTs). Direct electron transfer helps to mitigate errors from the instability in oxygen tension, eliminate use of a mediator and produce a device with low operating potential close to the redox potential of the enzymes. Supramolecular conjugates of SWNT-glucose oxidase (GOx-SWNT) may be produced via ultrasonic processing. Using a Plackett-Burman experimental design to investigate the process of tip ultrasonication, conjugate formation was investigated as a function of ultrasonication times and functionalized SWNTs of various tube lengths. Supramolecular conjugates formed from shorter, -OH functionalized SWNTs using longer sonication times gave the most favored combination for forming bioactive conjugates.

There has also been growing interest in the fabrication of CNT-enzyme supramolecular constructs that control the placement of SWNTs within tunneling distance of co-factors for enhanced electron transfer efficiency in generation 3 biosensors and advanced biofuel cells. These conjugate systems raise a series of questions such as: Which peptide sequences within the enzymes have high affinity for the SWNTs? And, are these high affinity sequences likely to be in the vicinity of the redox-active co-factor to allow for direct electron transfer? Phage display has recently been used to identify specific peptide sequences that have high affinity for SWNTs. Molecular dynamics simulations were

performed to study the interactions of five discrete peptides with (16,0) SWNT in explicit water as well as with graphene. The end residues appear to dominate the progression of adsorption regardless of character. Sequences identified by phage display share some homology with key enzymes (GOx, lactate oxidase and laccase) used in biosensors and enzyme-based biofuel cells.

Furthermore, the role of pyrrole electropolymerization as an additive technique for the biofabrication of side-by-side biotransducers for glucose and lactate with minimum cross-talk was investigated along with an electrodeposited layer of Fe/Ni hexacyanoferrate to serve as peroxide mediator, decorated with the electropolymerized PPy-Enzyme biorecognition layer, characterized *in vitro*, and implanted into the trapezius muscle of a piglet (*Sus scrofa*) hemorrhage model. Internal calibration, response under controlled hemorrhage conditions, and post–resection re-characterization were used to evaluate biotransducer performance.

ACKNOWLEDGMENTS

I would like to thank my advisor, Prof. Guiseppi-Elie, for showing me the need for more effective biosensors for use in trauma management and for guiding me in adding to this body of work in the scientific community. He has played a pivotal role in my academic and professional development in the field of bioengineering, biomolecular engineering and electrochemistry. I would also like to thank him for opportunities to expand my teaching abilities in some of his classes. I would like to thank my lab mates over the years Dr. Christian Kotanen, Dr. Nolan Wilson, Subhra Nag, Lorcan Ingham, Ruth Salas, Fouzan Alam, Jorge Hernandez, John Coleman, Dr. Deon Hines, Dr. Chaker Tlili, and Dr. Rachel Khan for their input and support. I wish to thank Aby Thyparambil and Tigran Abramyan for their input and support as well. I wish to thank the members of my dissertation committee Prof. Frank Alexis, Prof. Stephen Creager, Prof. Delphine Dean, Prof. Yaw Obeng for all of their valuable time, feedback and guidance. I would also like to thank Prof. Robert Latour for helpful discussions and support over the years. I would like to especially thank Dr. Frankie Felder and Prof. Martine LaBerge for their immense support when times were rough. A special thank you goes to our departmental fairy godmother, Maria Martin who is a great support for the graduate students in the Bioengineering department. I will like to thank members of the Deeper Life Bible Church (in Atlanta, GA and Charlotte, NC) for their emotional, spiritual and physical support during my period of studies. Finally, I am deeply grateful to my family for all their love, support, words of encouragement and prayers throughout this entire process.

Olukayode A. Karunwi

TABLE OF CONTENTS

Table of Contents (Continued) Page

LIST OF TABLES

List of Tables (Continued)

Table Page

LIST OF FIGURES

List of Figures (Continued)

Figure Page

List of Figures (Continued)

Figure Page

List of Figures (Continued)

Figure Page

List of Figures (Continued)

Figure Page

List of Figures (Continued)

Figure Page

CHAPTER ONE

ENZYME – CARBON NANOTUBE CONJUGATES FOR GENERATION-3 BIOSENSORS AND BIOFUEL CELLS

1.1 Abstract

Direct electron transfer between the redox active cofactors of oxidoreductases (e.g. glucose oxidase) and solid state graphitic electrodes facilitated by carbon nanotubes (CNT) has been shown. This eliminates the need for small molecules (e.g. oxygen) or polymeric mediators (e.g. poly(vinylferrocene)) and therefore allows development of Generation-3 biosensors and advanced biofuel cells. Relevant contributions in the development and modification of CNTs for use in biosensors and advanced biofuel cells are highlighted and critically evaluated. Enzyme-CNT conjugates may be physicochemical, electrostatic or covalent. Such conjugates may be efficient biocatalysts with unmatched stability and power density when compared to conventional low-temperature oxidation-reduction biocatalysts.

1.2 Introduction

There is a pressing need for fully implantable biosensors to allow the continual monitoring of various analytes that serve as markers of a wide variety of physiological conditions and pathologies [1, 2]. Among such analytes are glucose in diabetics and the fusion of glucose, lactate and succinate in victims of trauma-associated hemorrhage [3]. Over the years substantial progress has been made from generation-1 (Gen-1) to generation-2 (Gen-2) biotransducers and eventually moving towards generation-3 (Gen-3)

biotransducers. Design and development of Gen-3 biosensors that are reagentless, have long term *in vivo* stability, require no calibration, and allow for highly efficient electron transfer rates between redox centers and electrodes continues to be a major challenge and opportunity in biomedical diagnostics [4-6]. There is similarly a pressing need for implantable biofuel cells that may be well suited to trickle charge battery powered implantable medical devices (IMDs) or to serve as the primary source of power in implantable bioelectronics [7] [8]. The biofuel cell, which will power the biosensor, can be designed to make use of metabolically produced biofuel sources present within the body, such as glucose [9-12]. Both Gen-3 biosensors and advanced biofuel cells depend upon the judicious design, fabrication and engineering control of biomolecule-to-solid state (bio-abio) interfaces for biomolecule stability and efficient electron transfer. This review considers the current state of understanding of biomolecule-to-solid state interfaces formed from carbon nanotubes (CNTs) and enzymes. Moreover this review sets forth the rationale for why such conjugates may be useful in implantable Gen-3 biosensors as well as in the design of advanced biofuel cells to power diverse implantable medical devices (IMD). Finally the review identifies opportunities for further scholarship and technological development.

The first report of direct electron transfer (DET) involving the use of CNTs and oxidoreductase enzymes at graphitic electrodes is attributable to Guiseppi et al.[13]. The authors used simple adsorptive casting of glucose oxidase (GOx) onto CNT-modified glassy carbon electrodes (GCE) to achieve surface conjugates that demonstrated independence of oxygen tension, and hence DET between the FAD and the electrode, in

the catalytic conversion of glucose to gluconolactone. There has since been considerable progress in CNT-modified electrodes that exploit the unique properties (See section on Importance of CNTs in biosensors and biofuel cells) of CNTs in enhancing biosensor performance.

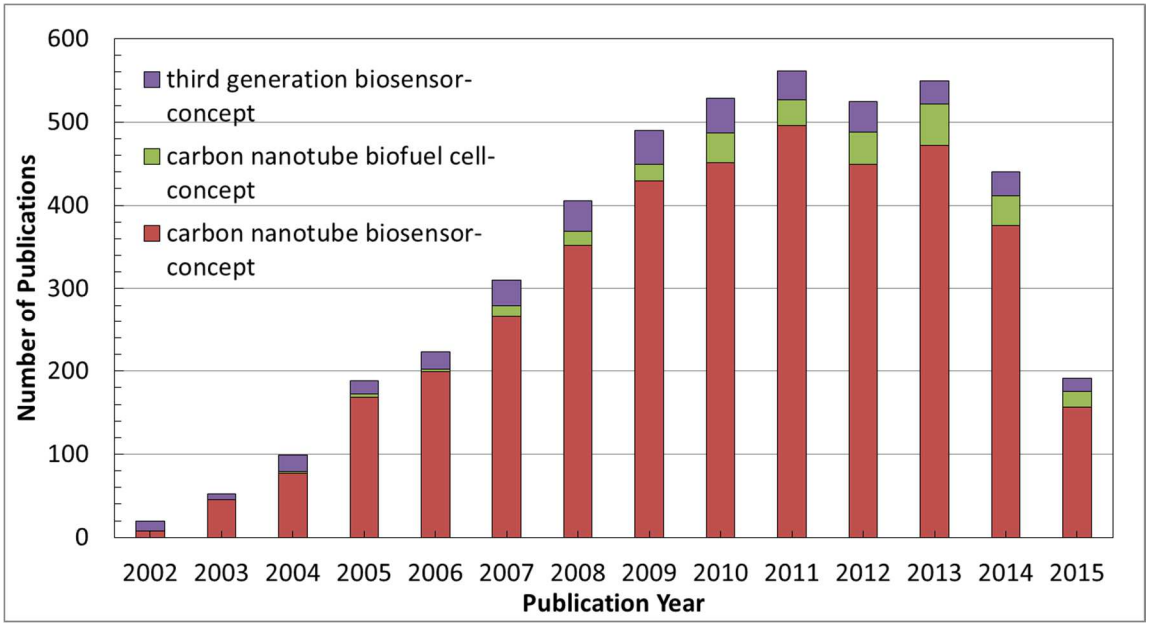

Figure 1*:* Growing interest in use of carbon nanotubes in biosensor and biofuel cell designs. A literature search carried out in the Chemical Abstract database using the terms "third generation biosensor", "carbon nanotube biofuel cell", and "carbon nanotube biosensor" with the "concept" option selected (as of April 23, 2015). Source: SciFinder Scholar.

Figure 1 shows the proliferation in publications involving DET of enzymes associated with CNTs as well as the use of CNTs in biosensors and biofuel cells. The development of CNT-oxidoreductase enzyme conjugates and the ability to achieve some modicum of stability of

such conjugates has enabled demonstration of optical [14, 15] and electrochemical Gen-3 biosensors [16]. Some of these Gen-3 biosensors have been developed by direct covalent coupling of the oxidoreductase enzymes to CNTs that were previously immobilized on platinum microdisc electrode arrays (MDEAs) to yield potentially implantable biotransducers [17]. Such implantable biosensors may be powered by integrated batteries, externally via induction, or internally by the use of a fully implantable enzymatic biofuel cell [18]. Since the fuel (e.g. glucose) of the biofuel cell will be supplied within the body, the cell can be made compact, not requiring a storage for fuel due to its availability *in situ*, and ability to provide sustained energy for the lifetime of the device [19].

There are numerous reports that use nanoparticles (NPs), such as gold NPs or silver NPs, conjugated with various biological molecules for sensing purposes. De et al. [20] give an excellent review on nanoparticle-biomolecular interactions and the applications of nanoparticles in biological sensing, delivery and imaging. While a broad spectrum of applications exists, there are yet questions surrounding reliable processes for directly conjugating enzymes to NPs [21], the acute and long-term health effects [22], manufacturing methods that are scalable and reproducible, as well as consistent metrics for properly characterizing NPs. In addition to these reasons, this review will focus on CNTs rather than NPs as follows.

CNTs, first identified by Sumio Iijima back in 1991 [23], have garnered a great reputation for possessing high mechanical properties (tensile strength ~30 GPa, Young Modulus ~1 TPa) and good electrical properties (resistivity of $10^{-4}\Omega$m, maximum current density of 10^{13} A/m^2). There are three principal methods for synthesizing CNTs: Arc

Discharge Method [24], Laser Ablation Method [25], Chemical Vapor Deposition (CVD) Method [26] (and a modified CVD method known as High Pressure Carbon Monoxide Method (HiPco)) [27]. These methods of synthesis and production are reviewed in detail elsewhere [28, 29] but summarized in **Table 1** because of the relevance of the manufacturing process, the mediator used, and the temperature during production, on the electrical properties of the CNTs as it impacts electron transfer. The manufacturing process used affects the distribution among single-walled carbon nanotubes (SWNTs) *vs.* multi-walled carbon nanotubes (MWNTs), metallic *vs.* semiconducting tubes, the aspect ratio of tubes, as well as their purity levels; all factors that influence electrical transport properties related to direct electron transfer in bioconjugates.

Table 1: Summary of principal characteristics of the three main methods of CNT synthesis (adapted from Baddour and Briens) [29]

Method	**Arc-discharge**	**Laser-ablation**	**CVD**
Pioneer	Iijima (1991)	Guo et al. (1995)[25]	Yacaman et al. (1993)[26]
How	CNT growth on graphite electrodes during direct current arc-discharge evaporation of carbon in presence of an inert gas	Vaporization of a mixture of carbon (graphite) and transition metals located on a target to form CNTs	Fixed bed method: acetylene decomposition over graphite supported iron particles at 700ºC
Yields	< 75%	< 75%	> 75%
SWNT or MWNT	Both	ONLY SWNT	Both
Advantage	Simple, inexpensive	Relatively high purity CNTs, room-temperature synthesis option with continuous laser	Simple, inexpensive, low temperature, high purity and high yields, aligned growth is possible, fluidized bed technique for large scale
Disadvantage	Purification of crude product is required, method cannot be scaled	Cannot produce MWNTs, method only adapted to lab-	CNTs usually are MWNTs, parameters must be closely

	up, must have high temperature	scale, crude product purification required	watched to obtain SWNTs

1.3 Enzyme-based Biosensors and Enzyme-based Biofuel Cells

1.3.1 Enzyme-based Biosensors

Biosensors are bioanalytical systems that enable point-of-concern real time measurement of analytes of biomedical, food, environment or industrial importance. Central to the biosensor is the biotransducer, the device that integrates molecular recognition of the bioreceptor with the chosen physicochemical transduction mode, and which produces a signal proportional to the analyte concentration that is processed and presented by the associated electronics [30]. The biotransducer is often falsely called the biosensor. Some possible transduction modes include electronic, optical, pyroelectric, piezoelectric and electrochemical. Biosensors are distinguished over biodetectors for being repeatable, updateable, quantitative and/or regenerable while detectors are not repeatable, not updateable, not quantitative and not regenerable. Advance®, Confirm®, ept® pregnancy test strips are examples of detectors of human chorionic gonadotropin (HCG) produced by the placenta while glucose biosensors such as Onetouch® can be used in critical care of diabetes or monitoring of a bioprocess. Commonly known implantable biosensor systems include short-term indwelling continuous glucose monitoring systems such as Dexcom's 2006 FDA-approved STS [31] and 2007 FDA-approved STS-7 Continuous Glucose Monitoring System for diabetics [32]. Newer implantable biosensor systems are being designed with intended use in trauma management [33].

1.3.1.1 Generation-1 (Gen-1) Biosensors

Since their discovery in the early 1960s, there has been considerable progress in the development and application of biotransducers and biosensors leading to various generations of biosensors. Wang [4] gives a detailed review on the various generations of electrochemical glucose biosensors. **Generation-1 (Gen-1) biosensors involve a measurement of reactant or product concentration** (e.g. oxygen consumption or peroxide formation) as a means to detect analyte levels (such as glucose). In Generation 1 amperometric enzyme biosensors, the hydrogen peroxide produced is electrochemically oxidized (+0.70 V *vs.* Ag/AgCl, $3MCl^-$) or reduced (+0.00 V *vs.* Ag/AgCl, $3MCl^-$) at a selected poise potential to generate a commensurate current. At a macro-electrode operating under diffusion-limited conditions, the Cottrell equation (equation 1 below) is adequate to describe the ensuing current. At microelectrodes with critical feature sizes less than the diffusion boundary layer thickness (ca. 25 microns), this equation may be modified to yield equation 2 below (at steady state, equation 2 reduces to equation 3).

$$i(t) = \frac{nFAD_0{}^{1/2}C_0}{\pi^{1/2}t^{1/2}} \qquad (1)$$

$$i(t) = \frac{nFAD_{app}^{1/2}C_0^*}{2\pi^{1/2}t^{1/2}} + \frac{nFAD_{app}C_0^*}{2r_e} \qquad (2)$$

$$i_{ss} = 4nFC_o^*D_{appt}r_e \qquad (3)$$

Where *i* (amperes) represents the current, n refers to the number of electrons involved in the reduction/oxidation reaction, F is Faraday's constant (96,485 C/mol), A is the area of the planar electrode in cm^2, C_0 and represent the initial concentration of the reducible analyte in mol/cm^3, D_{app} is the diffusion coefficient for the species of interest (cm^2/s), r_e refers to the radius of the electrode (cm) and t is the time (s). Because of the relationship

to the biocatalytic property of the immobilized enzyme, under diffusion-controlled conditions the amount of current produced is directly proportional to the concentration of the analyte. This allows the direct correlation of the ensuing steady state current of the amperometric enzyme biotransducer with the enzyme's kinetic parameters and the *Michaelis–Menten* Equation for an amperometric response becomes.

$$\frac{1}{I_{SS}} = \frac{K_M}{I_{max}} \frac{1}{C_S^*} + \frac{1}{I_{max}} \qquad (4)$$

Here I_{SS} is the steady-state current or response after substrate, S, addition, C* is the bulk concentration of substrate and I_{max} is the maximum current or response measured under enzyme saturated substrate conditions. The maximum current, I_{max}, and the Michaelis-Menten constant of the system, K_M (mM), may thus be determined, allowing evaluation of the contextual performance of the enzyme relative to some standard condition, such as in solution.

There are three key enzymes pertinent to this review. Two are part of the family of oxidoreductase enzymes; glucose oxidase (GOx) (beta-D-glucose:oxygen 1-oxidoreductase; EC. 1.1.3.4) and lactate oxidase (LOx) ((S)-2-hydroxy-acid:oxygen 2-oxidoreductase; EC 1.1.3.15). The third is laccase (benzenediol:oxygen oxidoreductase; EC 1.10.3.2) that generally serves as the cathode in enzymatic biofuel cells. The first two enzymes provide the molecular recognition capability to recognize their substrates glucose and lactate respectively. Accordingly, these substrates are targeted analytes in amperometric-enzyme biotransducers consuming oxygen and producing hydrogen peroxide. Hydrogen peroxide is a powerful oxidizing agent that readily oxidizes other organic molecules, including proteins/enzymes [34]. Normally, in biological systems,

hydrogen peroxide producing enzymes are closely associated with peroxidases (e.g. Catalase) that immediately and rapidly (high turnover rates) convert hydrogen peroxide to water. Also, the potential at which hydrogen peroxide is electrochemically oxidized allows the rapid oxidation of other molecules such as ascorbate and citrate that therefore contribute an interfering current. For the foregoing reasons, second generation biotransducers, based on the use of intermediary redox molecules called mediators were developed.

1.3.1.2 Generation-2 (Gen-2) Biosensors

After Shichiri's demonstration of *in-vivo* monitoring [35], considerable effort was applied, in the 1980s, to developing **Generation-2 (Gen-2) mediator-based glucose biosensors** [36, 37], introducing commercial screen-printed strips for self-monitoring of blood glucose [38, 39] and using modified electrodes and tailored membranes/coatings for improved sensor performance [40]. By the 1990s, the focus was directed towards establishing electrical communication between the redox active center of GOx and the electrode surface to facilitate mediated electron transfer (MET) [41-45]. MET promised lower operating potentials, fewer interferences, independence of oxygen, and in some cases enhanced electrocatalytic rates. Heller in particular introduced the use of flexible polymer with osmium redox sites [41, 42]. The 1990s also saw the advancement of minimally invasive subcutaneously implantable devices [46-49]. It is important to note that while glucose dehydrogenase (GDH) can be used for amperometric biosensing of glucose (due to its independence of oxygen), the issues of i) the need for an *in situ* source of NAD^+ ii) a suitable redox mediator to reduce the overvoltage for reoxidation of the resulting NADH product iii) lower stability than GOx, and iv) its poor cross reactivity [50] with maltose,

xylose, and galactose is believed to outweigh its benefits. These second generation biotransducers essentially replaced oxygen with a non-physiological electron acceptor (mediator) capable of shuttling electrons from the redox active center of the enzyme to the electrode surface. This shuttling of electrons between the redox site and the electrode has been a limiting factor in the development of these biotransducers as certain enzymes have their redox sites deeply buried within the globular structure of the enzyme. Some diffusional electron mediators, such as ferrocene derivatives, ferricyanide, conducting organic salts (for example tetrathiafulvalene-tetracyanoquinodimethane, TTF-TCNQ), quinone compounds, transition-metal complexes, and phenothiazine and phenoxazine compounds, have been shown to be useful to electrically connect GOx to electrodes [35-37]. Ferrocene derivatives have received a lot of attention due to their low (pH-independent) redox potentials and larger number of derivatives [51, 52]. In order to function properly, mediators should react rapidly with the reduced enzyme (large heterogeneous rate constant, k_{et}, to minimize competition with molecular oxygen) and possess good electrochemical properties (low pH-independent redox potential). The mediator will also need to be insoluble, nontoxic and chemically stable. In most cases, oxidation of the reduced enzyme by oxygen competitively occurs even in the presence of mediators and this limits the accuracy, especially when there are low levels of analyte and/or variable O_2 tension, such as in tissue hypoxia. Additionally, some derivatives, notably ferrocene, have been shown to be unstable following prolonged redox cycling and with extended continuous use [53]. This has led to the investigation of mediatorless biotransducers and the development of generation-3 biotransducers.

1.3.1.3 Generation-3 (Gen-3) Biosensors

Generation-3 (Gen-3) biosensors seek to eliminate the need for molecular mediators by developing a reagentless glucose biotransducer with a low operating potential (generally close to the enzyme redox potential). This leads to high selectivity and direct electron transfer. Ghindilis gives an overview regarding direct electron transfer catalyzed by GOx [54].

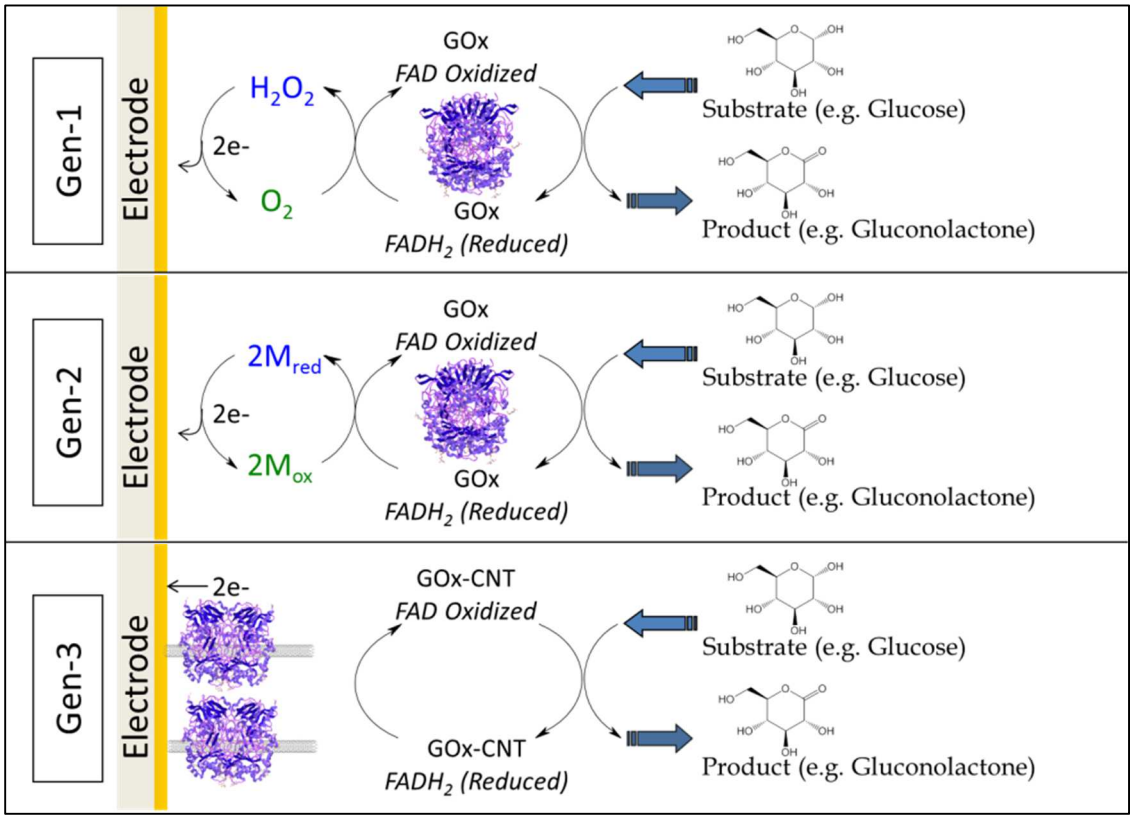

Figure 2 Illustrates the three generations of amperometric enzyme (glucose oxidase - GOx) biotranducers for glucose. Gen-1 is based on the measurement of peroxide concentration (natural oxygen cofactor), Gen-2 is based on the use of artificial redox mediators, and Gen-3 is based on the direct electron transfer between GOx-CNT conjugate and the electrode.

There is a surge in research activity directed towards Generation-3 (see **Fig. 1**) biosensors and/or biotransducers as this affords a number of key advantages over previous generations; i) the reduction of interference from endogenous and exogenous electroactive species, ii) improved selectivity and sensitivity; and iii) improvement in signal to noise. Reports on CNT-based biosensors have doubled in the last 3 years (**Fig.1**). Ultimately, there is the need to eliminate mediators and develop reagentless biotransducers. There is the search for directly transferring electrons from some system (for example an oxidoreductase enzyme) to an electrode. Efficient electron transfer at conventional electrodes has been reported for few redox enzymes (most notably glucose oxidase, GOx). Electrode configuration need to be optimally designed to ensure the electron-transfer distance between the immobilized enzyme and the electrode surface is made as short as possible. Although several reports claim DET between GOx and the electrode, very few give the right level of proof for this mediatorless detection. For example, one method to creating Gen-3 biotransducers is to use conducting organic salt electrodes based on charge-transfer complexes (for example tetrathiafulvalene-tetracyanoquinodimethane, TTF-TCNQ) [55, 56]. This has been proposed by various authors although the exact mechanism for the catalysis of GOx still remains embroiled in controversy. Cenas and Kulys [57] suggest that the electron transfer of GOx at TTF-TCNQ electrodes is mediated and involves the corrosion of the TTF-TCNQ to produce dissolved components of these organic salts that mediate the electron transfer of the enzyme. Yabuki et al. [58] and Koopal et al. [59] on the other hand suggest mediatorless glucose biosensors based on GOx|polypyrrole system. However, the relatively high anodic potential of this system suggests the

possibility of electron transfer by oligomeric pyrroles present on the surface. Guiseppi-Elie in 1994 [60] filed a patent on a GOx|polypyrrole system based on the measurement of change in electrical resistance of an electroactive polymer (such as polypyrrole, polyaniline or polythiophene). GOx was entrapped within this polymer film and the reaction of glucose with GOx produced hydrogen peroxide that oxidized the polymer film and made it more conductive. There is still room for improvement, development and understanding of how mediatorless third generation biotransducers operate.

1.3.2 Enzyme-based Biofuel Cells

In 1964, Yahiro et al. [61] described the first enzyme-based biofuel cell fabricated from glucose oxidase (GOx) as the anodic catalyst and glucose substrate as the fuel [61]. Since then, there has been an explosion of reports that advance the use of renewable and "clean" catalysts, reaction selectivity, fuel flexibility, as well as the ability to operate at milder temperatures.

Biofuel cells offer key advantages over traditional batteries. A good overview of enzymatic biofuel cells has been described by Neto et al. [62]. Enzymes, however, are not readily regenerated and may be denatured leading to shortened lifetimes. **Table 2** is a summary of some recent enzymatic biofuel cells reports detailing the substrates used as well as the power output from each system.

Table 2: Summary of enzymatic biofuel cells from recent papers from Neto et al. Reproduced with permission [62]

Immobilization methodology	**Substrate**	**Enzymatic system**	**Power output (mW/cm^2)**

Polyacrylic acid sodium salt	Glucose/O_2	Glucose dehydrogenase/Bilirubin oxidase	1.45 [63]
Modified Nafion® membrane	Ethanol	Dehydrogenase enzymes in cascade	1.01 [64]
Modified Nafion® membrane	Pyruvate	Dehydrogenase enzymes in cascade	0.93 [65]
Modified Nafion® membrane	Ethanol/O_2	Alcohol dehydrogenase/bilirubin oxidase	0.46 [66]
PAMAM dendrimers	Ethanol	Alcohol dehydrogenase	0.28 [67]
Conducting polymer copolymerized with 3-methylthiopene	Glucose/O_2	Glucose oxidase and bilirubin oxidase	0.15 [68]
Pyrroloquinoline onto gold electrodes	Lactate	Lactate dehydrogenase	0.14 [69, 70]
Cellulose-multiwall carbon nanotubes matrix	Fructose/O_2	D-fructose dehydrogenase/bilirubin oxidase	0.12 [71]
Sol-gel silica matrix/carbon nanotubes	Glucose/O_2	Glucose oxidase and bilirubin oxidase	0.12 [72]
"Ketjenblack" electrode	Glucose	Glucose dehydrogenase	0.052 [73]
Polypyrrole film	Glucose/O_2	Glucose dehydrogenase/laccase	0.042 [74]
Modified chitosan and Nafion ® membranes	Glucose	Glucose dehydrogenase	0.035 [75]
Ultra-small silicon nanoparticles	Glucose	Glucose dehydrogenase	0.0037 [69]
Glutaraldehyde	Ethanol	Quino-hemoprotein-alcohol dehydrogenase	0.0015 [76]

Implantable enzyme biofuel cells present an attractive alternative for powering fully implantable biosensor systems. When integrated, this creates a convenient closed loop system that may be safer while also reducing the demand placed on or need for other power sources. Biofuel cells comprise electrodes having immobilized biocatalyst that oxidize organic substrates, thus converting chemical energy to electrical energy [77]. Criteria for evaluating implantable biofuel cells, such as; the average power output, power density,

stability of components as well as the sustainability of power output continuously are summarized in **Table 3**.

Table 3: Key criteria used in the evaluation of the performance characteristics of implantable biofuel cells.

	Criteria for evaluating the performance of an implantable biofuel cell
1	Average power output (μW) and power density (μW/g or μW/cm^2)
2	Continuity of power output
3	Overall life-time / stability of components
4	Biocompatibility (includes foreign body response, toxicity of components and products)
5	Size and placement
6	Method of implantation
7	Ease of resection / removability
8	Wired or wireless communication between the sensor and instrumentation
9	Effect of external and internal fields
10	Proximity to target load / device

Improvements have since been made to the first enzymatic biofuel cell made by Yahiro [78-81]. Ramanavicius et al. [76] discuss an electrochemical based biofuel cell powered by ethanol. Since biological substances contain significant amounts of ethanol and other alcohols, alcohols offer one group of substrates useful for powering biofuel cells. Justin et al. [10] report a basic setup of a leukocyte biofuel cell wherein the enzymatic machinery resides within the living cell. The exact molecular mechanism of electronic discharge remains unclear.

Two prime issues to be addressed include the lifetime of the biofuel cell and the improvement of its power density. One possible way of improving power density is by increasing enzyme loading through advanced immobilization techniques and larger surface

areas and the lifetime of the biofuel cell could be improved via conjugation with CNT which could help produce stability to the enzyme structure.

1.4 Importance of CNTs in biosensors and biofuel cells

Rivas et al. [82] has given a review on the use of CNTs in electrochemical biosensing but did not address the original pioneering work on DET [13]. Several reports have shown the electroactivity of CNTs to be due to the presence of reactive functional groups on the surface of the tubes [83-85]. Higher charge densities have been shown in topological defects (such as pentagonal defects) [85]. This demonstrates the relationship between such defects and the electroactivity of CNTs. Electrocatalytic properties of CNTs have also been well documented. Compton et al. [86-88] reported on and rationalized why CNTs demonstrate enhanced electrocatalytic activity. It was proposed that this activity was due to edge-plane like sites located at tube ends and because of topologically defective areas on tubes. Other works have shown electrocatalytic activity due to the presence of CNTs that have been attributed to CNT dimensions, CNT electronic structure as well as intentional / non-intentional defect sites on tube surface [84-87, 89, 90]. Lower overvoltages and higher peak currents, evidence of electrocatalysis, have been observed in the voltammetric responses of various molecules on CNT-modified electrodes. Increase in peak currents, i_{pa} and i_{pc}, however may be attributable to increases in effective surface areas of electrodes modified by CNTs. Increase in the heterogeneous rate constant, k_{ct}, indicates catalytic activity. Due to these unique properties, CNTs have garnered a lot of attention in their use for preparing electrochemical biosensors [13, 91-100]. One key issue, in creating an electrochemical biosensor, is developing the appropriate method for modifying

electrode surfaces to receive CNTs [101]. See "Methods of Immobilization of CNT-Enzymes Conjugate" section.

1.4.1 Electronic Transport and Redox Properties of CNTs

Saito, Dresselhaus and Dresselhaus have provided a comprehensive review of the transport properties of CNTs [28]. CNTs transport properties are due to their sp^2 hybridized carbon architecture, their nano-size (which introduces quantum effects), essential one-dimensionality, and the impurities and defects in their structure. Complementary, Tans et al. [102] performed the first experiment giving a clear indication of ballistic transport associated with the discrete levels imposed by the finite length of a 1D CNT conductor. In this experiment CNTs were prepared by laser-ablation of carbon with an admixture of Ni/Co produced samples with a proliferation of armchair SWNTs and a uniform diameter of 1.38 nm. The SWNTs were deposited by spin-coating of a drop of SWNT suspension on top of a Si/SiO_2 substrate decorated with two 15-nm-thick Pt electrodes. An isolated SWNT was 3 microns long, with a section of 140 nm between the contacts to which a bias voltage, V_{bias}, was applied. A gate voltage, V_{gate}, applied via a third electrode was used to vary the electrostatic potential of the tube. A two-point resistance at room-temperature of 550 kΩ was observed. In a different four-point geometry setup, the SWNT was shown to have a contact resistance of 300 kΩ at room temperature and 1 MΩ at 4K. This observed phenomena can be understood as arising from well separated, discrete electron states that are quantum-mechanically coherent over long distance. In other words, steps in the quantum conductance and the charging effects associated with the minute capacitances of

the CNT and the gate. Britto et al. demonstrated via *Ab-initio* calculations that the improvement in electron transfer (relative to other materials) is due to the curvature of the tubes that originate changes in the energy bands close to the Fermi level [85]. Purposeful manipulation of the band structure by adsorption of metallic Cu or Au nanoparticles of different work functions can result in different electronic properties [103]. Likewise, changes in dielectric constant of the tube environment can potentiate its electronic properties [15]. Figure 3 below gives an overview of the various types of CNTs found.

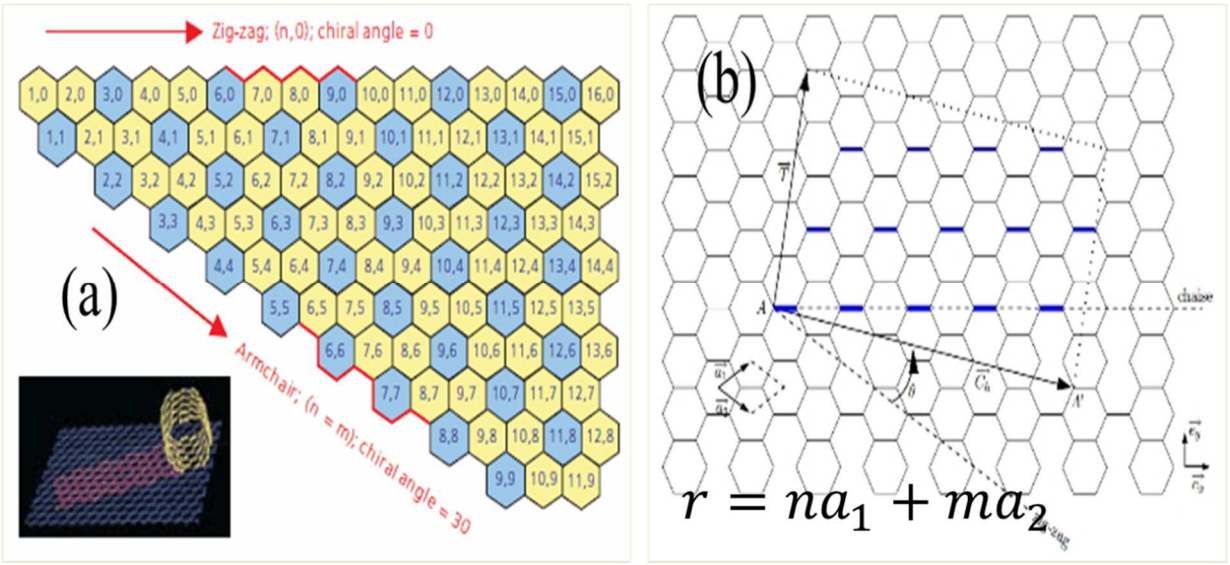

Figure 3: (a) A graphic (taken from Jansen [104]) displaying a Chirality Map which shows the various types of SWNTs that can be formed. The properties are governed by the way in which they are rolled as shown in the insert. The SWNT will be metallic in the armchair configuration, or when m-n is a multiple of 3. Metallic SWNT are indicated with blue while semiconducting SWNT are indicated with yellow. (b) Representation of the base vectors for the basic hexagon in a carbon sheet

It has been shown that the energy gap, E_g, for semiconducting nanotubes is inversely proportional to the nanotube diameter, d_t.[28, 105] regardless of the chiral angle of the semiconducting nanotube.

$$E_g = \frac{|t| a_{C-C}}{d_t}$$

Where | t | is the nearest neighbor C-C tight binding overlap energy (sometimes denoted by γ_0) and $a_{c\text{-}c}$ is the nearest neighbor C-C distance on a grapheme sheet. In 1998, Wildoer et al. in [106] were the first group to successfully test the vast amount of band-structure calculations that have appeared experimentally. They investigated 27 SWNTs of various chiral angles and diameters, and showed that the energy gap in SWNTs is inversely proportional to the tube diameter. Ouyang et al. [107] were able to use low-temperature scanning tunneling microscopy (STM) to characterize the atomic structure and local density of states (DOS) of metallic zigzag and armchair SWNTs (see Figure X for examples of zigzag and armchair SWNTs). They obtained energy gaps of 0.080 $\pm$ 0.005, 0.042 $\pm$ 0.004, and 0.029 $\pm$ 0.004 eV for (9,0), (12,0), and (15,0) zigzag SWNTs respectively and demonstrated that these "metallic" tubes should actually be classified as small-gap semiconductors. They also obtained pseudogaps with magnitudes ~80 to 100 meV for the (7,7), (8,8), (9,9), and (10,10) armchair SWNTs studied. In both cases, the magnitudes of the energy gap (or pseudogap) showed an inverse dependence on the radius of the SWNT. The result of this study was motivation for Matsuda et al. [108] to develop a more accurate method of predicting band gaps due to its importance in designing CNTs for electronics applications. **Figure 4** below shows a comparison between the various SWNTs and an enzyme of interest, glucose oxidase.

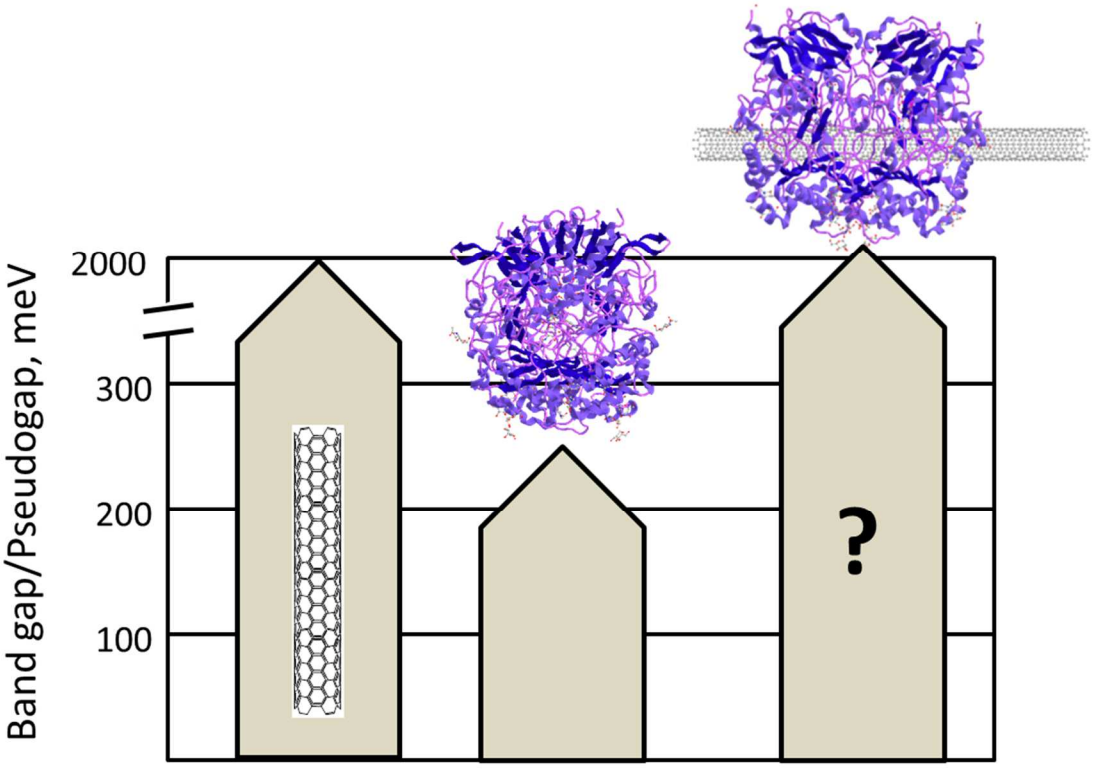

Figure 4: Energy band diagram comparing SWNTs [105-108], enzyme (glucose oxidase) and enzyme-SWNT conjugate

1.4.2 Individualization, Functionalization, Solubilization and Derivatization of Carbon Nanotubes:

For the refinement of existing Gen-3 biosensors and advanced enzyme biofuel cells that use CNTs as active supports, CNTs (normally spontaneously bundled into aggregates upon synthesis) must first be "individualized". For this, CNTs may need to be chemically modified to introduce biocompatablizing or reactive functional groups that will render the tubes processable in aqueous media, or for subsequent chemical covalent conjugation reactions. In addition, the functional groups may need to be derivatized by further reaction to introduce new chemical moieties [109]. Some reported methods include end and/or

sidewall functionalization [110, 111], use of surfactants with sonication [112], polymer wrapping of CNTs [113, 114], and protonation by superacids [115]. Some of these methods also involved "chopping" the CNTs into shorter lengths leading to a loss of the characteristic high aspect ratio and a compromise of the electronic properties [116].

Functionalization can be broadly divided into covalent and non-covalent functionalization. With covalent functionalization, there is a direct sidewall / tube end functionalization associated with a hybridization change from sp^2 to sp^3 and a simultaneous loss of conjugation. The chemical transformations from defect sites are generally involved in covalent functionalization. These defect sites could be the open ends or holes in the sidewalls terminated by –OH / –COOH groups or pentagon-heptagon irregularities in the hexagonal graphene framework. Non-covalent functionalization on the other hand is mainly based on supramolecular complexation using adsorption forces such as van der Waals and π-stacking interactions to engender intimate association between the CNT and the surfactant (such as enzymes). This has the key advantage of not adversely modifying the properties of the CNT directly and conversely being less stable than covalently functionalized CNTs. Both methods can be used to make CNTs more easily dispersible and the literature is rich with various techniques of modifying CNTs to achieve dispersion [117-119].

As an example, Kim et al. in 2003 [118], described a simple and efficient process for solubilizing CNTs using an enzyme (amylase), a linear polymer of D-glucose units, in aqueous dimethyl sulfoxide (DMSO-H_2O) mixed solvent. This process requires two key conditions, pre-sonication of CNTs in water and subsequent amylose treatment in an

optimum mixture of DMSO/H_2O. The first step, pre-sonication, separates SWNT bundles while the latter treatment ensures maximum cooperative interaction of SWNTs with amylose. This leads to immediate and complete "solubilization" of the tubes. The best solvent composition was found to be 10-20% DMSO, in which amylose assumes a random conformation (an interrupted loose helix). The resulting suspension was stable and showed no precipitation over several weeks.

Another simple and efficient example of solubilizing CNTs using an enzyme (GOx) is described by Guiseppi et al. [120] in deionized water. GOx-CNT suspensions were prepared by ultrasonication at 4^oC within a jacketed water bath using a Soniprep 150 equipped with an MSE exponential probe (tip diameter 3 mm, transformation ratio 7:1) ultratip sonicator (frequency 23 kHz). The resulting suspension showed stability and did not form any CNT aggregates over a month.

2 Enzyme-CNT Conjugation

2.1 Carbon Nanotubes in Amperometric Biosensors and Biofuel Cells

CNTs have the ability to access the embedded active site of oxidoreductase enzymes to achieve DET as well as to increase the surface concentration of enzymes due to their high 3D electroactive area. In its native environment, electron transfer within these enzymes of interest is achieved via enzymatic cofactors such as flavin adenine dinucleotide (FAD) in GOx or flavin mononucleotide (FMN) in LOx. While mediated electron transfer has been the dominant strategy employed for the electric wiring of the active sites of

enzymes to electrodes, redox mediators represent a limiting factor to stability in fuel cells as well as power output by decreasing the open circuit voltage.

With the demonstration of direct electron transfer via GOx-CNT conjugates [13, 100, 101], a new field of investigation has emerged with far reaching consequences for Gen-3 biotransducers and advanced enzyme biofuel cells. Notwithstanding, CNT-Enzyme conjugates have also shown some promise in targeted drug delivery [121] as well as in cancer therapy [122] [123]. In Gen-3 biotransducers and advanced enzyme biofuel cells the goal is to place the conductive SWNT nanostructure within tunneling distance of the enzyme's redox co-factor. This means forming a supra-molecular conjugate structure wherein the debundled nanotube effectively penetrates the glycoprotein shell and establishes, via the tube ends or the sidewall, facile electron transfer between the prosthetic group and the CNT. Finally, the supra-molecular conjugate must be immobilized on the electrode in such a manner as to facilitate tunneling from the SWNT to the electrode. (Draw the energy band diagram that illustrates this concept). Moreover, enzyme-SWNT conjugates should i) be stable and form homogeneous dispersions of individualized enzyme-SWNT conjugates; ii) preserve the electrical/electrochemical properties of the SWNTs; and iii) the active site and associated catalytic activity of the enzyme should not be compromised, and if possible, should be enhanced. Diverse methods of conjugation of enzymes with CNTs have produced evidence for direct electron transfer.

There are three principal techniques for making supramolecular conjugates of enzymes and CNTs; non-covalent conjugation, covalent conjugation, and hybrid conjugation (some combination of covalent and non-covalent methods). The non-covalent

approach is generally preferred since the physico-chemical properties of the CNT are preserved and the catalytic capability forged from molecular recognition by the enzyme can likewise be retained [120]. Covalent conjugation increases the chemical stability of the complex but chemically modifies the two components, often in uncontrolled ways, with concomitant undesired effects including subtle changes in enzyme structure with loss of activity and changes in the electronic and transport properties of the SWNTs. Hybrid techniques seek to maximize the benefits of both approaches while minimizing the potential deleterious effects. However, these approaches provide little control over orientation of the conjugate and provide little specificity regarding the sites of interaction of components.

2.2 Non-covalent Enzyme-CNT Conjugation Techniques

The association between enzymes and CNTs, as with other proteins, occurs spontaneously and there is evidence of the formation of supramolecular conjugates with proteins such as albumin and lysozyme [124]. The pioneering work of Guiseppi-Elie et al. [13] reported direct electron transfer between the redox active group, flavin adenine dinucleotide (FAD) of GOx and SWNT-modified glassy carbon electrodes (GCE). This was achieved by simple room temperature adsorption of GOx onto SWNT-modified GCE and onto SWNT paper. This study showed a large (~22x) increase in the effective working electrode area when modified with SWNT. Moreover, the work showed the necessary increase in k_{et} and demonstrated independence from molecular oxygen in amperometric glucose detection.

Surfactant facilitation of protein adsorptive conjugation is a noteworthy development. Graff et al. has demonstrated a non-covalent method of protein conjugation to SWNTs that uses a dilute solution of sodium cholate, a bile salt which acts as an effective surfactant to create a supramolecular SWNT-Con-A (concanavalin-A, a carbohydrate-binding protein) conjugate [125]. This suspension-dialysis process has been developed and successfully applied to non-covalent conjugation to horseradish peroxidase (HRP) by Palwai et al. [126]. In this work the HRP retained its biological activity and the conjugate showed little change in structure as determined by UV–Vis–NIR spectra. This system was subsequently used by Wang et al. to demonstrate, via l-cystine covalent immobilization of the conjugate to gold film electrodes, direct electron transfer in hydrogen peroxide (H_2O_2) detection [127]. A linear response to H_2O_2 was obtained over the range 1.0×10^{-12} to 1.0×10^{-11}M with a corresponding detection limit of 2.1×10^{-13}M. This method of non-covalent conjugate formation was found to produce dispersed and debundled supramolecular SWNT-GOx conjugates that were stable for 30 days and which retained 75% of the native enzymatic activity. The conjugates were also used in the fabrication of amperometric biosensors using the layer-by-layer (LbL) self-assembly process with alternate layers of the redox polymer, poly[(vinylpyridine)Os(bipyridyl)$_2$ $Cl^{2+/3+}$] (PVP-Os). Quite high current densities (2X vs. a planar electrode; 440 μA/cm^2) were observed in what is clearly a Gen-2 macromolecular mediated electron transfer system. Papain (papaya proteinase I), a cysteine protease (EC 3.4.22.2) enzyme present in papaya was physically adsorbed to carboxyl- and amine- functionalized MWCNTs. In a creative twist the conjugate was encapsulated via a papain-induced silicification reaction within a silica

coating. The silica-coated bioconjugates exhibited significantly improved thermal, pH and cycling stability without appreciable sacrifice of the enzyme's catalytic activity [128]. Lipases from *Candida rugosa* (CRL) were adsorbed onto MWCNTs, shown by TEM to be attached, and to retain 97% of their catalytic activity with 2.2- and 14-fold increase, compared to pristine enzyme, in their initial transesterification rates in nearly anhydrous hexane and water immiscible ionic liquid [Bmim] [PF6] respectively [129].

Another principal approach to creating supra-molecular conjugates is via ultrasonication. Ultrasonication, in relation to biomolecular conjugation, is a process whereby sound energy is transmitted through a medium via high frequency vibration at a probe tip. Ultrasonication creates a series of micro-cavities in the dispersion that results in shockwaves with pressures that reach 1,000s of atm and creates rapid microstreaming of liquid around the point of bubble collapse [130]. Using ultrasonication to process enzymes has been shown to have some effect on enzyme activity as well as enzyme structure (REF). Guiseppi-Elie et al. [131] studied tip ultrasonication (23 kHz) of glucose oxidase (GOx) over a range of times (10 min to 60 min) and showed that ca. 80% of activity was retained although not without some changes to alpha-, beta- and random secondary structure fractions. There was a monotonic reduction in α-helix and β-sheet fractions with extended sonication when compared to pristine GOx. When similar tip ultrasonication of GOx was done in the presence of SWCNTs, the authors showed similar reduction in α-helix and β-sheet fractions with extended sonication time, but also showed an improvement in the stability of the GOx enzyme activity. This they attributed to the dissipation of cavitation energy by the SWCNTs [120, 131].

Among these are such as deposition onto crystalline gold nanoparticle modified MWNT electrode shown by Rakhi et al. [132], cross-linking in a matrix of chitosan demonstrated by Wang et al.[133], electropolymerization within a polypyrrole film as shown by Wang et al. [134].

2.3 Covalent Enzyme-CNT Conjugation Techniques

Various groups have developed and applied different techniques for covalently conjugating biological materials to CNTs for various applications such as electronic devices [135], bioanalytical biosensors [136], as bioseparation aids [137] and as bactericidal coatings [138, 139]. Some examples of covalent conjugation techniques include the use of crosslinkers such as 1-ethyl-3-(3-dimethylaminopropyl) carbodiimide (EDC/EDAC) [140, 141], use of avidin-biotin interaction [142], and the use of homo-bifunctional cross-linker such as glutaraldehyde [140, 143]. Some methods employ a multistep route to the formation of covalent conjugates of SWNT and the biological entity. Baker used a multistep route to demonstrate the success of covalent linking with the goal of making building blocks for DNA complementary sequences and reversible biosensors [144].

One of the most common methods of covalent conjugation involves the use of EDC to activate the carboxylic acids of functionalized SWCNTs (f-SWNTs) which, upon reaction with the primary amine groups of enzymes yield amide bonds. One major challenge to the use of EDC is the potential for activation of acid groups on the targeted enzyme and the subsequent crosslinking to amine groups leading to intra- as well as inter-molecular crosslinks, the reduction in enzyme activity and the possible formation of cross-

linked aggregates [145]. To reduce most of these problems, EDC chemistry should be done in the presence of sulfo-NHS and in a slightly acidic buffer. Cang-Rong and Pastorin [146] reported the activity and structure of the enzyme amyloglucosidase (AMG) physically adsorbed or covalently attached to CNTs. They showed that catalytic efficiency was higher for the physically adsorbed samples compared to the covalently attached conjugates. This seems reasonable considering that covalent attachment modifies the secondary structure of the enzyme which could lead to some reduction in catalytic efficiency. The surfactant cetyltrimethyl ammonium bromide (CTAB) has been used by Gosh et al. to create reverse micelles containing active functionalized and derivatized SWCNTs. Surface-active lipase was found to be 2.5-fold more active with CTAB-CNT reversed micelles compared to that in the absence of the nanoconstructs but that the enzyme was deactivated in water. [147]. In the EDC-NHS conjugation of AcT (Perhydrolase S54V) to MWNTs, Dinu et al. [139] established that direct covalent conjugation resulted in retained specific activity of 7% of the native AcT activity, whereas the use of a PEG spacer ($dPEG_{12}$) raised this value to 24%. While spacers may support higher enzyme activity, they generally create conjugates wherein the CNT and Redox cofactor are well beyond the tunneling distance for effective change transfer.

2.4 Hybrid Conjugation Techniques

Hybrid conjugation involves the use of covalent and non-covalent techniques in conjunction with each other.

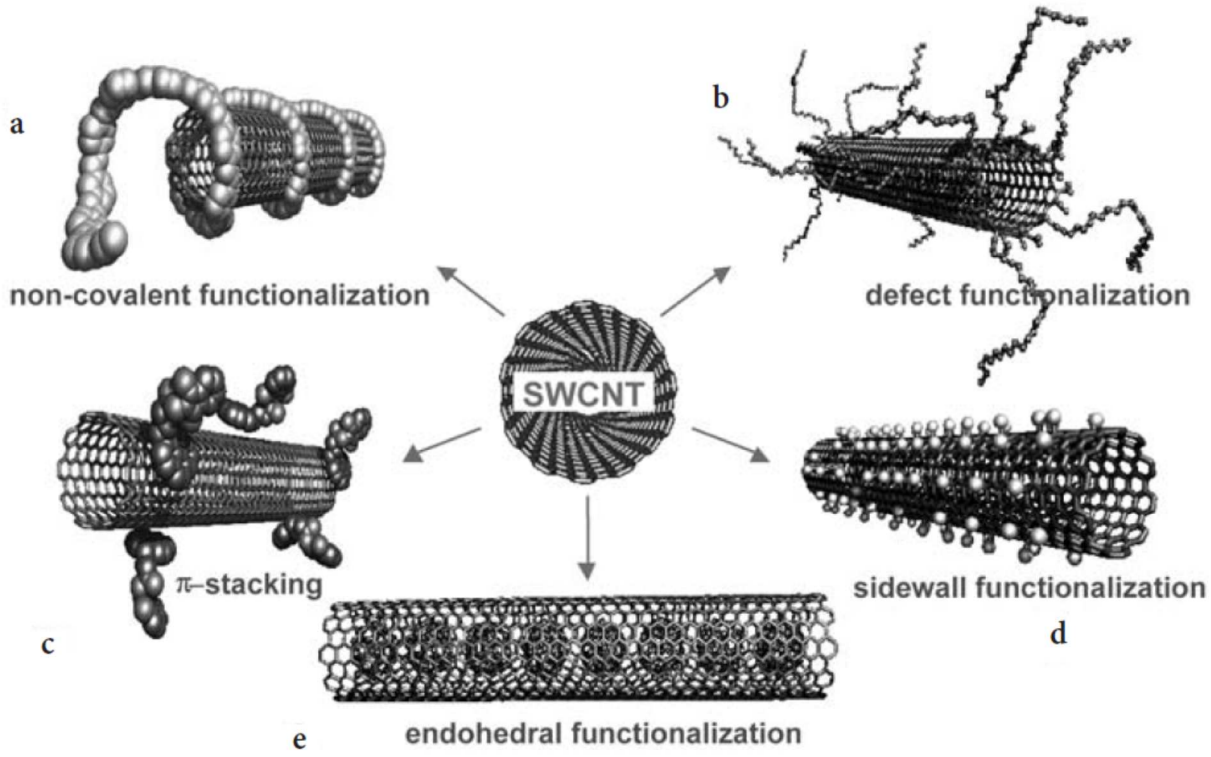

Figure 5: Different possibilities of the conjugation via functionalization of SWNTs. Reproduced with permission [117]

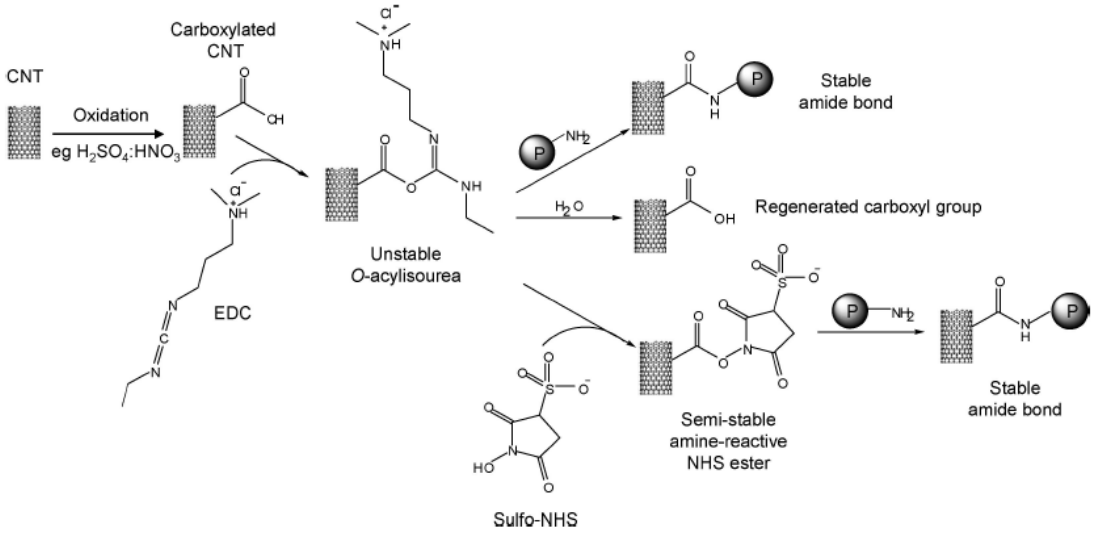

Figure 6: Schematic illustration of the covalent conjugation of proteins to carboxylated CNTs using EDC in the presence or absence of sulfo-NHS. Reproduced with permission [145]

The type of conjugation method used ultimately affects the robustness and stability of the conjugate. Each method has its tradeoffs and it is up to the user to decide on what constitutes acceptable loss (e.g. reduction in activity) versus benefits (e.g. long term viability, enhanced electron transfer efficiency, etc.).

One hybrid method uses the bi-functional favorable pi-stacking interface interactions of 1-pyrenebutanoic acid *N*-hydroxysuccinimide ester (PSE) with SWCNTs and its subsequent covalent coupling via the succinimide ester to primary amines of lysine and arginine of the enzyme GOx [148]. Similarly, lipase was immobilized using this hybrid method onto SWNTs in the ionic liquid, 1-butyl-3-methylimidazolium tetrafluoroborate (BMIM-BF4), and its performance compared with similar immobilization in buffer (20 mM phosphate, pH 7.2) and with simple non-facilitated adsorption in both buffer and sonic liquid. The resulting immobilized enzyme displayed the highest activity in the transesterification of 1-phenylethyl alcohol in the presence of vinyl acetate in toluene.

3 Methods of Immobilization of CNT-Enzyme Conjugates

Enzyme functionality can be stabilized and improved depending on the immobilization technique used [149]. There are four main methods of immobilizing CNT-Enzyme conjugates onto electrodes: adsorption, physical entrapment, covalent immobilization and binding. Entrapment involves the physical localization of the conjugate

within the void volume of a polymer or sol-gel membrane (e.g. hydrogel or aerogel entrapment) or within the microcavities of synthetic fibers (fiber entrapment) or reticulated carbonaceous materials in such a way as to prevent the release of the conjugate while allowing influx of analyte or fuel and release of product. A subset of the entrapment method is microencapsulation which involves enclosing the conjugate within spherical, semipermeable polymer membranes having diameters in the 1 – 100 micron range. Immobilization that uses electrostatic interactions, chelation, metal binding, covalent bond formation and hetero- or homo- bifunctional crosslinking is oftentimes mistakenly called binding. Binding refers specifically to the union of ligand (receptand) and its binding pair receptor characterized by an affinity or binding constant; typically $>10^{-4}$M.

Adsorption is a simple physicochemical immobilization technique involving the interaction of the conjugate with an insoluble support via van der Waals forces, hydrogen bonding or hydrophobic interactions [150]. Electrostatic interaction of charged conjugates (enzymes generally have a net negative charge) to oppositely charged solid supports containing ion-exchange residues likewise accommodates immobilization. Chelation or metal binding involves the use of transition metal compounds such as titanium and vanadium as a means of activating the surface of the support to allow direct chelate formation with conjugates. Covalent attachment is the formation of covalent (sigma and pi bonds) between components of the CNT-conjugates and dispersed meso-forms or insoluble physical supports. Finally, crosslinking addresses the formation of covalent bonds between components of the enzyme-CNT conjugate and the support or between the enzyme-CNT conjugate and itself by means of bi- or multi-functional reagents; leading to three

dimensional cross-linked aggregates which are completely insoluble in water but which do not require the use of water-insoluble carriers.

The work of Qiu et al. [151] illustrates an example of physical entrapment wherein GOx was entrapped within a multi-component chitosan membrane composite that was doped with ferrocene monocarboxylic acid-aminated silica nanoparticles conjugate and MWNTs. The authors reported good analytical performance (the sensor lost only 2.3% of its initial activity after more than 10 successive measurements over an 8 h period) and typical stability (retained 86% of initial activity when stored at 4^{o}C for >1 month and used intermittently). One notes however that the matrix possessed an enhanced mediator system (both ferrocene and MWNTs) and there was no direct conjugation of enzyme to the MWNTs. Although the authors investigated the effect of temperature on the biosensor, they used 25^{o}C for this work which may not have been appropriate considering that the sensor is more likely to be used at higher temperatures. Bourdillon et al. as far back as 1980 demonstrated the covalent attachment of GOx to a modified GCE [152] with the aim of improving electron transfer efficiency. Their method involves adsorbing enzymes on graphite or activated carbon followed by glutaraldehyde or soluble carbodiimide crosslinking. They obtained 40% yield of activity which was comparable to other data from that time. Stability of the enzyme electrode under storage conditions could be evidence for the covalent attachment process. CNT-enzyme conjugates can be similarly covalently coupled to glassy carbon electrodes (GCEs) using a common method of introducing carboxylic acid functional groups via various reduction chemistries and then using EDC-NHS chemistries to covalently tether the CNT-enzyme conjugates. One

method demonstrates improved stability of enzyme layers using phenyl-C_nH_{2n}-COOH moieties by electrochemical reduction of *in situ* generated aryldiazonium salts bearing carboxylic acid groups [153]. After introducing carboxyls groups, they were activated using EDC-NHS chemistries before depositing GOx onto the modified electrode as an initial grafting layer for subsequent crosslinking to other enzyme layers. The authors demonstrated that the initial grafted layer conferred stability (over 6 weeks) compared to non-grafted electrodes (1 week). Although this example discusses the coupling of enzymes, this can be extended to CNT-enzyme conjugates.

An alternative is the use of alkane thiol self-assembled monolayers (SAMs) on coinage metals such as gold as described by Guiseppi-Elie et al [154] wherein cysteamine (CA), which forms a highly disordered SAM, was compared to 11-amino-1-undecanethiol (11-AUT) which, by contrast, forms an ordered SAM. EDC-NHS covalent coupling of the terminal amines of the SAMs to mixed-acid chopped single-walled carbon nanotubes (HOOC–SWNT–COOH) produced an increase in the effective area of the MDEA-Au|CA|SWNT by 200% while that of MDEA-Au|11-AUT|SWNT was increased by 100%. Glutaraldehyde (GA), a prototypical bi-functional crosslinker widely used in enzyme immobilization, has been shown by Galhardo et al. [155] to have an adverse effect when used in CNT-enzyme crosslinking/immobilization. The authors investigated the use of a room temperature ionic liquid (1-butyl-2,3-dimethylimidazaolium tetrafluoroborate) and GA to immobilize GOx. In one approach a mixture of GOx, ionic liquid and GA was drop applied to a GCE and dried. In the other approach a mixture of GOx and ionic liquid was first cast and then a thin layer of GA was applied and allowed to react. The second approach

showed improved amperometric response time (12 *vs.* 15 s). The authors claimed that the ionic liquid interacted more strongly with the enzyme than with GA leading to stability of the enzymes thus enhancing the response in the first method and that the ionic liquid shields the enzymes from structural changes induced by GA. The second approach (17.1 $mA/cm^2/mmol^{-1}L$) had a 160% increase in sensitivity over the first approach (10.4 $mA/cm^2/mmol^{-1}L$) demonstrating efficient access of the active sites of the enzyme.

Printing is an attractive method for immobilization since it promotes cost efficient mass manufacturing on diverse substrates (rigid and flexible) as well as the opportunity to print complex patterns and accommodate specific spatial placement of conjugates. Smoland et al. [156] show the versatility of this method by investigating three conductive ink formulations containing enzymes (laccase) on various substrates. Ink 1 (carbon-based ink) contained some commercial carbon-based ink with carbon nanotubes, mediator and enzyme. Ink 2 (silver-based ink) contained commercial silver-based ink with carbon nanotubes, mediator and enzyme and Ink 3 (experimental) contained carbon nanotubes, α-sorbitol, polyvinyl alcohol, binder, mediator and enzyme. A novel, printed stand-alone enzyme fuel cell was fabricated using the experimental ink and was found to operate in a dry environment with the aid of some internal moisture reservoir. A voltage between 0.6 and 0.8 V could be maintained for several days under a 2.2 kΩ load in a well-controlled humidity environment. The dry printed layers maintained enzymatic activity for several months and could withstand some form of heat treatment without appreciable loss of activity. The authors suggest potential improvement with the addition of a dedicated moisture barrier and a selective membrane to separate both anode and cathode.

Most times a complex combination of the foregoing immobilization techniques is used. MacAodha et al. [157] have reported improvement in the stability of GOx-associated current through the inclusion of MWCNT into various enzyme/redox polymer films; some crosslinked with glutaraldehyde (GA) and others with poly(ethylene glycol) diglycidyl ether (PEGDGE). This approach combines physical entrapment and covalent crosslinking. They claim that the glucose oxidation current densities reported (1 mA/cm^2) for the MWCNT imbibed enzyme/redox polymer films crosslinked with GA vapors were the highest in 5 mM glucose. This effect is similar to that observed by Galhardo et al. where a thin layer of GA was applied to the enzyme/conjugate system [155].

Another good example of combination immobilization is found in the work of Fischback et al. where they developed and applied an enzyme immobilization technique called "enzyme precipitate coatings (EPCs)". This is achieved by first covalently attaching a monolayer of enzyme to the surface of CNTs, then precipitating the enzyme by the addition of ammonium sulfate. The enzymes were then cross-linked and covalently attached to the CNTs. Finally, the enzyme-coated CNTs were applied to carbon paper using Nafion® as a binder within which to entrap them. This system proved highly stable and produced a current density >0.7 mA/cm^2 at 0.18V for over 45 h using a glucose solution under ambient conditions [158]. Gao et al. used electrodeposition to achieve initiation of the layer-by-layer technique for GOx-SWCNT conjugate immobilization with an alternate redox polymer layer of water-soluble poly(1-vinylimidazole) (PVI) complexed with $[Os(bpy)_2Cl]^+$ (PVI-Os) [159]. The screen printed carbon electrodes (SPCEs) functionalized with multilayers of PVI-Os|GOx-SWCNT was stabilized by further

electrodeposition of PVI-Os [160, 161]. The authors demonstrated enhanced catalytic current with an increase in the number of deposited layers, rapid response (~ 5 s), a linear range from 0.5 – 6.0 mM, detection limit of 0.1 mM glucose and a sensitivity of 16.4 μA $mM^{-1}cm^{-2}$. The biosensor maintained 90% of initial activity with intermittent evaluation of the biosensor every 5 days for 30 days while stored at 4ºC. Selectivity tests (response to glucose in the presence of uric acid, ascorbic acid and 4-acetamidophenol) were done by adding a Nafion membrane to the electrode surface. The Nafion helped mitigate interference from ascorbic and uric acids although the overall biosensor response was reduced. While the results obtained are encouraging, diabetic patients with glucose levels as high as 33 mM may need to dilute their blood so it fits within the working range of this biosensor. Jose et al. [162] fabricated electrodes by electrospinning a solution of DMF containing polyacrylonitrile (PAN) 8% (w/w) and $HAuCl_4$ 10% (w/w) (heated at 80ºC until solution was clear). The resulting electrospun fiber was then soaked in sodium borohydride (1 mM) to reduce the Au^{3+} within the fiber to Au^0. This reduced fiber was washed in dilute HCl (10 mM) and distilled water to completely remove all sodium borohydride. Following this, the fiber was soaked in a $HAuCl_4$ solution (0.1 mg/mL) containing hydroxyl amine (0.02 mg/mL) leading to a completely coated fiber with gold nanoparticles via electroless deposition (taking advantage of the crystalline gold present in and on the fiber and using these as nucleating sites to deposit gold nanoparticles). Electrophoresis was then used to deposit carboxyl functionalized MWCNT uniformly on the fiber surface. Finally enzymes were covalently coupled to the carboxyl groups on the MWCNTs using EDC-NHS chemistry. They were able to achieve enhanced surface area (surface coverage of 1.1 x 10-

^{12} mol cm^{-2}) of the electrospun fiber due to MWCNT coating as well as demonstrate direct electron transfer via the MWCNT coating with an electron transfer rate constant of 1.12 s^{-1}. The sensor produced a linear response to glucose concentration up to 30.0 mM, sensitivity of 0.47 μA mM^{-1} cm^{-2} and a detection limit of 4 μM.

While there are many possible immobilization techniques, most frequently authors seek to combine a high loading method (such as entrapment within a polymer matrix) with specific anchorage (for example via chemical crosslinking) to increase overall sensitivity and detection limit of the resulting biosensor or to enhance the power density of a biofuel cell.

Concerns have been raised regarding the cytotoxicity of CNTs [163-165]. There are still ongoing investigations into the exact nature of possible cytotoxic effects. Most of the toxic effects arise from the high aspect ratio of the CNTs; similar to asbestos fiber effects but may also arise from the electrical properties as CNTs become associated with redox co-factors that are naturally inaccessible but may now be within tunneling distance of CNTs. There have also been claims of reducing cytotoxicity by functionalizing CNTs [165]. This area is still being debated since Salvador-Morales et al. [166] concluded that while functionalization of CNTs can lower toxicity of CNTs, the functional groups could have toxicity implications of their own. Functionalizing still does not address the toxic effect arising from the high aspect ratio of the CNTs.

The fabrication of multi-analyte biotransducers continues to be a major technical challenge when the length scales of the individual transducer elements are on the order of microns (Zimmermann, Fienbork et al. 2004,Park, Kim et al. 2006,Kotanen and Guiseppi-

Elie 2013). Such biotransducers are critical for in vivo (intramuscular) wireless biosensor systems (Endo, Yonemori et al. 2009) that allow for immediate and continual pre-hospital and ICU monitoring of lactate and glucose to inform patient specific interventions that will improve survivability from trauma-associated or postoperative hemorrhage (Endo, Yonemori et al. 2009,Kotanen and Guiseppi-Elie 2013). Continued examination of interstitial compartments using biosensors will aid in understanding the temporal relationships among biomarkers of physiological stress in these environments and how they relate to hemorrhagic shock states (Uyehara and Sarkar 2013).

4 Conclusion

The relevant contributions in the development and modification of CNTs for use in biosensors and advanced biofuel cells have been highlighted in this review. The various processes used in the synthesis of CNTs (both smaller single-walled and larger multi-walled) affects materials properties (purity level, electrical, electrochemical) as well as other physicochemical properties relevant for bio-electrochemical devices. CNTs demonstrate ballistic electron transport which make them efficient electron transfer materials. The relationship between topological defects on CNTs and CNT electroactivity has also been established. This has led to the preparation of modified electrode surfaces, using CNTs and/or enzymes, where CNT-based electrochemical biosensors and their bioanalytical performance are influenced by the association between the CNT and the enzyme. The debundling and solubilization of CNTs may be achieved through conjugation with enzymes. Enzyme-CNT conjugates may be physicochemical, electrostatic or covalent. Methods of enzyme-CNT conjugation influences bio-electrochemical

performance. Such conjugates may be efficient biocatalysts that are unmatched in stability and power density when compared to conventional low-temperature oxidation-reduction catalysts of fuel cells.

There is also a need to develop next generation biosensors/biofuel cells that are capable of detecting multi-analytes using biotransducers on the order of microns. The use of direct electron transfer between oxidoreductases facilitated by carbon nanotubes in conjunction with a catalytic layer for improved signal transduction could be key.

Some issues to be addressed in this dissertation include:

- What role does the process of tip ultrasonication play in the formation of supramolecular conjugates?
- How do functionalization and tube lengths of single-walled carbon nanotubes affect conjugate formation and stability of the ensemble?
- What sort of key findings can be gleaned from molecular dynamics simulation of peptide sequences with high affinity for carbonaceous materials?
- What sort of biofabrication process will be used to make a dual responsive device for implantation in animals and eventually humans?

5 Acknowledgements

This work was supported by the US Department of Defense (DoDPRMRP) grant PR023081/DAMD17-03-1-0172, by the Consortium of the Clemson University Center for Bioelectronics, Biosensors and Biochips (C3B) and by ABTECH Scientific, Inc.

6 References (in EndNote-X5)

[1] C.N. Kotanen, F.G. Moussy, S. Carrara, A. Guiseppi-Elie, Biosensors and Bioelectronics, 35 (2012) 14-26.

[2] S. Carrara, S. Ghoreishizadeh, J. Olivo, I. Taurino, C. Baj-Rossi, A. Cavallini, M. Op de Beeck, C. Dehollain, W. Burleson, F.G. Moussy, A. Guiseppi-Elie, G. De Micheli, Sensors, 12 (2012) 11013-11060.

[3] A. Guiseppi-Elie, in: USPTO (Ed.), Anthony Guiseppi-Elie, USA, 2011.

[4] J. Wang, Chemical Reviews, 108 (2007) 814-825.

[5] J. Okuda-Shimazaki, N. Kakehi, T. Yamazaki, M. Tomiyama, K. Sode, Biotechnology Letters, 30 (2008) 1753-1758.

[6] M. Falk, Z. Blum, S. Shleev, Electrochimica Acta, 82 (2012) 191-202.

[7] S. Neto, J. Forti, A. De Andrade, Electrocatalysis, 1 (2010) 87-94.

[8] W. Jia, C. Jin, W. Xia, M. Muhler, W. Schuhmann, L. Stoica, Chemistry – A European Journal, 18 (2012) 2783-2786.

[9] S. Barton, J. Gallaway, P. Atanassov, Chem. Rev, 104 (2004) 4867-4886.

[10] G. Justin, Y. Zhang, M. Sun, R. Sclabassi, in, IEEE, 2005, pp. 4096-4099.

[11] S. Calabrese Barton, J. Gallaway, P. Atanassov, Chemical Reviews, 104 (2004) 4867-4886.

[12] H.-Y. Wang, A. Bernarda, C.-Y. Huang, D.-J. Lee, J.-S. Chang, Bioresource Technology, 102 (2011) 235-243.

[13] A. Guiseppi-Elie, C. Lei, R.H. Baughman, Nanotechnology, 13 (2002) 559.

[14] P.W. Barone, S. Baik, D.A. Heller, M.S. Strano, Nat Mater, 4 (2005) 86-92.

[15] A.A. Boghossian, J. Zhang, P.W. Barone, N.F. Reuel, J.H. Kim, D.A. Heller, J.H. Ahn, A.J. Hilmer, A. Rwei, J.R. Arkalgud, C.T. Zhang, M.S. Strano, ChemSusChem, 4 (2011) 848-863.

[16] J. Wang, Chemical Reviews, 108 (2008) 814-825.

[17] A. Guiseppi-Elie, A.R.A. Rahman, N.K. Shukla, Elctrochimica Acta, 55 (2010) 4247–4255.

[18] X. Wei, J. Liu, Front. Energy Power Eng. China, 2 (2008) 1-13.

[19] T. Dissanayake, D. Budgett, A.P. Hu, S. Malpas, L. Bennet, in: IFMBE Proceedings of the 2008 "13th International Conference on Biomedical Engineering", IFMBE, Singapore, 2008.

[20] M. De, P.S. Ghosh, V.M. Rotello, Advanced Materials, 20 (2008) 4225-4241.

[21] S. Rana, Y.C. Yeh, V.M. Rotello, Current Opinion in Chemical Biology, 14 (2010) 828-834.

[22] M.R. Gwinn, V. Vallyathan, Environmental Health Perspectives, 114 (2006) 1818.

[23] S. Iijima, Nature, 354 (1991) 56-58.

[24] Y. Ando, S. Iijima, JAPANESE JOURNAL OF APPLIED PHYSICS PART 2 LETTERS, 32 (1993) 107-107.

[25] T. Guo, P. Nikolaev, A. Thess, D. Colbert, R. Smalley, Chemical Physics Letters, 243 (1995) 49-54.

[26] M. Jose Yacaman, M. Miki Yoshida, L. Rendon, J. Santiesteban, Applied physics letters, 62 (1993) 202-204.

[27] M.J. Bronikowski, P.A. Willis, D.T. Colbert, K. Smith, R.E. Smalley, Journal of Vacuum Science & Technology A: Vacuum, Surfaces, and Films, 19 (2001) 1800.

[28] G.D. R. Saito, M. S. Dresselhaus, Physical Properties of Carbon Nanotubes, Imperial College Press, 1998.

[29] C.E. Baddour, C. Briens, International journal of chemical reactor engineering, 3 (2005) 3.

[30] A. Guiseppi-Elie, S. Brahim, A.M. Wilson, in: T. Skotheim, J.R. Reynolds (Eds.) Handbook of Conducting Polymers: Conjugated Polymer Processing and Applications, Taylor and Francis, New York, 2007, pp. 12:11 - 12:45.

[31] U.S.FDA, in: M. Devices (Ed.), U.S. Food and Drug Administration, 10903 New Hampshire Ave., Silver Spring, MD 20993, USA, 2006.

[32] U.S.FDA, in: M. Devices (Ed.), US Food and Drug Administration, 10903 New Hampshire Ave., Silver Spring, MD 20993, USA, 2007.

[33] A. Guiseppi-Elie, J Anal and Bioanal Chem, 339 (2010) 403-419.

[34] R. Kohen, A. Nyska, Toxicologic Pathology, 30 (2002) 620–650.

[35] M. Shichiri, Y. Yamasaki, R. Kawamori, N. Hakui, H. Abe, The Lancet, 320 (1982) 1129-1131.

[36] A.E.G. Cass, G. Davis, G.D. Francis, H.A.O. Hill, W.J. Aston, I.J. Higgins, E.V. Plotkin, L.D.L. Scott, A.P.F. Turner, Analytical chemistry, 56 (1984) 667-671.

[37] J.E. Frew, H.A.O. Hill, Analytical chemistry, 59 (1987) 933-944.

[38] P.I. Hilditch, M.J. Green, The Analyst, 116 (1991) 1217.

[39] D. Matthews, R. Holman, E. Bown, J. Steemson, A. Watson, S. Hughes, D. Scott, Lancet, 1 (1987) 778.

[40] R.W. Murray, A.G. Ewing, R.A. Durst, Analytical chemistry, 59 (1987) 379-390.

[41] Y. Degani, A. Heller, Journal of Physical Chemistry, 91 (1987) 1285-1289.

[42] T.J. Ohara, R. Rajagopalan, A. Heller, Analytical chemistry, 66 (1994) 2451-2457.

[43] I. Willner, V. Heleg-Shabtai, R. Blonder, E. Katz, G. Tao, A.F. Bückmann, A. Heller, Journal of the American Chemical Society, 118 (1996) 10321-10322.

[44] Y. Xiao, F. Patolsky, E. Katz, J.F. Hainfeld, I. Willner, Science, 299 (2003) 1877.

[45] P. Bartlett, S. Booth, D. Caruana, J. Kilburn, C. Santamaria, Analytical chemistry, 69 (1997) 734-742.

[46] G. Reach, G.S. Wilson, Analytical chemistry, 64 (1992) 381-386.

[47] D.S. Bindra, Y. Zhang, G.S. Wilson, R. Sternberg, D.R. Thevenot, D. Moatti, G. Reach, Analytical chemistry, 63 (1991) 1692-1696.

[48] E. Csöregi, D. Schmidtke, A. Heller, Wired" Glucose Oxidase," Anal. Chem, 67 (1995) 1240-1244.

[49] D.W. Schmidtke, A.C. Freeland, A. Heller, R.T. Bonnecaze, Proceedings of the National Academy of Sciences of the United States of America, 95 (1998) 294.

[50] U. Food, in, 2011.

[51] G.J. Tustin, V.G.H. Lafitte, C.E. Banks, T.G.J. Jones, R.B. Smith, J. Davis, N.S. Lawrence, Journal of Organometallic Chemistry, 692 (2007) 5173-5182.

[52] C.E. Banks, A.S. Yashina, G.J. Tustin, V.G.H. Lafitte, T.G.J. Jones, N.S. Lawrence, Electroanalysis, 19 (2007) 2518-2522.

[53] Z. Wang, H. Möhwald, C. Gao, Langmuir, 27 (2010) 1286-1291.

[54] A.L. Ghindilis, P. Atanasov, E. Wilkins, Electroanalysis, 9 (1997) 661-674.

[55] W.J. Albery, P.N. Bartlett, D.H. Craston, Journal of Electroanalytical Chemistry and Interfacial Electrochemistry, 194 (1985) 223-235.

[56] F. Palmisano, P.G. Zambonin, D. Centonze, M. Quinto, Analytical chemistry, 74 (2002) 5913-5918.

[57] N. Cenas, J. Kulys, Journal of Electroanalytical Chemistry and Interfacial Electrochemistry, 128 (1981) 103-113.

[58] S. Yabuki, H. Shinohara, M. Aizawa, J. Chem. Soc., Chem. Commun., (1989) 945-946.

[59] C.G.J. Koopal, B. de Ruiter, R.J.M. Nolte, J. Chem. Soc., Chem. Commun., (1991) 1691-1692.

[60] A. Guiseppi-Elie, in, Google Patents, 1994.

[61] A. Yahiro, S. Lee, D. Kimble, Biochimica et Biophysica Acta (BBA)-Specialized Section on Biophysical Subjects, 88 (1964) 375-383.

[62] S.A. Neto, J. Forti, A. De Andrade, Electrocatalysis, 1 (2010) 87-94.

[63] H. Sakai, T. Nakagawa, Y. Tokita, T. Hatazawa, T. Ikeda, S. Tsujimura, K. Kano, Energy & Environmental Science, 2 (2009) 133-138.

[64] D. Sokic-Lazic, S.D. Minteer, Biosensors and Bioelectronics, 24 (2008) 939-944.

[65] D. Sokic-Lazic, S.D. Minteer, Electrochemical and Solid-State Letters, 12 (2009) F26.

[66] S. Topcagic, S.D. Minteer, Electrochimica Acta, 51 (2006) 2168-2172.

[67] J. Forti, S. Aquino Neto, V. Zucolotto, P. Ciancaglini, A. de Andrade, Biosensors and Bioelectronics, (2010).

[68] T. Kuwahara, T. Homma, M. Kondo, M. Shimomura, Synthetic Metals, 159 (2009) 1859-1864.

[69] S. Lee, B. Choi, A. Tsutsumi, Biotechnology Letters, 31 (2009) 851-855.

[70] S. Lee, B. Choi, A. Tsutsumi, Journal of Chemical Engineering of Japan, 42 (2009) 596-599.

[71] X. Wu, F. Zhao, J.R. Varcoe, A.E. Thumser, C. Avignone-Rossa, R.C.T. Slade, Biosensors and Bioelectronics, 25 (2009) 326-331.

[72] J. Lim, P. Malati, F. Bonet, B. Dunn, Journal of the Electrochemical Society, 154 (2007) A140.

[73] T. Miyake, M. Oike, S. Yoshino, Y. Yatagawa, K. Haneda, H. Kaji, M. Nishizawa, Chemical Physics Letters, 480 (2009) 123-126.

[74] A. Habrioux, G. Merle, K. Servat, K. Kokoh, C. Innocent, M. Cretin, S. Tingry, Journal of Electroanalytical Chemistry, 622 (2008) 97-102.

[75] T.L. Klotzbach, M. Watt, Y. Ansari, S.D. Minteer, Journal of Membrane Science, 311 (2008) 81-88.

[76] A. Ramanavicius, A. Kausaite, A. Ramanaviciene, Biosensors and Bioelectronics, 24 (2008) 761-766.

[77] I. Willner, G. Arad, E. Katz, Bioelectrochemistry and Bioenergetics, 44 (1998) 209-214.

[78] J. Brockris, S. Srinivasan, Fuel cells: their electrochemistry, McGraw-Hill,New York, 1969.

[79] G. Govil, A. Saran, J Indian Chem Soc, 59 (1982) 1226-1228.

[80] W. Aston, A. Turner, Biotechnology & genetic engineering reviews, 1 (1984) 89-120.

[81] G. Palmore, G. Whitesides, Enzymatic conversion of biomass for fuels production, 566 (1994) 271–290.

[82] G.A. Rivas, M.D. Rubianes, M.C. Rodríguez, N.F. Ferreyra, G.L. Luque, M.L. Pedano, S.A. Miscoria, C. Parrado, Talanta, 74 (2007) 291-307.

[83] M. Dresselhaus, Y. Lin, O. Rabin, A. Jorio, A. Souza Filho, M. Pimenta, R. Saito, G. Samsonidze, G. Dresselhaus, Materials Science and Engineering: C, 23 (2003) 129-140.

[84] H. Hiura, T.W. Ebbesen, K. Tanigaki, Advanced Materials, 7 (1995) 275-276.

[85] P.J. Britto, K.S.V. Santhanam, A. Rubio, J.A. Alonso, P.M. Ajayan, Advanced Materials, 11 (1999) 154-157.

[86] C.E. Banks, R.G. Compton, Analyst, 131 (2005) 15-21.

[87] C.E. Banks, T.J. Davies, G.G. Wildgoose, R.G. Compton, Chemical communications, (2005) 829-841.

[88] C.E. Banks, R.G. Compton, Analyst, 130 (2005) 1232-1239.

[89] K. Balasubramanian, M. Burghard, Small, 1 (2005) 180-192.

[90] P. Ajayan, O. Zhou, Carbon Nanotubes, (2001) 391-425.

[91] A. Merkoçi, M. Pumera, X. Llopis, B. Pérez, M. del Valle, S. Alegret, TrAC Trends in Analytical Chemistry, 24 (2005) 826-838.

[92] A. Merkoçi, Microchimica Acta, 152 (2006) 157-174.

[93] J.J. Gooding, Electrochimica Acta, 50 (2005) 3049-3060.

[94] J. Wang, Electroanalysis, 17 (2005) 7-14.

[95] M. Jiang, Y. Lin, in: Encyclopedia of Sensors, Pacific Northwest National Laboratory (PNNL), Richland, WA (US), Environmental Molecular Sciences Laboratory (EMSL), 2006, pp. 25-51.

[96] E. Katz, I. Willner, ChemPhysChem, 5 (2004) 1084-1104.

[97] M. Valcarcel, B.M. Simonet, S. Cardenas, B. Suarez, Analytical and bioanalytical chemistry, 382 (2005) 1783-1790.

[98] C.E. Banks, A. Crossley, C. Salter, S.J. Wilkins, R.G. Compton, Angewandte Chemie International Edition, 45 (2006) 2533-2537.

[99] A. Guiseppi-Elie, S. Brahim, G. Wnek, R. Baughman, NanoBioTechnology, 1 (2005) 83-92.

[100] F. Tasca, W. Harreither, R. Ludwig, J.J. Gooding, L. Gorton, Analytical chemistry, 83 (2011) 3042-3049.

[101] J.J. Gooding, R. Wibowo, J. Liu, W. Yang, D. Losic, S. Orbons, F.J. Mearns, J.G. Shapter, D.B. Hibbert, J Am Chem Soc, 125 (2003) 9006-9007.

[102] S.J. Tans, M.H. Devoret, H. Dai, A. Thess, R.E. Smalley, L. Geerligs, C. Dekker, Nature, 386 (1997) 474-477.

[103] C. Yu, Y. Ryu, L. Yin, H. Yang, ACS Nano, 5 (2011) 1297-1303.

[104] R. Jansen, P. Wallis, Material Matters, 4 (2009) 23-27.

[105] C.H. Olk, J.P. Heremans, Journal of materials research, 9 (1994) 259-262.

[106] J.W.G. Wildoer, L.C. Venema, A.G. Rinzler, R.E. Smalley, C. Dekker, Nature, 391 (1998) 59-62.

[107] M. Ouyang, J.-L. Huang, C.L. Cheung, C.M. Lieber, Science, 292 (2001) 702-705.

[108] Y. Matsuda, J. Tahir-Kheli, W.A. Goddard III, Journal of Physical Chemistry Letters, 1 (2010) 2946-2950.

[109] J.L. Bahr, J.M. Tour, Chemistry of Materials, 13 (2001) 3823-3824.

[110] J. Chen, M.A. Hamon, H. Hu, Y. Chen, A.M. Rao, P.C. Eklund, R.C. Haddon, Science, 282 (1998) 95-98.

[111] D. Tasis, N. Tagmatarchis, V. Georgakilas, M. Prato, Chemistry – A European Journal, 9 (2003) 4000-4008.

[112] M. Islam, E. Rojas, D. Bergey, A. Johnson, A. Yodh, Nano letters, 3 (2003) 269-273.

[113] A. Star, J.F. Stoddart, D. Steuerman, M. Diehl, A. Boukai, E.W. Wong, X. Yang, S.-W. Chung, H. Choi, J.R. Heath, Angewandte Chemie International Edition, 40 (2001) 1721-1725.

[114] M.J. O'Connell, P. Boul, L.M. Ericson, C. Huffman, Y. Wang, E. Haroz, C. Kuper, J. Tour, K.D. Ausman, R.E. Smalley, Chemical Physics Letters, 342 (2001) 265-271.

[115] S. Ramesh, L.M. Ericson, V.A. Davis, R.K. Saini, C. Kittrell, M. Pasquali, W. Billups, W.W. Adams, R.H. Hauge, R.E. Smalley, The Journal of Physical Chemistry B, 108 (2004) 8794-8798.

[116] C. Wang, S. Guo, X. Pan, W. Chen, X. Bao, Journal of Materials Chemistry, 18 (2008) 5782-5786.

[117] A. Hirsch, O. Vostrowsky, Functional molecular nanostructures, (2005) 193-237.

[118] O.K. Kim, J. Je, J.W. Baldwin, S. Kooi, P.E. Pehrsson, L.J. Buckley, Journal of the American Chemical Society, 125 (2003) 4426-4427.

[119] J.H.T. Luong, S. Hrapovic, D. Wang, F. Bensebaa, B. Simard, Electroanalysis, 16 (2004) 132-139.

[120] A. Guiseppi-Elie, S.-H. Choi, K. Geckeler, B. Sivaraman, R. Latour, NanoBioTechnology, 4 (2008) 9-17.

[121] A. Bianco, K. Kostarelos, M. Prato, Current Opinion in Chemical Biology, 9 (2005) 674-679.

[122] J. Meng, J. Duan, H. Kong, L. Li, C. Wang, S. Xie, S. Chen, N. Gu, H. Xu, X.-D. Yang, Small, 4 (2008) 1364-1370.

[123] R.P. Feazell, N. Nakayama-Ratchford, H. Dai, S.J. Lippard, Journal of the American Chemical Society, 129 (2007) 8438-8439.

[124] D. Nepal, K.E. Geckeler, Small, 2 (2006) 406-412.

[125] R.A. Graff, J.P. Swanson, P.W. Barone, S. Baik, D.A. Heller, M.S. Strano, Advanced Materials, 17 (2005) 980-984.

[126] N.R. Palwai, D.E. Martyn, L.F.F. Neves, Y. Tan, D.E. Resasco, R.G. Harrison, Nanotechnology, 18 (2007) 235601.

[127] Y. Wang, J. Du, Y. Li, D. Shan, X. Zhou, Z. Xue, X. Lu, Colloids and Surfaces B: Biointerfaces, 90 (2012) 62-67.

[128] Q. Wang, L. Zhou, Y. Jiang, J. Gao, Enzyme and Microbial Technology, 49 (2011) 11-16.

[129] S. Shah, K. Solanki, M.N. Gupta, Chem Cent J, 1 (2007) 30.

[130] S.L. Peshkovsky, A.S. Peshkovsky, Ultrasonics Sonochemistry, 14 (2007) 314-322.

[131] A. Guiseppi-Elie, S.-H. Choi, K.E. Geckeler, Journal of Molecular Catalysis B: Enzymatic, 58 (2009) 118-123.

[132] R.B. Rakhi, K. Sethupathi, S. Ramaprabhu, The Journal of Physical Chemistry B, 113 (2009) 3190-3194.

[133] Y. Wang, W. Wei, X. Liu, X. Zeng, Materials Science and Engineering: C, 29 (2009) 50-54.

[134] J. Wang, M. Musameh, Analytica Chimica Acta, 539 (2005) 209-213.

[135] A. Minett, N. Carolan, D. Leane, R. O'Kennedy, G. Wallace, in: Iconn, Brisbane, Qld, Australia, 2006, pp. 290-293.

[136] J. Li, Y.B. Wang, J.D. Qiu, D. Sun, X.H. Xia, Analytical and bioanalytical chemistry, 383 (2005) 918-922.

[137] D.T. Mitchell, S.B. Lee, L. Trofin, N. Li, T.K. Nevanen, H. Söderlund, C.R. Martin, Journal of the American Chemical Society, 124 (2002) 11864-11865.

[138] R.C. Pangule, S.J. Brooks, C.Z. Dinu, S.S. Bale, S.L. Salmon, G. Zhu, D.W. Metzger, R.S. Kane, J.S. Dordick, ACS Nano, 4 (2010) 3993-4000.

[139] C.Z. Dinu, G. Zhu, S.S. Bale, G. Anand, P.J. Reeder, K. Sanford, G. Whited, R.S. Kane, J.S. Dordick, Advanced Functional Materials, 20 (2010) 392-398.

[140] K. Fu, W. Huang, Y. Lin, D. Zhang, T.W. Hanks, A.M. Rao, Y.-P. Suna, Journal of Nanoscience and Nanotechnology, 2 (2002) 457-461.

[141] N.W. Shi Kam, T.C. Jessop, P.A. Wender, H. Dai, Journal of the American Chemical Society, 126 (2004) 6850-6851.

[142] M. O'Connor, S. Kim, A. Killard, R. Forster, M. Smyth, F. Papadimitrakopoulos, J. Rusling, The Analyst, 129 (2004) 1176-1180.

[143] M. Shim, N.W. Shi Kam, R.J. Chen, Y. Li, H. Dai, Nano letters, 2 (2002) 285-288.

[144] S.E. Baker, W. Cai, T.L. Lasseter, K.P. Weidkamp, R.J. Hamers, Nano letters, 2 (2002) 1413-1417.

[145] Y. Gao, I. Kyratzis, Bioconjugate Chemistry, 19 (2008) 1945-1950.

[146] J.T. Cang-Rong, G. Pastorin, Nanotechnology, 20 (2009) 255102.

[147] M. Ghosh, S. Maiti, S. Dutta, D. Das, P.K. Das, Langmuir, 28 (2012) 1715-1724.

[148] V.A. Karachevtsev, S.G. Stepanian, A.Y. Glamazda, M.V. Karachevtsev, V.V. Eremenko, O.S. Lytvyn, L. Adamowicz, The Journal of Physical Chemistry C, 115 (2011) 21072-21082.

[149] C. Mateo, J.M. Palomo, G. Fernandez-Lorente, J.M. Guisan, R. Fernandez-Lafuente, Enzyme and Microbial Technology, 40 (2007) 1451-1463.

[150] B.M. Brena, F. Batista-Viera, Immobilization of enzymes and cells, 22 (2006) 15.

[151] J.D. Qiu, J. Guo, R.P. Liang, M. Xiong, Electroanalysis, 19 (2007) 2335-2341.

[152] C. Bourdillon, J. Bourgeois, D. Thomas, Journal of the American Chemical Society, 102 (1980) 4231-4235.

[153] M. Pellissier, F. Barrière, A.J. Downard, D. Leech, Electrochemistry Communications, 10 (2008) 835-838.

[154] A. Guiseppi-Elie, A.R.A. Rahman, N.K. Shukla, Electrochimica Acta, 55 (2010) 4247-4255.

[155] K.S. Galhardo, R.M. Torresi, S.I. Torresi, Electrochimica Acta, (2011).

[156] M. Smolander, H. Boer, M. Valkiainen, R. Roozeman, M. Bergelin, J.E. Eriksson, X.C. Zhang, A. Koivula, L. Viikari, Enzyme and Microbial Technology, 43 (2008) 93-102.

[157] D. MacAodha, M.L. Ferrer, P.Ó. Conghaile, P. Kavanagh, D. Leech, Physical Chemistry Chemical Physics, (2012).

[158] M. Fischback, K.Y. Kwon, I. Lee, S.J. Shin, H.G. Park, B.C. Kim, Y. Kwon, H.T. Jung, J. Kim, S. Ha, Biotechnology and Bioengineering, 109 (2011) 318-324.

[159] T.J. Ohara, R. Rajagopalan, A. Heller, Analytical chemistry, 65 (1993) 3512-3517.

[160] Q. Gao, Y. Guo, W. Zhang, H. Qi, C. Zhang, Sensors and Actuators B: Chemical, (2010).

[161] Q. Gao, Y. Guo, J. Liu, X. Yuan, H. Qi, C. Zhang, Bioelectrochemistry, 81 (2011) 109-113.

[162] M.V. Jose, S. Marx, H. Murata, R.R. Koepsel, A.J. Russell, Carbon, (2012).

[163] J. Kolosnjaj, H. Szwarc, F. Moussa, Bio-Applications of Nanoparticles, (2007) 181-204.

[164] D. Cui, F. Tian, C.S. Ozkan, M. Wang, H. Gao, Toxicology Letters, 155 (2005) 73-85.

[165] C.M. Sayes, F. Liang, J.L. Hudson, J. Mendez, W. Guo, J.M. Beach, V.C. Moore, C.D. Doyle, J.L. West, W.E. Billups, K.D. Ausman, V.L. Colvin, Toxicology Letters, 161 (2006) 135-142.

[166] C. Salvador-Morales, P. Townsend, E. Flahaut, C. Vénien-Bryan, A. Vlandas, M.L.H. Green, R.B. Sim, Carbon, 45 (2007) 607-617.

CHAPTER TWO

SUPRAMOLECULAR GLUCOSE OXIDASE-SWNT CONJUGATES FORMED BY ULTRASONICATION: EFFECT OF TUBE LENGTH, FUNCTIONALIZATION AND PROCESSING TIME

2.1 Abstract

2.1.1 Background

Generation-3 (Gen-3) biosensors and advanced enzyme biofuel cells will benefit from direct electron transfer to oxidoreductases facilitated by single-walled carbon nanotubes (SWNTs). Supramolecular conjugates of SWNT-glucose oxidase (GOx-SWNT) may be produced via ultrasonic processing. Using a Plackett-Burman experimental design to investigate the process of tip ultrasonication (23 kHz), conjugate formation was investigated as a function of ultrasonication times (0, 5, 60 min) and functionalized SWNTs of various tube lengths (SWNT-X-L), (X = -OH or -COOH and L = 3.0 μm, 7.5 μm).

2.1.2 Results

Enzyme activity (K_M, k_{cat}, k_{cat}/K_M, v_{max} and n (the Hill parameter)) of pGOx (pristine), sGOx (sonicated) and GOx-SWNT-X-L revealed that sonication of any duration increased both K_M and k_{cat} of GOx but did not change k_{cat}/K_M. Functionalized tubes had the most dramatic effect, reducing both K_M and k_{cat} and reducing k_{cat}/K_M. UV-Vis spectra over the range of 300 to 550 nm of native enzyme-bound FAD (λ_{max} at 381 and 452 nm) or the

blue-shifted solvated FAD of the denatured enzyme (λ_{max} at 377 and 448 nm) revealed that ultrasonication up to 60 minutes had no influence on spectral characteristics of FAD but that the longer SWNTs caused some partial denaturation leading to egress of FAD. Circular dichroism spectral analysis of the 2° structure showed that sonication of any duration caused enrichment in the α-helical content at the sacrifice of the unordered sequences in GOx while the presence of SWNTs, regardless of length and/or functionality, reduced the β-sheet content of pristine GOx. Surface profiling by white light interferometry revealed that ultrasonciction produced some aggregation of GOx and that GOx effectively debundled the SWNT.

2.1.3 Conclusions

Supramolecular conjugates formed from shorter, -OH functionalized SWNTs using longer sonication times (60 min) gave the most favored combination for forming bioactive conjugates.

Keywords: supra-molecular conjugates, SWNT, ultrasonic processing, glucose oxidase, biosensors, biofuel cells

2.2.Introduction

There is pressing need for the design, development and understanding of bio-abio interfaces that permit direct electron transfer of redox enzymes with metallic, carbonaceous or semiconductor electrodes permitting the development of generation-3 (Gen-3) biosensors (Kotanen, Moussy, Carrara and Guiseppi-Elie 2012) and advanced biofuel cells

(Neto, Forti and De Andrade 2010). Such biosensors will enable fully implantable continual monitoring of various analytes that serve as markers of a wide variety of physiological conditions and pathologies. Among these are glucose in diabetics (Klonoff 2005) and glucose, lactate and succinate in victims of trauma associated hemorrhage (Guiseppi-Elie 2011). Design and development of Gen-3 biosensors that are reagentless, have long term *in vivo* stability, and require no calibration continues to be a major challenge and opportunity in biomedical diagnostics (Wang 2007; Okuda-Shimazaki, Kakehi, Yamazaki, Tomiyama and Sode 2008; Falk, Blum and Shleev 2012). There is similarly a pressing need for the development of implantable (Calabrese Barton, Gallaway and Atanassov 2004; Wang, Bernarda, Huang, Lee and Chang 2011) biofuel cells that could trickle charge battery powered biomedical devices or to serve as the primary source of power in implantable bioelectronics (Falk, Andoralov, Blum, Sotres, Suyatin, Ruzgas, Arnebrant and Shleev 2012; Jia, Jin, Xia, Muhler, Schuhmann and Stoica 2012). The biofuel cell (Davis and Higson 2007), which will power the biosensor, can be designed to make use of fuel sources present within the body (Barton, Gallaway and Atanassov 2004; Justin, Zhang, Sun and Sclabassi 2005). Both types of biotransduction devices depend upon the design, fabrication and engineering control of biomolecule-to-solid state (bio-abio) interfaces for stable biomolecular recognition (Rubenwolf, Kerzenmacher, Zengerle and von Stetten 2011) and efficient electron transfer (Kannan, Renugopalakrishnan, Filipek, Li, Audette and Munukutla 2008; Kotanen, Moussy, Carrara and Guiseppi-Elie 2012).

Several methods have been proposed over the years to address the foregoing challenge. Among these are generation-1 (Gen-1) biotransducer devices that

electrochemically monitor the reactants or products of an enzyme catalyzed reaction, generaton-2 (Gen-2) devices benefit from the use of a free or tethered redox mediators that intercede between charge generation and discharge at an electrode, and Gen-3 biotransducers that allow direct electron transfer across the bio-abio interface (Wang 2007; Min, Ryu and Yoo 2010). Generation-3 biosensors have been achieved by the use of electrical "wiring" using conductive electroactive polymers (CEPs) (Guiseppi-Elie 1998) or the identification of enzymes that facilitate this at nano-structured surfaces (Liu, Tian and Xia 2008). Among the recent novel approaches for establishing an efficient biotransduction mechanism is the use of single walled carbon nanotubes (SWNT)-enzyme conjugates. Guiseppi-Elie et al., in a series of papers (Brahim, Shukla and Guiseppi-Elie 2006), were the first to demonstrate direct electron transfer between flavin adenine dinucleotide (FAD) containing glucose oxidase (GOx) (Guiseppi-Elie, Lei and Baughman 2002) and copper containing pseudoazurin (Guiseppi-Elie, Brahim, Wnek and Baughman 2005) at glassy carbon electrodes that was enabled by SWNT-enzyme conjugates formed by adsorption. These exciting results have since generated an avalanche of publications that have ushered in a new vista of study (Karunwi and Guiseppi-Elie 2012). SWNTs possessing high mechanical properties (tensile strength ~30 GPa, Young Modulus ~1 TPa) and good electrical properties (resistivity of $10^{-4}\Omega$m, maximum current density of 10^{13} A/m^2) and FAD-containing GOx (β-D-glucose:oxygen 1-oxidoreductase; EC. 1.1.3.4) are suitable model candidates for conjugation and study in the context of Gen-3 biosensors and advanced biofuel cells.

Bioconjugates of GOx-SWNT may be enabled by simple mixing with the supramolecular association being driven by the entropy of mixing and facilitated by the interaction between hydrophobic motifs of the enzyme and the extended pi-structure of the CNTs (Cang-Rong and Pastorin 2009). However, this is a slow and inefficient process. Guiseppi-Elie et al. have recently reviewed the ever broadening motivations and approaches to forming physical and covalent conjugates between enzymes and SWNTs (Karunwi and Guiseppi-Elie 2012) and have shown that ultrasonic processing (Guiseppi-Elie, Choi and Geckeler 2009), the use of cavitation energy, while representing some modest compromise of enzyme activity, may prove a viable route to facilitate rapid and reproducible conjugation of GOx-SWNT suitable for biosensor and biofuel cell applications (Guiseppi-Elie, Choi, Geckeler, Sivaraman and Latour 2008). Here we expand this work and present detailed investigation of the use of tip ultrasonication (23 kHz) for various sonication times (0, 5 min, 60 min) in the presence of SWNTs of different functionalities (X = -OH or -COOH) and of different tube lengths (L = 3.0 μm, 7.5 μm) (SWNT-X-L), on the activity, stability and structure of GOx component of the conjugate. The activity of the enzyme was monitored by HRP-coupled colorimetric bioassay, UV-Vis spectroscopy has been used to monitor the association of the FAD with its apoenzyme, circular dichroism (CD) and white light *interferometric i*maging have been used to monitor changes in the secondary structure of the enzyme within the GOx-SWNT conjugate.

2.3 Experimental methods

2.3.1 Materials and reagents

SWNTs (purity, 95 wt. %) were purchased from Bucky USA (Houston, TX, USA) and were used as received. These tubes were un-functionalized and un-sorted by length and were referred to as Bucky tubes or simply Bucky in this manuscript. Functionalized SWNTs possessing –OH and –COOH groups with two different tube lengths (3.0 μm, 7.5 μm) were purchased from NanoLab, Inc. (Waltham, MA, USA) and used as received. In summary, SWNTs-OH and SWNTs-COOH of different lengths (~3.0 μm and ~7.5 μm) were first produced using chemical vapor deposition (CVD) of a carbon-carrying feedstock [methane (CH_3)] delivered at a controlled rate over a catalyst bed of iron nanoparticles deposited on a fumed silica support at 700 °C. SWNTs were subsequently purified in HF/HCl and the resulting product rinsed in deionized water until pH neutral, then drained and annealed. SWNTs were produced with high purity and with little or no amorphous carbon through careful control of the catalyst size, process time, temperature, and pressure [38]. SWCNTs were produced at 1−1.5 nm in diameter with ~7.5 μm of length and subsequently ball milled to produce the shorter version (~ 3.0 μm) so that the chemical composition of the two different lengths would be the same. Energy-dispersive X-ray spectroscopic analysis (SEM-EDX) provided by the manufacturer confirmed that the SWCNTs contained 95.93 wt% carbon and 4.07wt% of other elements (including Na, Al, Si, S, and Fe). End and sidewall -COOH functionalization (1.0-7.0 atom%) was achieved by the use of 1:3 HNO_3:H_2SO_4, 8M acid under refluxing conditions (~80 °C, 4 hours). For end and sidewall -OH functionalization (1.0–7.0 atom%), the carboxylated nanotubes are

returned to the reflux apparatus but this time in a KOH solution. FTIR and Raman spectroscopies for these samples are included in the Supporting Materials section.

Glucose oxidase (EC 1.1.3.4 from *Aspergillus niger*, G7141-250KU, type X-S, 146,000 units/g solid; lyophilized powder containing approximately 75% protein) was purchased from Sigma Aldrich (St. Louis, MO, USA) and used as received. For the high-speed centrifugation of the GOx-SWNT suspension after ultrasonication, ultracentrifuge tubes (OakRidge Bottle, polycarbonate 16 X 83 mm and polypropylene sealing caps) were purchased from Fisher Scientific (Pittsburg, PA, USA). Horseradish peroxidase (HRP) (EC 1.11.1.7, P-8250-50KU, type II, 60 purpurogallin units/mg solid), sodium acetate buffer 2,2'-azino-bis(3-ethylbenzothiazoline-6-sulphonic acid) (ABTS) and β-D(+)-glucose substrate solution were purchased from Sigma (St. Louis, MO, USA). The 96-well plates for the enzymatic bioassays were purchased from Falcon (BD Biosciences, Franklin Lakes, NJ USA) and DI water was generated by a Milli-Q® Ultrapure Water Purification System.

2.3.2 Preparation of the GOx-SWNT conjugate dispersions:

Aqueous suspensions of appropriate weights of functionalized SWNTs of various lengths (SWNT-X-L where X = –OH or –COOH groups and L = 3.0 μm 7.5 μm) (5 mg) and GOx (5 mg) were prepared in 5.0 mL of DI water (1 mg/ml each component). Suspensions were prepared by ultrasonication at 4ºC within a jacketed water bath using a Soniprep 150 (MSE, UK) equipped with an MSE exponential probe (tip diameter 3 mm, transformation ratio 7:1) ultratip sonicator (frequency 23 kHz) at two different time intervals, 5 min and 60 min (0 min (control)). The GOX-SWNT conjugates were collected

from the supernatant following high-speed centrifugation (33,000 x g for 4 h at 4°C) using a high-speed Sorval Evolution RC Centrifuge (Thermo Scientific, IL, USA) equipped with a SS-34 rotor (Guiseppi-Elie, Choi, Geckeler, Sivaraman and Latour 2008). Following centrifugation, all samples were collected and stored in the refrigerator at 4°C. **Scheme 1** illustrates and summarizes this procedure. TEMs images of SWCNT-GOx conjugates prepared by this method have been previously published (Guiseppi-Elie, Choi, Geckeler, Sivaraman and Latour 2008).

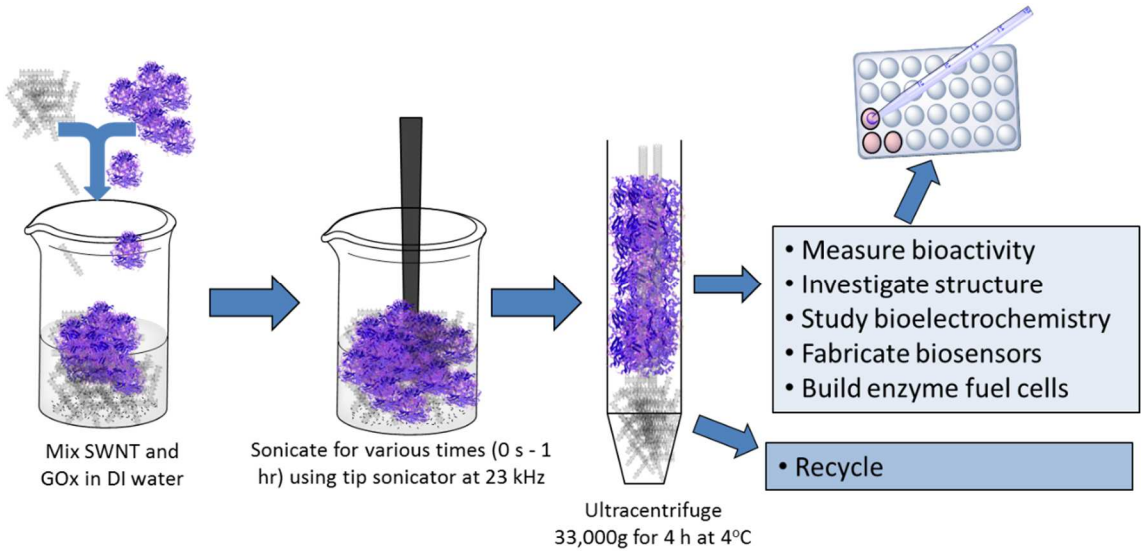

Scheme 1. Supra-molecular complex formation via ultrasonic processing and ultracentrifugation

2.3.3 Enzyme assays

All samples containing GOx were subjected to the standard HRP-coupled enzymatic assay (Bergmeyer, Gawehn and Grassl 1974) protocol recommended by Sigma Aldrich. This assay is a coupled enzyme assay wherein the enzyme catalyzed reaction is

linked to the decomposition of hydrogen peroxide with horseradish peroxidase (HRP) and the oxidation of the chromogenic reagent, 2,2'-azino-bis(3-ethylbenzothiazoline-6-sulphonic acid) (ABTS). ABTS was used in place of *o*-dianisidine for more stable results. **Scheme 2** shows the three step process for generating the colorimetric glucose dose response.

Step I

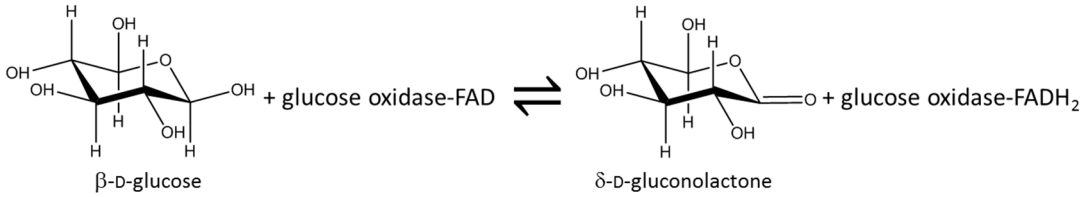

Step II

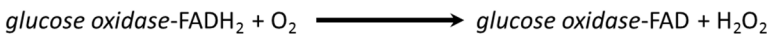

Step III

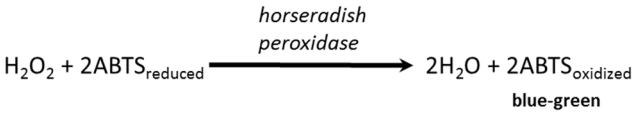

Scheme 2. Assay of glucose oxidase activity via an HRP-linked colorimetric response using ABTS.

The following reagents were prepared and used for the enzymatic assay experiments: A, 48 mM sodium acetate buffer, pH 5.1 (adjusted with 1 M HCl) at 37ºC which contained 0.1 mg/ml of sodium azide; B, 0.16 mM ABTS in reagent A; C, varying

concentrations of mutarotated β-D (+) glucose substrate in DI water; D, reaction cocktail consisting of reagent B and C (24:5 v/v), equilibrated to 37°C and adjusted to pH 5.1 with 1 M HCl or 1 M NaOH; E, HRP solution containing 60 purpurogallin units/ml in DI water; F sample of interest (pristine GOx, GOx-SWNT conjugate, etc). The reactions were carried out by mixing 91.9 µl of freshly prepared D and 68.1 µl of E (contains 6 units HRP) in a 96-well plate. The mixture was equilibrated at 37°C in the plate reader and the absorbance at 405 nm monitored for about 10 minutes until it was constant. Finally, 40 µl of F (contains 0.004 mg solid/ml GOx) was added and the increase in absorbance at 405 nm was monitored every 10 s for about 5 min. Using the maximum/initial linear rate yielded the change in absorbance per minute which was converted to units of enzyme activity (µmol/min) using an extinction coefficient of 36.8 $mM^{-1}cm^{-1}$ at 405 nm (Re, Pellegrini, Proteggente, Pannala, Yang and Rice-Evans 1999). One enzyme unit is defined as the amount of enzyme required to oxidize 1 µmol of β-D glucose per minute at 37°C. The initial rate data was used to determine the enzyme kinetic parameters (v_{max}, K_M, n, k_{cat}, and k_{cat}/K_M) through nonlinear curve fitting of the Hill function (Equation 1), and where appropriate, the Lineweaver-Burk plot in conjunction with the Michaelis-Menten equation.

$$v = v_{max}\left(\frac{{C_S}^n}{{K_M}^n + {C_S}^n}\right) \quad (1)$$

Statistical analysis of triplicate data via t-test statistic was used to establish a *p*-value.

2.3.4 UV/Vis spectroscopy

UV-Vis spectroscopy was performed using a Synergy Mx Monochromator-based Multi-mode Microplate Reader running Gen5 software. For this, 200 µl of each of the ultrasonicated aqueous GOx-SWNT conjugate solution and control samples (pristine GOx, sonicated GOx without SWNT) was placed in a 96-well plate and the UV/Vis absorption spectra recorded over the wavelength range 230 – 900 nm. The range 300 – 500 nm was specifically isolated and analyzed for its relevance to FAD-apoenzyme association (O'Malley and Weaver 1972; Shin, Youn, Han, Kang and Hah 1993). Since many buffers and common buffer additives have a strong absorbance in the far UV region, the aqueous GOx-SWNT and control sample solutions were prepared buffer free.

2.3.5 Circular dichroism spectroscopy

The Circular Dichroism (CD) (Kelly, Jess and Price 2005) measurements were performed at 25^{o}C in a 1.0 cm quartz cuvette (Stama Cells, Atascadero, CA, USA) over the wavelength range 190-300 nm on a Jasco J-810 spectropolarimeter (Jasco, Easton, MD, USA) fitted with a xenon lamp. Each scan was the average of six accumulations using a scan rate of 2 nm/min and 0.1 nm resolution. The CD spectra for 0.005 mg/mL concentration of GOx solution and those of the various GOx-SWNT-X-L conjugates were obtained in nanopure water. These spectra were then deconvoluted using the CDPro software package and the secondary structural components for the native protein and the nanotube-protein conjugates were determined using the CONTINLL-4, CONTINLL-7 (Provencher and Gloeckner 1981), CDSSTR-4, CDSSTR-7 (Johnson 1999) computer

program. Data cut was applied to the CD spectra (data pitch: 0.1 nm) as well as smoothing to the final curves. A mean residue weight of 110 Da was used for GOx while calculating the molar ellipticity $[\theta]_{MRW}$ (in deg cm^2/dmol).

2.3.6 Surface profile imaging

An automated Contour GT-K1 Optical Profiler (Bruker Nano Surfaces Division, USA) was used to provide high resolution 3D surface images and obtain surface roughness using white light interferometric technology (Schmit 2005). Composites were prepared on 1.0 cm x 2.0 cm x 0.05 cm platinum planar metal electrodes (PME 118-Pt; ABTECH Scientific Inc., Richmond, VA, USA) and imaged under dry conditions. The samples imaged include: i) Blank PME 118-Pt, ii) Physically adsorbed GOx (20 μL of 1 mg/mL) on PME 118-Pt, iii) Physically adsorbed GOx-SWNT (20 μL of 1 mg/mL) on PME 118-Pt, iv) Physically adsorbed sonicated (60 min) GOx (20 μL of 1 mg/mL) on PME 118-Pt, and v) Physically adsorbed SWNT (20 μL of 1 mg/mL) on PME 118-Pt.

2.4 Results and discussion

Ultrasonication at 23 kHz has been known to cause an increase in temperature (up to ~35ºC) within 5 minutes and prolonged sonication can increase the temperature of aqueous solutions up to more than 60ºC (Raso, Mañas, Pagán and Sala 1999). To eliminate the possible confounding effects of thermal denaturation, all samples were ultrasonicated at ice bath temperatures. **Scheme 1** summarizes the several steps in GOx-SWNT supra-molecular complex formation via ultrasonic processing and ultracentrifugation. Ultrasonication, a process of using cavitation energy to achieve rapid mixing (RSC 2012),

is well known to accelerate enzyme-catalyzed reactions but it also induces enzyme inactivation through a potentiation of structure and activity of native enzymes (Özbek and Ülgen 2000; Shah and Gupta 2008). The challenge in the design of biomaterials for molecular bioelectronics is to engineer such conjugates with a minimum loss of biofunctionality while conferring some strategic technical advantage; in this case, form the GOx-SWNT supra-molecular conjugate with a minimum loss of bioactivity.

The investigation of the influence of tube length, tube functionalization and ultrasonicaton time on enzyme kinetic parameters, FAD-apoenzyme stability, and protein structure, is amenable to a Plackett-Burman design of experiment approach to identify optimum conditions for further investigation (Haaland 1989).

Table 1. Plackett-Burman design of experiments (Minitab16) to identify optimal conditions for the ultrasonic processing of GOx-SWNT supra-molecular conjugates.

Input Parameters	**High (+)**	**Low (-)**
Ultrasonication Time	60 minutes	5 minutes
Tube functionality	-OH	-COOH
SWNT length	~7.5 microns (long)	~3 microns (short)

Output Parameters	
Enzyme activity	K_M, k_{cat} and k_{cat}/K_M
Enzyme stability	FAD absorption, λ_{max}

Enzyme structure	Sum of α-helix and β-sheet

Table 1 shows the parameter space that was defined by low (-) and high (+) input parameter values. Here ultrasonication time (Low = 5 min and High = 60 min), tube functionalization (Low = –OH and High = –COOH) and tube length (Low = 3.0 μm and High = 7.5 μm). The three output variables studied were; i) the K_M, k_{cat} and k_{cat}/K_M of the enzyme conjugate all expressed relative to the pristine GOx as measured under the same conditions, ii) the extent of the blue shift (λ_{max}) in the absorbance maximum of the FAD-apoenzyme at 381 and 452 nm, and iii) the sum of α-helix and β-sheet in the CD spectra.

2.4.1 Assays of enzymatic activity

In order to investigate the effect of ultrasonication on enzyme activity, enzyme activity assays of pristine GOx, sonicated GOx and the various GOx-SWNT-X-L conjugates were determined using the colorimetric GOx-HRP coupled enzymatic assay method. Because enzyme function and fidelity of the active site are strongly connected to the overall structure of the enzyme, these experiments were critical in rationalizing the retained biological activity following ultrasonication as well as after supramolecular conjugate formation by ultrasonication. The enzyme kinetic parameters were determined using varying concentrations of β-D(+) glucose at constant pGOx, sGOx and GOx-SWNT-X-L concentrations and by using both the Lineweaver-Burke and Hill plot methods for comparative purposes. **Figure 1A** shows a typical plot of the enzyme kinetic data, **Figure 1B** shows a typical the Lineweaver-Burk plot, and **Figure 1C** shows the aggregate

relationship between K_M, k_{cat}, k_{cat}/K_M for pristine GOx, sonicated GOx (5 and 60 min) and selected GOx-SWNT-X-L conjugates. **Table 2** presents and compares K_M, k_{cat}, k_{cat}/K_M (the specificity constant; a reflection of the efficiency of the enzyme), v_{max} and n (the Hill parameter) for pristine GOx from this work and various literature sources, sonicated GOx and the various sGOx-SWNT-X-L conjugates.

Table 2. Presents and compares v_{max}, K_M, k_{cat}, k_{cat}/K_M (a reflection of the efficiency of the enzyme) and *n* (the hill parameter) for pristine GOx, sonicated GOx and the various GOx-SWNT-X-L conjugates. (Error bars ± 95% confidence interval)

	v_{max} (mM/s)	**K_M (mM)**	**k_{cat} (/s)**	**k_{cat}/K_M (/mM·s)**	**n**
Pristine GOx	0.00344±0.0008	9.01±4.1	17.1±2.7	2.06±0.68	1.86±0.08
Sonicated GOx-5min	0.00916±0.0010	26.5±7.8	48.7±6.1	1.89±0.35	1.37±0.10
Sonicated GOx-60min	0.00888±0.0009	27.0±1.6	44.8±4.9	1.66±0.082	1.46±0.10
GOx-COOH-medium-5min	0.00351±0.0009	15.5±1.7	17.7±5.3	1.13±0.22	1.14±0.13
GOx-COOH-medium-60min	0.00190±0.0008	6.82±1.9	8.86±4.8	1.25±0.40	1.82±0.17

GOx-OH-medium-60min	0.00115±0.0008	3.11±1.8	5.97±4.8	1.74±0.62	1.57±0.05
GOx-OH-Long-60min	0.00140±0.0008	3.76±2.0	7.01±4.7	1.77±0.34	2.93±0.06
GOx-Bucky-60min	0.00322±0.0009	11.0±5.7	16.1±4.6	1.64±0.67	1.40±0.19

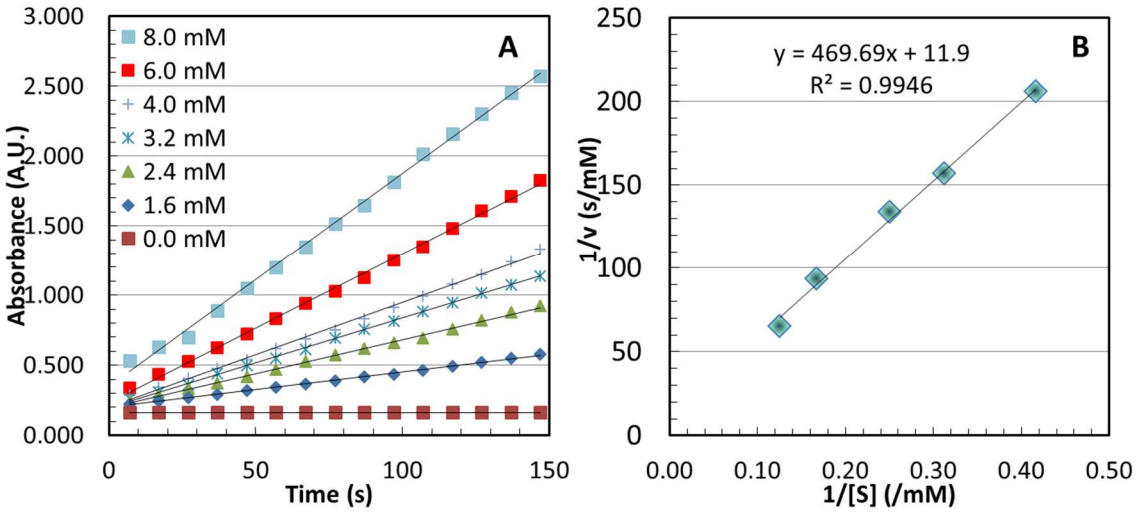

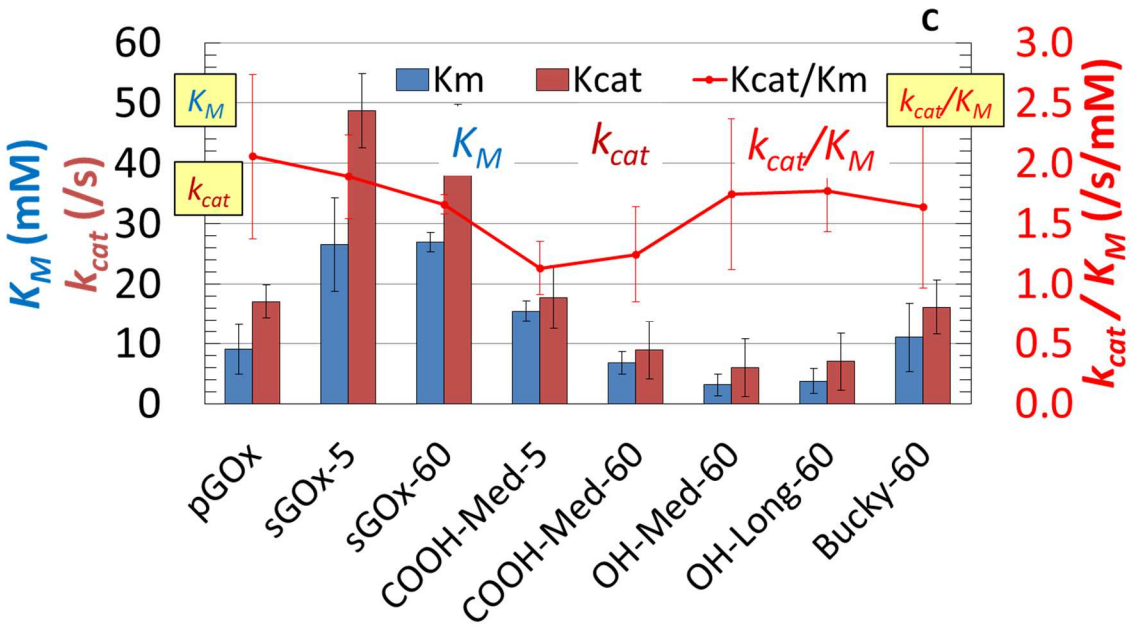

Figure 1. A) Typical plot of enzyme kinetic data B) Typical Lineweaver-Burk double reciprocal plot from which to extract kinetic parameters. C) Relationship between K_M, k_{cat}, and k_{cat}/K_M (a reflection of the efficiency of the enzyme) for pristine GOx, sonicated GOx (5 min, 60 min) and selected SWNT-X-L-GOx conjugates. The greatest contribution to change in enzyme efficiency is seen from functionalities of SWNTs.

Sonication of pristine GOx, whether for 5 or 60 minutes, produced a significant increase in both K_M and k_{cat}. However, the specificity constant (k_{cat}/K_M) was not significantly altered. That is, the effect of sonication was to change the specific rate and the affinity in the same direction and magnitude, and this result was produced whether a short time (5 min) or a long time (60 min) was used. In all cases, the presence of SWNTs was to attenuate the magnitude of change induced by these sonication effects.

Looking at the trend in the specificity constant (k_{cat}/K_M), sonication times did not have as much of an influence as did the length and functionality of the SWNTs. The –OH functionalized SWNT (SWNT-OH), although of lower K_M and k_{cat} values, retained higher enzyme efficiency compared to SWNT-COOH. The length of the tubes did not have as much of an effect on enzyme efficiency. Sonication times likewise did not affect overall efficiency of the enzyme. The extent of sonication, whether short (5 min) or long (60 min) appears inconsequential to enzyme activity under any circumstance. One reason the SWNT-OH conjugates had greater enzyme efficiency than the SWNT-COOH could be due to the carboxyl groups strongly interacting with the amine groups found on the surface of the enzyme thereby slightly altering access to the active site of the enzyme. The sonication times had little effect on the overall enzyme efficiency and this is thought to be a result of the energy damping effects conferred by the high aspect ratio SWNTs. That is, the tubes effectively absorbed and dissipated the cavitation energy that would otherwise induce denaturation/aggregation of the GOx.

Globular proteins such as GOx present an abundance of their polar amino acid side groups on the surface of the enzyme. Functionalized tubes rich in –OH and -COOH groups will strongly hydrogen bond and electrostatically interact with these groups creating conjugates that are topological. There is a strong possibly that these will affect the active site of the enzyme while not gaining proximal access to the deeply buried cofactor. Non-functionalized SWNTs however will more likely interact with the hydrophobic motifs of the enzyme that are deeply buried and proximal to the cofactor.

2.4.2 UV/Vis spectroscopy of FAD-apoenzyme association

In order to determine the effect of ultrasonication on sonicated GOx, including the possible partial aggregation, partial denaturation, or ultrasonically induced self-chemical modification involving reactions of its UV-absorbing amino acid residues, UV-Vis absorption spectrophotometric analyses were performed. The UV-Vis spectra over the range of 300 to 550 nm was specifically investigated to obtain information pertinent to the binding state of the FAD bound to the native enzyme (absorption maxima at 381 and 452 nm) or the spectrum of the solvent denatured enzyme (FAD absorption maxima at 377 and 448 nm). A blue shift is expected (Swoboda and Massey 1965) on going from enzyme-bound FAD to free solvated FAD and apoenzyme in solution. This is important to ensure supramolecular conjugates were not denatured by losing FAD. The UV-Vis absorption spectra of pristine FAD and sonicated FAD were measured in triplicate. **Figure 2A** shows that there is no change in the FAD signature upon the application of ultrasonication energy typically used in creating these supramolecular conjugates. This confirmed that ultrasonication, up to 60 min had no influence on spectral characteristics of FAD in solution. The UV-Vis absorption spectra of pristine GOx, ultrasonicated GOx (5 min), and ultrasonicated GOx (60 min) in the presence of SWNTs of different functionality and lengths were similarly measured in triplicate. Spectral peaks were deconvoluted and the absorbances at λ_{max} 381nm and 452 nm (FAD bound in GOx) and λ_{max} 377 nm and 448 nm (partially denatured GOx), expressed as ratios 381 nm / 377 nm and 452 nm / 448 nm, as a measure of the extent of denaturation by ultrasonication times, SWNT lengths and SWNT functionalities. **Figure 2B** shows that there was some statistical difference ($p < 0.05$)

between the low time (5 min) of sonicated GOx and high time (60 min) of sonicated GOx but no statistical difference between each sonicated GOx system compared to pristine GOx.

Similar to the effect of sonication time on enzyme kinetic parameters, sonication appears to induce some subtle changes in the distribution among FAD-associated and FAD de-associated enzyme; the extent of sonication however, whether 5 min or 60 min, appears inconsequential to this change. This suggests that some number of GOx molecules may be vulnerable to the influence of the disruptive force brought on by the cavitation energy of sonication.

A greater effect on FAD egress (enzyme denaturation) was seen from the influence of tube lengths rather than from the tube functionalities of the SWNT and/or the sonication times. This effect is better shown in the plot of the ratios of bound to free FAD (**Figure 2D**) where the greatest change is seen among the varying lengths of the SWNTs rather than functionality or ultrasonication time.

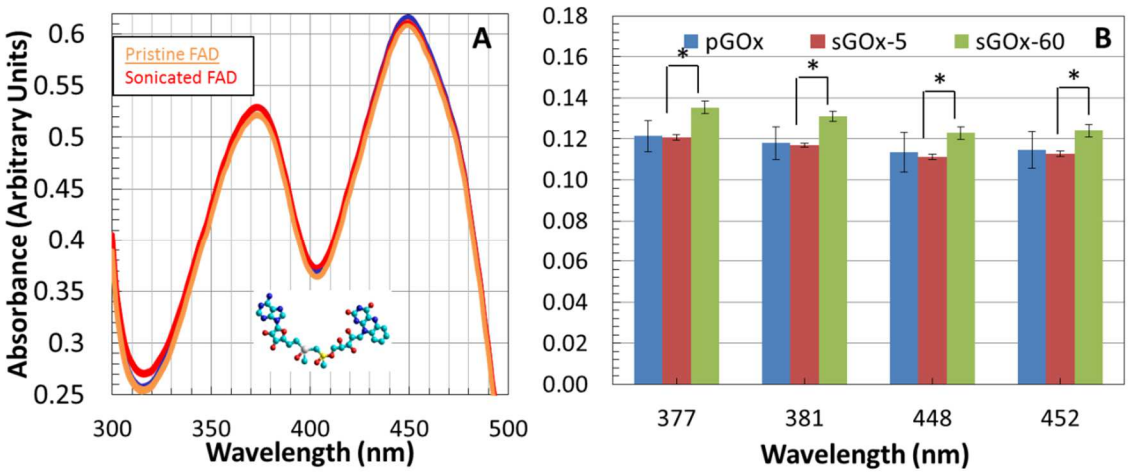

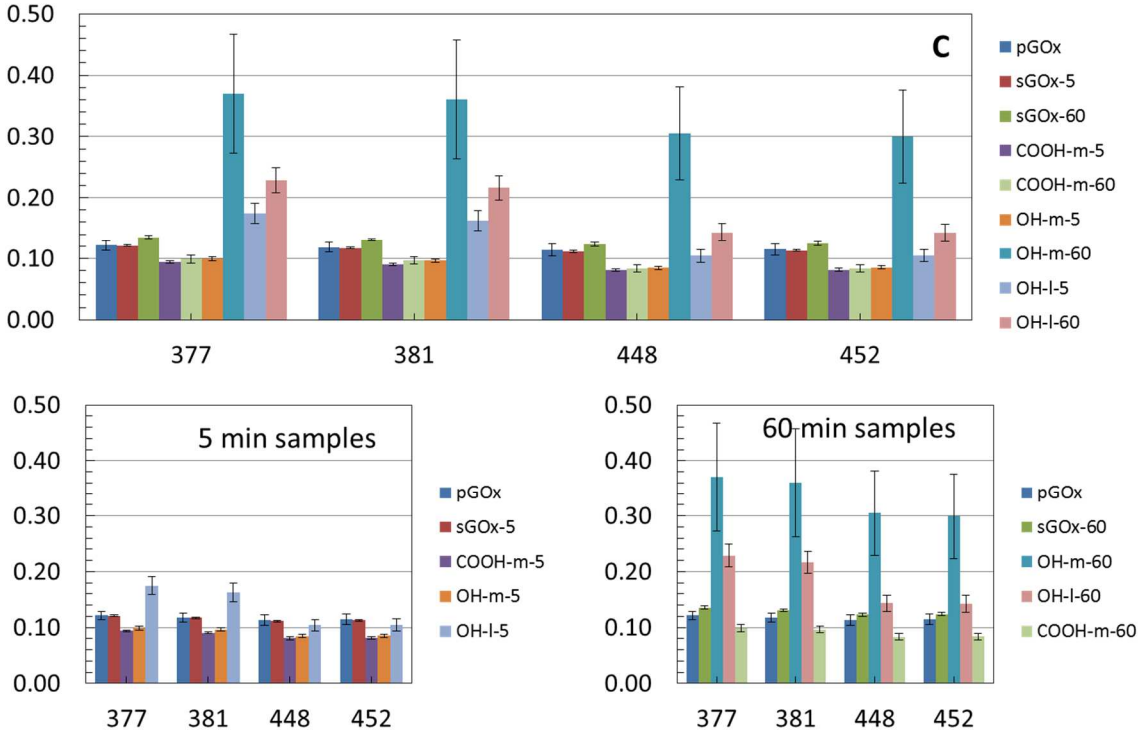
C
0.50
0.40
0.30
0.20
0.10
0.00
377
381
448
452
pGOx
sGOx-5
sGOx-60
COOH-m-5
COOH-m-60
OH-m-5
OH-m-60
OH-l-5
OH-l-60

5 min samples
0.50
0.40
0.30
0.20
0.10
0.00
377
381
448
452
pGOx
sGOx-5
COOH-m-5
OH-m-5
OH-l-5

60 min samples
0.50
0.40
0.30
0.20
0.10
0.00
377
381
448
452
pGOx
sGOx-60
OH-m-60
OH-l-60
COOH-m-60

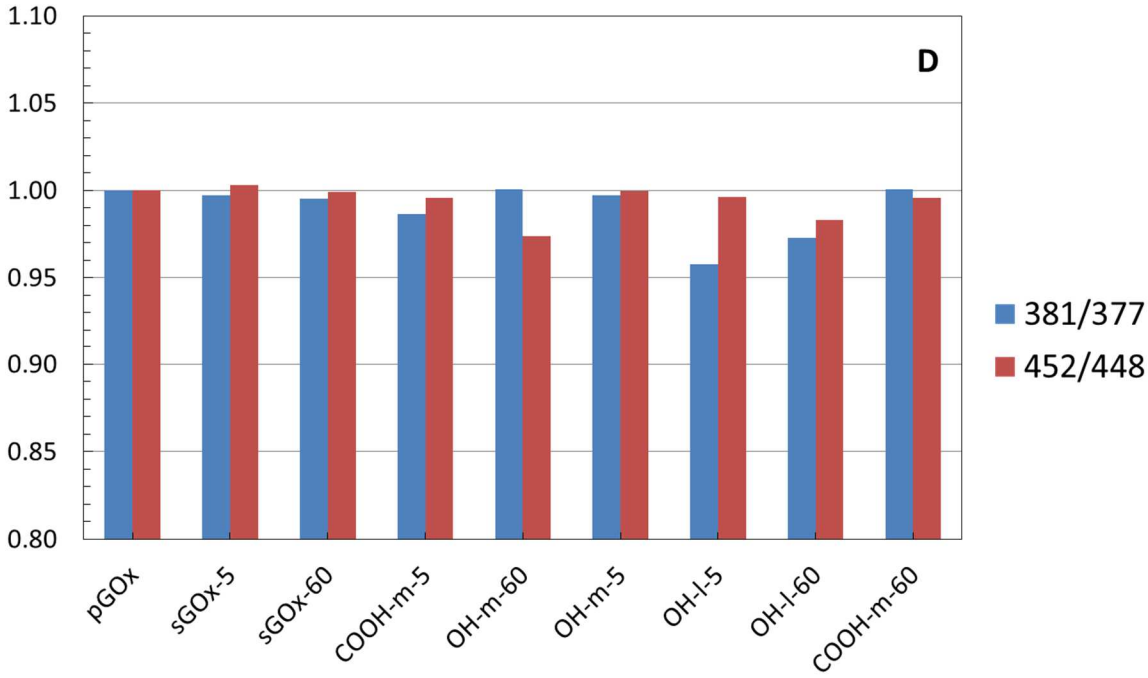
D
1.10
1.05
1.00
0.95
0.90
0.85
0.80
pGOx
sGOx-5
sGOx-60
COOH-m-5
OH-m-60
OH-m-5
OH-l-5
OH-l-60
COOH-m-60
381/377
452/448

Figure 2. A) Triplicate measures of the UV/Vis spectra of pristine and sonicated (5 min) Flavin Adenine Dinucleotide (FAD) in DI water (0.1 mg/mL). B) Changes in the FAD signature in pristine GOx: Bound at 381 and 452 nm; Denatured at 377 and 448 nm. * $p < 0.05$. C) Changes in the FAD signature in GOx-SWNT-X-L: Bound at 381 and 452 nm; Denatured at 377 and 448 nm. D) Ratio of 381 nm to 377 nm and 452 nm to 448 nm in the FAD signature in GOx-SWNT-X-L: Ratio in pristine GOx normalized to 1.

2.4.3 Circular dichroism spectroscopy for the structure of GOX-SWNT conjugates

Circular dichroism was used to study the changes to 2° structure that accompanied ultrasonication of GOx, both in the absence and presence of SWNT variants. To understand the conformational changes of the pristine (p) and ultrasonicated (s) samples (pGOx, sGOx, GOx-SWNT-X-L) plots of molar ellipticity *vs.* wavelength were produced (a typical plot is shown in **Figure 3A**) and from these plots were extracted the fractions of α-helix, β-sheet, turns and random sequences. **Table 3** gives the fractions, sum of fractions and the relative change of each structural component relative to pristine GOx. This analysis shows that there was no statistical difference in the "sum of the fractions" when comparing pristine GOx to sGOx (5 min, 60 min) although the α-helix fractions and unordered fractions did show significant difference ($p < 0.05$) (**Figure 3B**). Sonication, (whether 5 min or 60 min) causes a significant enrichment in the α-helical content. This occurs at the sacrifice of the unordered sequences with no change in the β-sheet content. Again, we see

that time of ultrasonication, 5 min or 60 min, is inconsequential to the structural change of the enzyme.

Table 3. Percentage distribution of secondary structural elements and sum of α-helix and β-sheet fractions in pristine GOx, sonicated GOx (5 min and 60 min) and various GOx-SWNT-X-L conjugates.

	α-Helix	**β-Sheet**	**Sum**	**Turn**	**Random Coil**
Pristine GOx	16	31	47	13	40
Sonicated GOx – 5 min	37	26	63	15	22
Sonicated GOx – 60 min	37	25	62	12	26
GOx-Bucky – 60 min	45	18	63	12	24
GOx-SWNT-OH-long-5 min	36	20	56	10	34
GOx-SWNT-OH-long-60 min	48	17	65	9	27
GOx-SWNT-OH-medium-5 min	47	17	64	16	20
GOx-SWNT-OH-medium-60 min	42	18	60	18	22
GOx-SWNT-COOH-medium-5 min	50	15	65	18	17
GOx-SWNT-COOH-medium-60 min	37	23	60	16	24

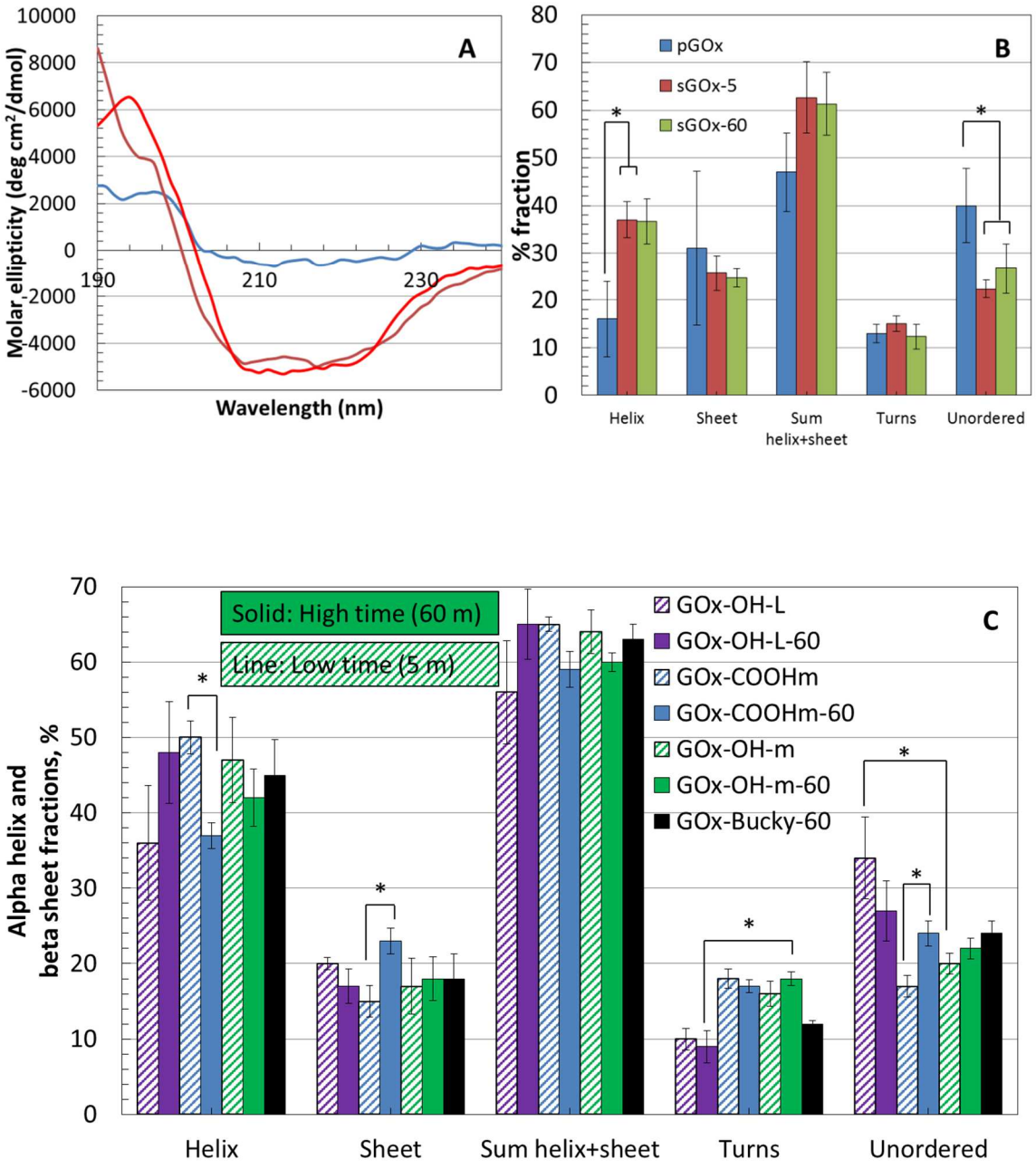

Figure 3. A) Far-UV CD spectra of pristine GOx. B) Changes in the secondary structure of GOx following ultrasonication for 5 and 60 min compared to pristine GOX (0 min). * $p < 0.05$. C) Changes in the secondary structure of GOx-SWNT-X-L. Among the three

parameters of interest, length of SWNT had the greatest effect on structure compared to functionality and sonication time. * $p < 0.05$.

When looking closely at the changes to the structure of GOx in the supramolecular GOx-SWNT-X-L conjugates (**Figure 3C**), the greatest contributor to a significant change in the secondary structure of the enzyme was tube length. Tube length contributes a significant change ($p < 0.05$) in the unordered fractions [e.g. OH-M-5 *vs.* OH-L-5 and (Unordered $p = 0.024$) and OH-M-60 *vs.* OH-L-60 (Unordered $p = 0.0006$)] of the secondary structure of the enzyme while sonication times (whether 5 min or 60 min) did not show any significant difference. Ultrasonication, as a process, regardless of the presence of SWNTs, causes an increase in the sum of α-helix, β-sheet components at the sacrifice of the unordered sequences. On the other hand, ultrasonication in the presence of SWNTs, regardless of length and functionality, reduced the β-sheet content of pristine GOx suggesting their unambiguous role in disrupting intramolecular hydrogen bonding. SWNTs therefore have a unique interaction with GOx in the presence of ultrasonication that opposes the action of ultrasonication taken alone. In general, ultrasonication times (5 min or 60 min) did not show any significant difference among the various conjugates (similar to the action in the absence of SWNTs) except in the case of COOH-M-5 vs. COOH-M-60 where there was a significant reduction ($p = 0.003$) in the α-helix content, a significant increase ($p = 0.014$) in the β-sheet component, and a significant increase ($p = 0.011$) in the unordered portion with increased ultrasonication time. Thus –COOH functionalized tubes clearly acted uniquely compared to –OH functionalized and Bucky tubes. This shift in

ordered fractions can be attributed to the interaction of the carboxyl groups on the SWNTs with the surface amine groups on GOx. Such a difference in mode of action could arise from a release of surface pressure (Dai, Li and Jiang 1999) and the induced structural transformations, which may affect the active site of the enzyme.

2.4.4 Surface profile imaging

White light interferometry (Wyant 2002; Schmit 2005; Goicoechea, Zamarreño, Matias and Arregui 2009) was used to produce 3D surface images of adsorbed pGOx, sGOx, and GOx-SWNT-X-L conjugates on platinum electrodes. **Figure 4** shows the surface morphology using non-contact optical profiling of: A) blank PME 118-Pt, B) physically adsorbed GOx (20 μL of 1 mg/mL), C) physically adsorbed GOx-SWNT (20 μL of 1 mg/mL), D) physically adsorbed sonicated GOx (60 min; 20 μL of 1 mg/mL) and E) physically adsorbed SWNT (20 μL of 1 mg/mL) on PME 118-Pt. These images clearly show that what was a generally uniform, featureless metallic surface became roughed by the presence of adsorbed GOx aggregates. From these images were extracted average surface roughness (Sa, nm) and the developed surface area ratio (Sdr, unitless) [Sdr = (texture surface area – plan surface area) / plan surface area] and these are tabulated in **Table 4**. In both cases the data are also referenced to the blank Pt electrode.

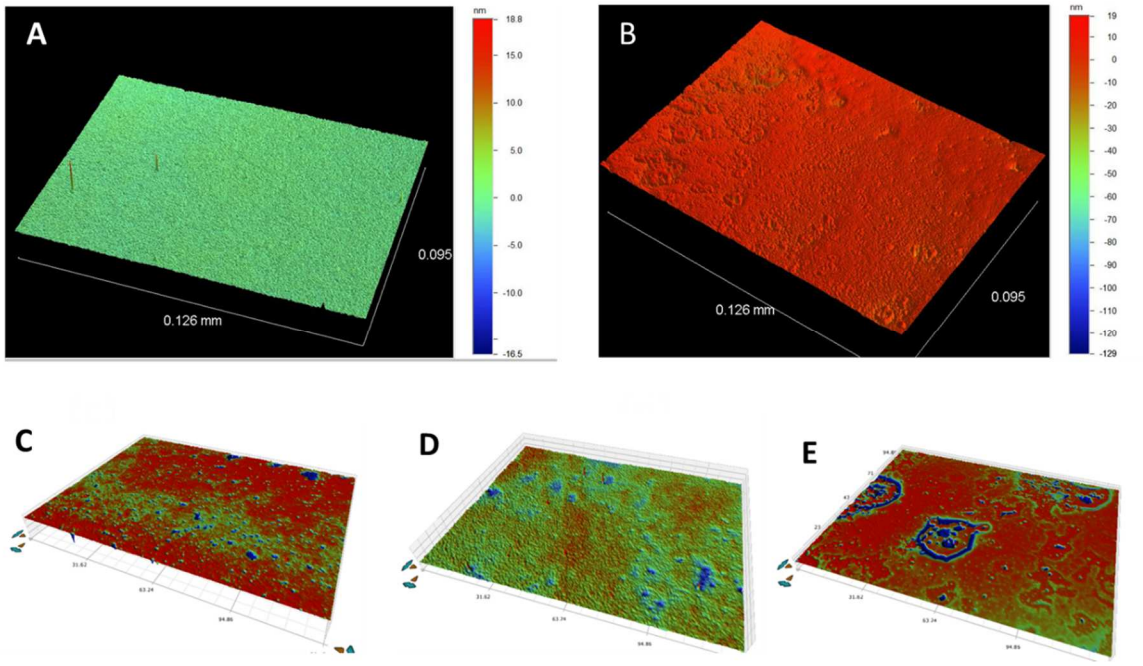

Figure 4. Surface morphology using non-contact optical profiling of: A) Blank PME 118-Pt, B) Physically adsorbed GOx (20 mL of 1 mg/mL) on PME 118-Pt, C) Physically adsorbed GOx-SWNT (20 mL of 1 mg/mL)on PME 118-Pt, D) Physically adsorbed sonicated (60 min) GOx (20 mL of 1 mg/mL) on PME 118-Pt, and E) Physically adsorbed SWNT (20 mL of 1 mg/mL) on PME 118-Pt.

Table 4. A comparison of the surface profiles of pristine GOx, sonicated (60 min) GOx, SWNT and GOx-SWNT examined as determined by non-contact optical profiling.

Materials	Sa (Average Roughness), nm	Ratio to blank	Sdr (developed surface area ratio)	Ratio to blank
Pt	0.254	1.00	0.114	1.00
Pt|pGOx	1.928	7.59	0.122	1.07
Pt|sGOx-SWNT	9.408	37.04	0.0025	0.02
Pt|sGOx	10.688	42.08	0.0071	0.06
Pt|SWNT	66.222	260.72	0.0431	0.38

The surface roughness may by inference be related to the aggregation state of the protein and SWNT following adsorption and drying on the Pt substrate. The Pt|sGOx and Pt|sGOx-SWNT both show similar surface roughness but produce surface roughness that is ca. 5X that produced by the pristine GOx. This confirms that ultrasonication likely produced aggregation of the GOx, independent of the presence of the SWNT. The structural changes, particularly the increase in α-helix content, are consistent with the formation of GOx aggregates. On the other hand, the Pt|SWNT produced a surface which was 7X that produced by the Pt|sGOx-SWNT. This confirms that the GOx effectively de-aggregates the SWNTs bundles and produces a surface structure that is governed by the protein member of the conjugate pair. This suggests that the SWNTs are effectively individualized, or are at least of bundle sizes less than that of the protein aggregates.

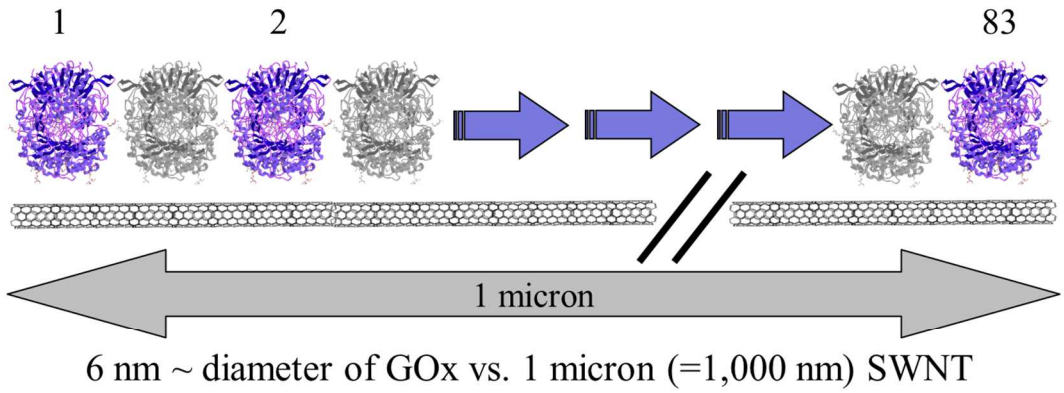

Protein	Molecular Weight [kDa]	EC Number	Diameter [nm]
Glucose Oxidase	160	232-601-0	6
Bovine Serum Albumin	66	232-936-2	14

~ 83 GOx / SWNT

~ 35 BSA / SWNT

Figure 5. Back of the envelope calculation showing optimal number of glucose oxidase (GOx) and bovine serum albumin (BSA) that could adsorb to the sides of a single-walled carbon nanotube (SWNT). First order approximation assumes ONE enzyme space in between successive enzymes using the average diameter of the enzyme and protein.

2.4.5 Optimal processing conditions

The design of experiments approach allows us to rapidly converge upon generally optimized processing conditions for producing GOx-SWNT supramolecular conjugates with minimum loss of enzyme activity for the best retained activity. The experimental design suggested 12 unique experiments that were conducted in triplicate and resulted in 36 separate test samples. From an analysis of the experimental data, shorter SWNTs

functionalized with –OH groups and provided with longer sonication times (no difference with respect to shorter sonication times) gave the best combination for forming bioactive conjugates. There are other issues of course. For example, are these short, –OH functionalized SWNTs conductive? Can the bioactive conjugate support direct electron transfer? Can these bioactive conjugates be immobilized onto solid or porous electrodes to promote direct electron transfer appropriate for Gen-3 biosensors and advanced biofuel cells?

2.5 Conclusions

These investigations reveal that tube length of SWNTs has the greatest overall effect compared to sonication times and functionalities on FAD retention and enzyme structure while functionality of the SWNT has a greater effect on the kinetic efficiency of the enzyme. One possibility for this could be the higher density of tube ends with the shorter SWNTs compared to the longer ones for the same weight of SWNTs. A high level of enzyme activity was conserved for all conjugates. Shorter SWNTs supported conjugate formation with no loss of FAD and conserved enzymatic structure while the longer SWNTs caused some partial denaturation leading to the egress of FAD. Ultrasonication, regardless of time used short or long, promotes GOx aggregation as evidenced by the increase in α-helix content and the surface roughness data. Ultrasonication, as a processing technique, has an almost instantaneous effect on GOx structure and activity that appears to be the associated with aggregate formation. SWNT stabilizes the GOx from ultrasonic denaturation by absorbing and dissipating portions of ultrasonic energy put into creating conjugates. Future studies will characterize the electron transfer kinetics as well as perform

amperommetry measurements to determine efficacy in biosensors and biofuel cells. In addition, long term viability studies will be run to ensure the implantable biosensors have a relatively long shelf life.

Abbreviations

GOx: glucose oxidase; pGOx: pristine glucose oxidase; sGOx: sonicated glucose oxidase; FAD: flavin adenine dinucleotide; HRP: horseradish peroxidase; SWNT: single-walled carbon nanotube; PME: planar metal electrode; Pt: Platinum; Gen-3: Generation-3; CD: circular dichroism; k_{cat}: the turnover number of an enzyme; K_M: The Michales constant – an inverse measure of the affinity of an enzyme for its substrate

2.6 References

Banks, C. E. and R. G. Compton (2005). "Exploring the electrocatalytic sites of carbon nanotubes for NADH detection: an edge plane pyrolytic graphite electrode study." Analyst **130**(9): 1232-1239.

Banks, C. E. and R. G. Compton (2005). "New electrodes for old: from carbon nanotubes to edge plane pyrolytic graphite." Analyst **131**(1): 15-21.

Banks, C. E., T. J. Davies, G. G. Wildgoose and R. G. Compton (2005). "Electrocatalysis at graphite and carbon nanotube modified electrodes: edge-plane sites and tube ends are the reactive sites." Chemical communications(7): 829-841.

Barton, S., J. Gallaway and P. Atanassov (2004). "Enzymatic biofuel cells for implantable and microscale devices." Chem. Rev **104**(10): 4867-4886.

Berendsen, H. J. C., J. P. M. Postma, W. F. van Gunsteren, A. DiNola and J. R. Haak (1984). "Molecular dynamics with coupling to an external bath." The Journal of chemical physics **81**(8): 3684-3690.

Bergmeyer, H., K. Gawehn and M. Grassl (1974). "Glucose oxidase: assay method." Methods of enzymatic analysis **1**: 457-460.

Brahim, S., N. K. Shukla and A. Guiseppi-Elie (2006). Nanobiosensors: Carbon Nanotubes in Bioelectrochemisty. Nanotechnology in Biology and Medicine. T. Vo-Dinh. New York, CRC Press**:** 397-410.

Bussi, G., D. Donadio and M. Parrinello (2007). "Canonical sampling through velocity rescaling." The Journal of chemical physics **126**(1): 014101-014107.

Calabrese Barton, S., J. Gallaway and P. Atanassov (2004). "Enzymatic Biofuel Cells for Implantable and Microscale Devices." Chemical Reviews **104**(10): 4867-4886.

Cang-Rong, J. T. and G. Pastorin (2009). "The influence of carbon nanotubes on enzyme activity and structure: investigation of different immobilization procedures through enzyme kinetics and circular dichroism studies." Nanotechnology **20**(25): 255102.

Consortium, T. U. (2013). "Update on activities at the Universal Protein Resource (UniProt) in 2013." Nucleic Acids Research **41**(D1): D43-D47.

Cui, X., V. A. Lee, Y. Raphael, J. A. Wiler, J. F. Hetke, D. J. Anderson and D. C. Martin (2001). "Surface modification of neural recording electrodes with conducting polymer/biomolecule blends." Journal of Biomedical Materials Research **56**(2): 261-272.

Dai, G., J. Li and L. Jiang (1999). "Conformation change of glucose oxidase at the water–air interface." Colloids and Surfaces B: Biointerfaces **13**(2): 105-111.

Darden, T., D. York and L. Pedersen (1993). "Particle mesh Ewald: An N [center-dot] log(N) method for Ewald sums in large systems." The Journal of chemical physics **98**(12): 10089-10092.

Davis, F. and S. P. Higson (2007). "Biofuel cells--recent advances and applications." Biosens Bioelectron **22**(7): 1224-1235.

Duan, Y., C. Wu, S. Chowdhury, M. C. Lee, G. Xiong, W. Zhang, R. Yang, P. Cieplak, R. Luo, T. Lee, J. Caldwell, J. Wang and P. Kollman (2003). "A point-charge force field for molecular mechanics simulations of proteins based on condensed-phase quantum mechanical calculations." Journal of computational chemistry **24**(16): 1999-2012.

Eisenberg, D., R. M. Weiss, T. C. Terwilliger and W. Wilcox (1982). "Hydrophobic moments and protein structure." Faraday Symposia of the Chemical Society **17**(0): 109-120.

Falk, M., V. Andoralov, Z. Blum, J. Sotres, D. B. Suyatin, T. Ruzgas, T. Arnebrant and S. Shleev (2012). "Biofuel cell as a power source for electronic contact lenses." Biosens Bioelectron **37**(1): 38-45.

Falk, M., Z. Blum and S. Shleev (2012). "Direct electron transfer based enzymatic fuel cells." Electrochimica Acta **82**(0): 191-202.

Fried, J. R. (2003). Conformations, Solutions and Molecular Weight. Polymer Science and Technology. Upper Saddle River, NJ, Prentice Hall**:** 582.

Ghosh, T., A. E. García and S. Garde (2001). "Molecular dynamics simulations of pressure effects on hydrophobic interactions." Journal of the American Chemical Society **123**(44): 10997-11003.

Godawat, R., S. N. Jamadagni and S. Garde (2009). "Characterizing hydrophobicity of interfaces by using cavity formation, solute binding, and water correlations." Proceedings of the National Academy of Sciences **106**(36): 15119-15124.

Goicoechea, J., C. R. Zamarreño, I. R. Matias and F. J. Arregui (2009). "Utilization of white light interferometry in pH sensing applications by mean of the fabrication of nanostructured cavities." Sensors and Actuators B: Chemical **138**(2): 613-618.

Guiseppi-Elie, A. (1998). Chemical and Biological Sensor Devices Having Electroactive Polymer Thin Films Attached to Microfabricated Devices and Possessing Immobilized Indicator Moieties. USPTO. USA, ABTECH Scientific, Inc. **5,766,934**.

Guiseppi-Elie, A. (2011). Implantable biochip for managing trauma-induced hemorrhage USPTO. USA, Anthony Guiseppi-Elie. **20120088997**.

Guiseppi-Elie, A., S. Brahim, G. Wnek and R. Baughman (2005). "Carbon-nanotube-modified electrodes for the direct bioelectrochemistry of pseudoazurin." NanoBioTechnology **1**(1): 83-92.

Guiseppi-Elie, A., S.-H. Choi, K. Geckeler, B. Sivaraman and R. Latour (2008). "Ultrasonic Processing of Single-Walled Carbon Nanotube–Glucose Oxidase Conjugates: Interrelation of Bioactivity and Structure." NanoBiotechnology **4**(1-4): 9-17.

Guiseppi-Elie, A., S.-H. Choi, K. Geckeler, B. Sivaraman and R. Latour (2008). "Ultrasonic Processing of Single-Walled Carbon Nanotube–Glucose Oxidase Conjugates: Interrelation of Bioactivity and Structure." NanoBioTechnology **4**(1): 9-17.

Guiseppi-Elie, A., S.-H. Choi and K. E. Geckeler (2009). "Ultrasonic processing of enzymes: Effect on enzymatic activity of glucose oxidase." Journal of Molecular Catalysis B: Enzymatic **58**(1–4): 118-123.

Guiseppi-Elie, A., C. Lei and R. H. Baughman (2002). "Direct electron transfer of glucose oxidase on carbon nanotubes." Nanotechnology **13**(5): 559.

Guiseppi-Elie, A., A. R. A. Rahman and N. K. Shukla (2010). "SAM-modified microdisc electrode arrays (MDEAs) with functionalized carbon nanotubes." Electrochimica Acta **55**(14): 4247-4255.

Haaland, P. D. (1989). Experimental Design in Biotechnology. New York, CRC Press.

Hansen, C. M. (2007). Hansen solubility parameters: a user's handbook, CRC Press, 2007.

Hao, F., P. Dong, J. Zhang, Y. Zhang, P. E. Loya, R. H. Hauge, J. Li, J. Lou and H. Lin (2012). "High Electrocatalytic Activity of Vertically Aligned Single-Walled Carbon Nanotubes towards Sulfide Redox Shuttles." Sci. Rep. **2**.

Hernandez, Y., M. Lotya, D. Rickard, S. D. Bergin and J. N. Coleman (2009). "Measurement of multicomponent solubility parameters for graphene facilitates solvent discovery." Langmuir **26**(5): 3208-3213.

Hess, B., H. Bekker, H. J. C. Berendsen and J. G. E. M. Fraaije (1997). "LINCS: A linear constraint solver for molecular simulations." Journal of computational chemistry **18**(12): 1463-1472.

Hess, B., C. Kutzner, D. Van Der Spoel and E. Lindahl (2008). "GROMACS 4: Algorithms for highly efficient, load-balanced, and scalable molecular simulation." Journal of chemical theory and computation **4**(3): 435-447.

Hildebrand, J. H. and R. L. Scott (1950). The Solubility of Nonelectrolytes, Reinhold, New York.

Jia, W., C. Jin, W. Xia, M. Muhler, W. Schuhmann and L. Stoica (2012). "Glucose Oxidase/Horseradish Peroxidase Co-immobilized at a CNT-Modified Graphite Electrode: Towards Potentially Implantable Biocathodes." Chemistry – A European Journal **18**(10): 2783-2786.

Johnson, W. C. (1999). "Analyzing protein circular dichroism spectra for accurate secondary structures." Proteins: Structure, Function, and Bioinformatics **35**(3): 307-312.

Jorgensen, W. L., J. Chandrasekhar, J. D. Madura, R. W. Impey and M. L. Klein (1983). "Comparison of simple potential functions for simulating liquid water." The Journal of chemical physics **79**(2): 926-935.

Jorgensen, W. L., D. S. Maxwell and J. Tirado-Rives (1996). "Development and testing of the OPLS all-atom force field on conformational energetics and properties of organic liquids." Journal of the American Chemical Society **118**(45): 11225-11236.

Justin, G., Y. Zhang, M. Sun and R. Sclabassi (2005). Biofuel cells: a possible power source for implantable electronic devices, IEEE.

Kannan, A. M., V. Renugopalakrishnan, S. Filipek, P. Li, G. F. Audette and L. Munukutla (2008). "Bio-Batteries and Bio-Fuel Cells: Leveraging on Electronic Charge Transfer Proteins." Journal of Nanoscience and Nanotechnology **8**: 1-13.

Karunwi, O. and A. Guiseppi-Elie (2012). "CNT-Enzyme Conjugates for Gen-3 Biosensors and Biofuel Cells " Nano Today **In preparation**.

Karunwi, O. and A. Guiseppi-Elie (2013). "Supramolecular glucose oxidase-SWNT conjugates formed by ultrasonication: effect of tube length, functionalization and processing time." Journal of Nanobiotechnology **11**(1): 6.

Kelly, S. M., T. J. Jess and N. C. Price (2005). "How to study proteins by circular dichroism." Biochimica et Biophysica Acta (BBA)-Proteins & Proteomics **1751**(2): 119-139.

Kim, D.-H., M. Abidian and D. C. Martin (2004). "Conducting polymers grown in hydrogel scaffolds coated on neural prosthetic devices." Journal of Biomedical Materials Research Part A **71A**(4): 577-585.

Kim, J. and K.-H. Yoo (2013). "Glucose oxidase nanotube-based enzymatic biofuel cells with improved laccase biocathodes." Physical Chemistry Chemical Physics **15**(10): 3510-3517.

Klonoff, D. C. (2005). "Continuous Glucose Monitoring Roadmap for 21st century diabetes therapy." Diabetes care **28**(5): 1231-1239.

Kotanen, C. N., F. G. Moussy, S. Carrara and A. Guiseppi-Elie (2012). "Implantable Enzyme Amperometric Biosensors." Biosensors and Bioelectronics: (in press).

Kotanen, C. N., F. G. Moussy, S. Carrara and A. Guiseppi-Elie (2012). "Implantable enzyme amperometric biosensors." Biosensors and Bioelectronics **35**(1): 14-26.

Kyte, J. and R. F. Doolittle (1982). "A simple method for displaying the hydropathic character of a protein." Journal of Molecular Biology **157**(1): 105-132.

Lee, K., H. J. Lim, S. J. Yang, Y. S. Kim and C. R. Park (2013). "Determination of solubility parameters of single-walled and double-walled carbon nanotubes using a finite-length model." RSC Advances **3**(14): 4814-4820.

Liu, H., Y. Tian and P. Xia (2008). "Pyramidal, Rodlike, Spherical Gold Nanostructures for Direct Electron Transfer of Copper, Zinc-Superoxide Dismutase: Application to Superoxide Anion Biosensors." Langmuir **24**(12): 6359-6366.

Lobanov, M. Y., N. S. Bogatyreva and O. V. Galzitskaya (2008). "Radius of gyration as an indicator of protein structure compactness." Molecular Biology **42**(4): 623-628.

Meirovitch, H., S. Rackovsky and H. A. Scheraga (1980). "Empirical Studies of Hydrophobicity. 1. Effect of Protein Size on the Hydrophobic Behavior of Amino Acids." Macromolecules **13**(6): 1398-1405.

Min, K., J. Ryu and Y. Yoo (2010). "Mediator-free glucose/O2; biofuel cell based on a 3-dimensional glucose oxidase/SWNT/polypyrrole composite electrode." Biotechnology and Bioprocess Engineering **15**(3): 371-375.

Neto, S., J. Forti and A. De Andrade (2010). "An Overview of Enzymatic Biofuel Cells." Electrocatalysis **1**(1): 87-94.

Neto, S. A., J. C. Forti and A. R. Andrade (2010). "An Overview of Enzymatic Biofuel Cells." Electrocatalysis **1**(1): 87-94.

O'Malley, J. J. and J. L. Weaver (1972). "Subunit structure of glucose oxidase from Aspergillus niger." Biochemistry **11**(19): 3527-3532.

Okuda-Shimazaki, J., N. Kakehi, T. Yamazaki, M. Tomiyama and K. Sode (2008). "Biofuel cell system employing thermostable glucose dehydrogenase." Biotechnology Letters **30**(10): 1753-1758.

Özbek, B. and K. Ö. Ülgen (2000). "The stability of enzymes after sonication." Process Biochemistry **35**(9): 1037-1043.

Provencher, S. W. and J. Gloeckner (1981). "Estimation of globular protein secondary structure from circular dichroism." Biochemistry **20**(1): 33-37.

Raso, J., P. Mañas, R. Pagán and F. J. Sala (1999). "Influence of different factors on the output power transferred into medium by ultrasound." Ultrasonics sonochemistry **5**(4): 157-162.

Raut, V. P., M. A. Agashe, S. J. Stuart and R. A. Latour (2005). "Molecular Dynamics Simulations of Peptide−Surface Interactions." Langmuir **21**(4): 1629-1639.

Re, R., N. Pellegrini, A. Proteggente, A. Pannala, M. Yang and C. Rice-Evans (1999). "Antioxidant activity applying an improved ABTS radical cation decolorization assay." Free Radical Biology & Medicine **26**(9/10): 1231–1237.

RSC (2012). "Ultrasonication." RSC Chemical Methods Ontology (CMO) Retrieved March 24, 2012, 2012.

Rubenwolf, S., S. Kerzenmacher, R. Zengerle and F. von Stetten (2011). "Strategies to extend the lifetime of bioelectrochemical enzyme electrodes for biosensing and biofuel cell applications." Applied Microbiology and Biotechnology **89**(5): 1315-1322.

Saifuddin, N., A. Z. Raziah and A. R. Junizah (2013). "Carbon Nanotubes: A Review on Structure and Their Interaction with Proteins." Journal of Chemistry **2013**: 18.

Sarupria, S. and S. Garde (2009). "Quantifying water density fluctuations and compressibility of hydration shells of hydrophobic solutes and proteins." Physical review letters **103**(3): 037803.

Schmit, J. (2005). INTERFEROMETRY | White Light Interferometry. Encyclopedia of Modern Optics. E.-i.-C. B. D. Guenther. Oxford, Elsevier**:** 375-387.

Shah, S. and M. Gupta (2008). "The effect of ultrasonic pre-treatment on the catalytic activity of lipases in aqueous and non-aqueous media." Chemistry Central Journal **2**(1): 1.

Shin, K.-S., H.-D. Youn, Y.-H. Han, S.-O. Kang and Y. C. Hah (1993). "Purification and characterisation of d-glucose oxidase from white-rot fungus Pleurotus ostreatus." European Journal of Biochemistry **215**(3): 747-752.

Silverman, B. D. (2001). "Hydrophobic moments of protein structures: Spatially profiling the distribution." Proceedings of the National Academy of Sciences **98**(9): 4996-5001.

Stevens, F. J. (2008). "Homology versus analogy: possible evolutionary relationship of immunoglobulins, cupredoxins, and Cu,Zn-superoxide dismutase." J Mol Recognit **21**(1): 20-29.

Swoboda, B. E. P. and V. Massey (1965). "Purification and properties of the glucose oxidase from Aspergillus niger." Journal of Biological Chemistry **240**(5): 2209-2215.

Wang, H.-Y., A. Bernarda, C.-Y. Huang, D.-J. Lee and J.-S. Chang (2011). "Micro-sized microbial fuel cell: A mini-review." Bioresource Technology **102**(1): 235-243.

Wang, J. (2007). "Electrochemical Glucose Biosensors." Chemical Reviews **108**(2): 814-825.

Wang, S., E. S. Humphreys, S.-Y. Chung, D. F. Delduco, S. R. Lustig, H. Wang, K. N. Parker, N. W. Rizzo, S. Subramoney, Y.-M. Chiang and A. Jagota (2003). "Peptides with selective affinity for carbon nanotubes." Nat Mater **2**(3): 196-200.

Willats, W. T. (2002). "Phage display: practicalities and prospects." Plant Molecular Biology **50**(6): 837-854.

Wyant, J. C. (2002). White light interferometry. AeroSense 2002, International Society for Optics and Photonics.

Yu, T., Y. Gong, T. Lu, L. Wei, Y. Li, Y. Mu, Y. Chen and K. Liao (2012). "Recognition of carbon nanotube chirality by phage display." RSC Advances **2**(4): 1466-1476.

Yuan, W., Y. Zhou, Y. Li, C. Li, H. Peng, J. Zhang, Z. Liu, L. Dai and G. Shi (2013). "The edge- and basal-plane-specific electrochemistry of a single-layer graphene sheet." Sci. Rep. **3**.

Zhu, Z., L. Garcia-Gancedo, A. J. Flewitt, H. Xie, F. Moussy and W. I. Milne (2012). "A Critical Review of Glucose Biosensors Based on Carbon Nanomaterials: Carbon Nanotubes and Graphene." Sensors **12**(5): 5996-6022.

CHAPTER THREE

MOLECULAR DYNAMICS SIMULATIONS OF PEPTIDE-SWCNT INTERACTIONS RELATED TO ENZYME CONJUGATES FOR BIOSENSORS AND BIOFUEL CELLS

3.1 Abstract

With the demonstration of direct electron transfer between the redox active prosthetic group, flavin adenine dinucleotide (FAD), of glucose oxidase (GOx) and single-walled carbon nanotubes (SWCNT), there has been growing interest in the fabrication of CNT-enzyme supramolecular constructs that control the placement of SWCNTs within tunneling distance of co-factors for enhanced electron transfer efficiency in generation 3 biosensors and advanced biofuel cells. These conjugate systems raise a series of questions such as: Which peptide sequences within the enzymes have high affinity for the SWCNTs? And, are these high affinity sequences likely to be in the vicinity of the redox-active co-factor to allow for direct electron transfer? Phage display has recently been used to identify specific peptide sequences that have high affinity for SWCNTs. Molecular dynamics simulations were performed to study the interactions of five discrete peptides with (16,0) SWCNT in explicit water as well as with graphene. From the progression of the radius of gyration, Rg, the peptides studied were concertedly adsorbed to both the SWCNT and graphene. Peptide properties calculated using individual amino acid values, such as hydrophobicity indices, did not correlate with the observed adsorption behavior as quantified by Rg, indicating that the adsorption behavior of the peptide was not based on

the individual amino acid residues. However, the Rg values, reflective of the physicochemical embrace of the surface (SWCNT or graphene) had a strong positive correlation with the solubility parameter, indicating concerted, cooperative interaction of peptide segments with the materials. The end residues appear to dominate the progression of adsorption regardless of character. Sequences identified by phage display share some homology with key enzymes (GOx, lactate oxidase and laccase) used in biosensors and enzyme-based biofuel cells. These analogous sequences appear to be buried deep within the shell of fully folded proteins and as such are expected to be close to the redox-active prosthetic group.

Keywords: peptides, SWCNTs, enzymes, conjugates, simulations.

3.2 Introduction

With the advent of demonstrated direct electron transfer between the redox active cofactors of oxidoreductase enzymes such as glucose oxidase and solid state electrodes facilitated by single walled carbon nanotubes (SWCNTs), there is the potential to eliminate the need for small molecule or polymeric mediators in the development and commercialization of Generation-3 biosensors and advanced biofuel cells. Guiseppi et al.(Guiseppi-Elie, Brahim et al. 2002) were the first to demonstrate direct electron transfer between the redox active prosthetic group of glucose oxidase, flavin adenine dinucleotide (FAD), and single-walled carbon nanotubes. Since then there has been a large number of publications on the subject. (Zhu, Garcia-Gancedo et al. 2012; Saifuddin, Raziah et al. 2013)

SWCNT-oxidoreductase enzyme conjugates have been developed by the covalent coupling of oxidoreductase enzymes directly to carboxylic acid functionalized nanotubes (HOOC-SWCNT-COOH). These covalent conjugates have been immobilized onto various electrodes such as microdisc electrode arrays (MDEAs) to simultaneously take advantage of the high flux associated with radial diffusion and direct electron transfer.(Guiseppi-Elie, Rahman et al. 2010) Such covalent conjugation has the potential to adversely impact the enzymes active site and compromise its catalytic activity. Furthermore, the acid functionalization of the SWCNT is known to compromise its electronic properties.(Banks and Compton 2005; Banks and Compton 2005; Banks, Davies et al. 2005) As an alternative to covalent conjugation, non-covalent conjugation techniques that exploit the secondary forces between peptide sequences of the enzyme and the SWCNTs have been proposed and used to produce supra-molecular SWCNT-oxidoreductase enzyme conjugates.(Owino, Arotiba et al. 2008) Recent investigations have reported on the tremendous surfactant properties of GOx and on the changes to the structure and activity of GOx upon ultrasonic processing for the non-covalent conjugation of GOx with SWCNTs.(Karunwi and Guiseppi-Elie 2013) The interaction between the SWCNT and the enzyme has been investigated for its impact to the activity and change in structure of the protein as a function of SWCNT functionality, tube length and ultrasonic processing time.(Karunwi and Guiseppi-Elie 2013)

The goal in creating these supramolecular enzyme-SWCNT constructs is to achieve placement of the SWCNT within tunneling distance of the co-factor, FAD, so that electron transfer to the SWCNT can then lead to ballistic conduction of the electron to the

supporting electrode. On the other hand, the conjugate should not lead to appreciable loss of enzymatic activity.

In the study of enzyme-based amperometric biosensors(Kotanen, Moussy et al. 2012) and advanced enzyme-based implantable biofuel cells(Neto, Forti et al. 2010; Jia, Jin et al. 2012) the enzymes glucose oxidase (GOx), important in the measurement of glucose for diabetes management and as an anodic biocatalyst in enzyme fuel cells, lactate oxidase (LOx), important in the measurement and monitoring of lactate in victims of trauma, and laccase (Lac), important as a cathodic biocatalyst in enzyme fuel cells, each features prominently in the literature.(Kim and Yoo 2013)

A series of questions naturally arise:

- Which peptide sequences within these enzymes are most likely to have high affinity for the SWCNTs?
- Where within the subject enzymes are the SWCNTs predominantly associated?
- Are these high affinity sequences likely to be in the vicinity of the redox-active co-factor to allow for direct electron transfer?

Elementary inspection would suggest that the high degree of hydrophobicity of pristine SWCNTs will lead to their association with the more hydrophobic and non-charged motifs of the enzyme. Such highly hydrophobic motifs are not likely to be in the vicinity of the active site where the binding of highly hydrophilic molecules such as glucose, lactate and 2,2'-azino-bis(3-ethylbenzthiazoline-6-sulphonic acid) (ABTS) occurs.

3.3 Peptide Sequences

Phage display is a molecular expression technique by which foreign peptides may be expressed at the surface of phage particles.(Willats 2002) The phage thus becomes a vehicle for the expression and replication of large variants of that peptide which may be screened for desired properties, for example, specific binding properties. Recently, phage display and site-directed mutagenesis (SDM) have been used to identify specific peptide sequences that have high affinity to SWCNT(Wang, Humphreys et al. 2003) and to distinguish the chirality of SWCNTs. (Yu, Gong et al. 2012) The peptides identified by Wang et al. are shown in Table 1 and form the basis for the current molecular dynamics (MD) simulations to study the interactions of these five discrete peptides with SWCNTs. Furthermore, ongoing computational work has shown that the interaction of the nine amino acid sequence TGTGVGTGT with a prototypical hydrophobic (-CH3-terminated) and hydrophilic (-OH-terminated) self-assembled monolayer (SAM) suggest a strong role for the displacement of water.(Raut, Agashe et al. 2005) Hence, MD investigations of peptide-SWCNT interactions must account for the role of water.

Table 1. Peptides with selective affinity for SWCNTs as determined by phage display and site directed mutagenesis(Wang, Humphreys et al. 2003)	
HWKHPWGAWDTL	Sequence identified by phage display
HWKHPSGAWDTL	Replace W with S via SDM to show reduction in binding affinity
HNWYHWWMPHNT	Hydrophobicity as a function of amino acid location along the chain for 3 binding sequences revealing a tendency for a
HWSAWWIRSNQS	

HHWHHWCMPHKT	hydrophobic region in the middle and short hydrophilic sequence as either end

In general, a peptide may be globally described by its hydrophobicity index derived from the residue contributions and/or its solubility parameter, similarly derived from group contributions. Both are useful considerations when exploring the potential for dissolution of peptides. Recently, Lee et al(Lee, Lim et al. 2013) have reported on and rationalized solubility parameters of SWCNTs. Here we explore the relationships between these key global attributes and the pattern of adsorption of the above peptides as revealed by MD simulations.

3.4 Methods

Molecular dynamics (MD) simulations were performed to study the interactions of five discrete peptides with SWCNT in explicit water (**Table 2**). The simulations were performed in the isothermal-isobaric ensemble (NPT) at 300 K and 1 bar. The simulations were run for 35 ns each (time step of 2 fs). In the starting configurations, the peptide was placed at least 3 nm away from the SWCNT (**Fig. 1**). The SWCNT was a (16,0) zig-zag of ϕ = 1.270 nm. This initial position allowed the peptide to sample various configurations before reaching the nanotube surface, and also allowed an evaluation of the spontaneity of the peptide to adsorb onto the SWCNT. The nanotube was held rigid in the simulation. AMBER03 force field(Duan, Wu et al. 2003) was used to represent the peptides, OPLS force field(Jorgensen, Maxwell et al. 1996) was used to represent the SWCNT and TIP3P(Jorgensen, Chandrasekhar et al. 1983) water model was used to represent water. Each simulation system comprised one peptide chain, one SWCNT and water molecules

as shown in **Fig. 1(a)**. The number of water molecules varied based on the peptide chain. In all systems there were at least 15800 water molecules (**Table 2**).

Table 2. Peptides studied - These peptides have been reported to have affinity for

No.	Peptide sequence	No. of water
1	His-Trp-Lys-His-Pro-Trp-Gly-Ala-Trp-Asp-Thr-Leu	15868
2	His-Trp-Lys-His-Pro-Ser-Gly-Ala-Trp-Asp-Thr-Leu	15876
3	His-Asn-Trp-Tyr-His-Trp-Trp-Met-Pro-His-Asn-Thr	15861
4	His-Trp-Ser-Ala-Trp-Trp-Iso-Arg-Ser-Asn-Gln-Ser	15867
5	His-His-Trp-His-His-Trp-Cys-Met-Pro-His-Lys-Thr	15857

Similar molecular dynamics (MD) simulations were performed to study the interactions of these five discrete peptides with a graphene sheet in explicit water. These simulations allowed a comparative assessment of the possible role of curvature on peptide binding. In these simulations, a 8x8 nm2 graphene sheet was placed at the center of a 9x9x9 nm3 simulation box with explicit water (see Fig. 1(b)). Note that the graphene sheet was non-periodic. Representative snapshots of the starting configuration of the SWCNT-peptide-water and graphene-peptide-water systems used in the simulations are shown in Fig. 1. The OPLS force field was used to represent the graphene sheet and the non-bonded parameters of the carbon atoms (i.e., Lennard-Jones parameters) were the same as those specified for the carbon atoms in the SWCNT simulations. MD simulations were performed using GROMACS v4.5.5(Hess, Kutzner et al. 2008). Periodic boundary conditions were applied and electrostatic interactions were calculated using the Particle

Mesh Ewald (PME) method.(Darden, York et al. 1993) Velocity rescaling algorithm(Bussi, Donadio et al. 2007) was used to maintain constant temperature and Berendsen algorithm(Berendsen, Postma et al. 1984) was used to maintain constant pressure. The peptide and water were coupled to separate thermostats each with a time constant of 0.5 ps. The time constant of 0.5 ps was used for the barostat with the compressibility approximated by that of pure water at the system pressure. LINCS algorithm was used to constrain the bonds involving hydrogen atoms in water and the peptides.(Hess, Bekker et al. 1997) The coordinates of the atoms were captured and stored every picosecond for further analysis.

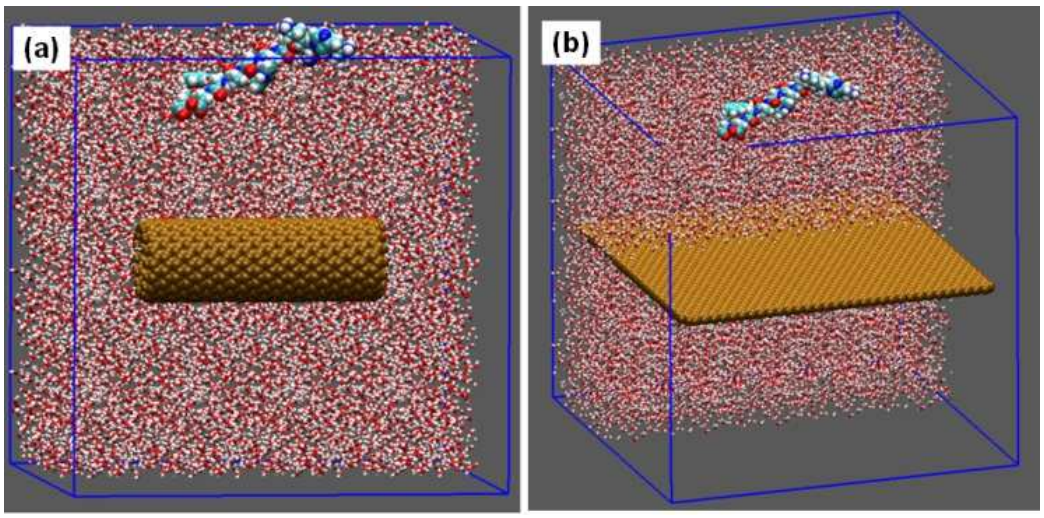

Fig. 1: Snapshots of the starting configuration of the (a) SWCNT-peptide-water and (b) graphene-peptide-water simulation systems. SWCNT and graphene sheet are shown in brown with spacefill representation, the peptide is shown in spacefill with atoms colored as cyan for carbon, red for oxygen, blue for nitrogen and white for hydrogen. Water

molecules are shown in red (oxygen) and white (hydrogen). Subset of water molecules are not shown for visual clarity.

The solubility parameter(Hildebrand and Scott 1950) (δ) (eq. (1) and (2)) when used in conjunction with Flory-Huggins theory(Fried 2003) (eq. (3)) supports general guidelines for the chemical compatibility and miscibility of organic components such as solvents and/or polymers.

$$\delta^2 = \frac{\Delta E}{V_m}. \qquad (1)$$

$$\delta^2 = \delta_d^2 + \delta_p^2 + \delta_h^2 = \frac{\Delta E_d}{V_m} + \frac{\Delta E_p}{V_m} + \frac{\Delta E_h}{V_m}. \qquad (2)$$

$$\chi = \chi_H + \chi_S = \frac{V_m}{RT}(\delta_1 - \delta_2)^2 + \chi_S.$$

$$= \frac{V_m}{RT}\left[\left(\delta_{d_1} - \delta_{d_2}\right)^2 + \left(\delta_{p_1} - \delta_{p_2}\right)^2 + \left(\delta_{h_1} - \delta_{h_2}\right)^2\right] + \chi_S. \qquad (3)$$

where δ is the total solubility parameter (the Hildebrand solubility parameter), ΔE is the cohesive energy, the subscripts d, p, and h represent the dispersion forces, polar interactions, and hydrogen bonding contributions, respectively, V_m is the molar volume, χ is the Flory-Huggins interaction parameter, the enthalpy term χ_H can be calculated from either the Hildebrand-Scatchard regular solution theory or the Hansen solubility parameter

theory,(Hansen 2007) χ_S is the residual entropy contribution, *R* is the gas constant, *T* is the temperature, and the subscripts 1 and 2 refer to the solvent and solute, respectively. Using this formalism, and Hansen solubility parameter values of each individual amino acid, the solubility parameter of each of the five candidate peptides was calculated (**Table 3**) These Hansen solubility parameter values were calculated using the Hansen solubility parameter in practice (HSPiP) program

The combined consensus hydrophobicity scale (CCS)(Eisenberg, Weiss et al. 1982; Kyte and Doolittle 1982) was used to calculate the hydrophobic index for each peptide (**Table 3**). The CCS was derived from two consensus scales; a general consensus scale (GCS) based on 160 normalized and filtered hydrophobicity index (Hi) scales of all types found in the literature, and an experimental consensus scale (XCS) based on 33 normalized and filtered Hi literature scales obtained by purely experimental methods.

Pearson Correlation Coefficient, *r*, (also Pearson Product Moment Correlation) was used to measure the quality of the relation between various peptide attributes. This is shown in equation (4) where *x* represents one set of parameters and *y* represents another.

$$r = \frac{n(\sum xy) - (\sum x)\sum y}{\sqrt{[n\sum x^2 - (\sum x)^2][n\sum y^2 - (\sum y)^2]}} \qquad (4)$$

The possible values of *r* range from -1 to 1. A high correlation has *r* values from 0.5 to 1.0 or -0.5 to -1.0, medium correlation from 0.3 to 0.5 or -0.3 to -0.5, a low correlation from 0.1 to 0.3 or -0.1 to -0.3 and no correlation gives a value of 0.

3.5 Results and Analysis

3.5.1 Progression in the radius of gyration

The progression in the radius of gyration, R_g, (a measure of compactness) of the peptide is a logical parameter to monitor the peptide configurations, as it progresses towards the carbon surfaces.(Lobanov, Bogatyreva et al. 2008) The final Rg value, along with contact information of individual residues with the carbon surfaces, together conveys information on the segmental interaction of the peptide with the carbon surface. All peptides studied demonstrated spontaneous adsorption onto the SWCNT. **Fig. 2(a)** is a plot of the radius of gyration, R_g, of the five peptides as they progress towards their spontaneous adsorption on to the surface of the SWCNT.

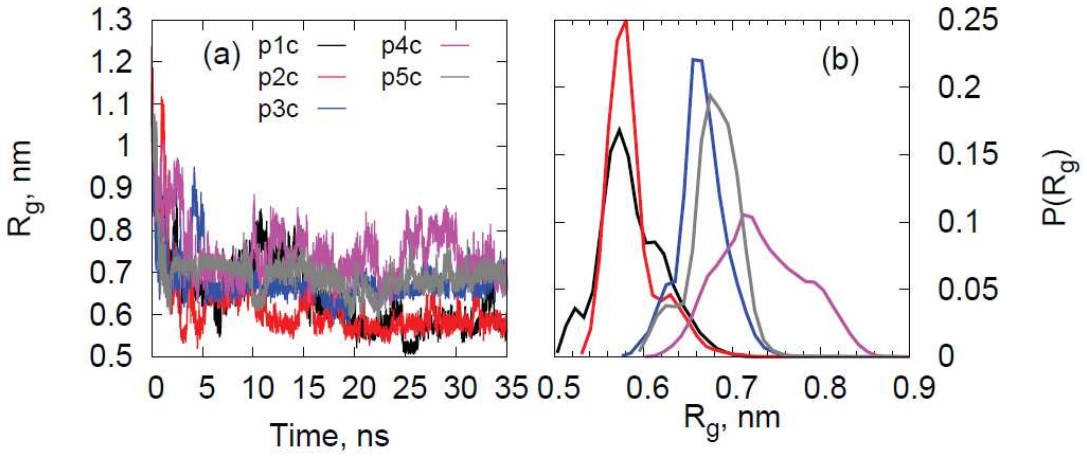

Fig. 2: (a) Radius of gyration, R_g, of peptides during the simulations of SWCNT-peptide-water systems. All peptides displayed collapsed configurations relative to their initial

extended configurations. (b) Distribution of R_g for the five peptides in the vicinity of the SWCNT calculated over 25 – 35 ns. Clearly, while all five peptides adsorbed to the surface of the SWCNT, their configurations on the SWCNT surface were quite varied. Peptides 1 and 2 were more compact, while peptide 4 was the most extended on the SWCNT surface. Color code: Black: peptide-1; red: peptide-2; blue: peptide-3; magenta: peptide-4; gray: peptide-5. Naming convention of pNc represents peptide-N-on-SWCNT, where N=1, 2, 3, 4 or 5.

The decrease in the R_g values during the first few nanoseconds of the simulation is consistent with the adsorption of the peptides to the SWCNT. The peptides tend to become more compact relative to the extended states from which the simulations were started in the vicinity of the SWCNT. Interestingly, the distribution of the R_g values varies among the different peptides. As seen in **Fig. 2(b)**, the distribution of the R_g, values varies with the peptide sequence. Peptides 1 and 2 were more compact, while peptide 4 was the most extended following adsorption onto the SWCNT surface. Both peptides 1 and 2 have hydrophobic residues at the C- and N-terminal regions. Also, peptide 1 and 2 differ in only one residue at the 6^{th} position. Peptide 1 has TRP, which is replaced by SER in peptide 2. In contrast to peptides 1 and 2, residues 9-12 are non-hydrophobic in both peptides 3 and 5, while residues 8-12 in peptide 4 are non-hydrophobic.

Fig. 3 illustrates the interactions discussed in the previous section as it relates to peptides 3 and 4 with the (16,0) SWCNT and graphene respectively. Peptide-4 has most of its hydrophobic residue in contact with the SWCNT while orienting the non-hydrophobic

residues towards water (**Fig. 3(c)**). In contrast, some non-polar residues are further away from the SWCNT and closer to water in case of peptide-3.(**Fig. 3(a)**).

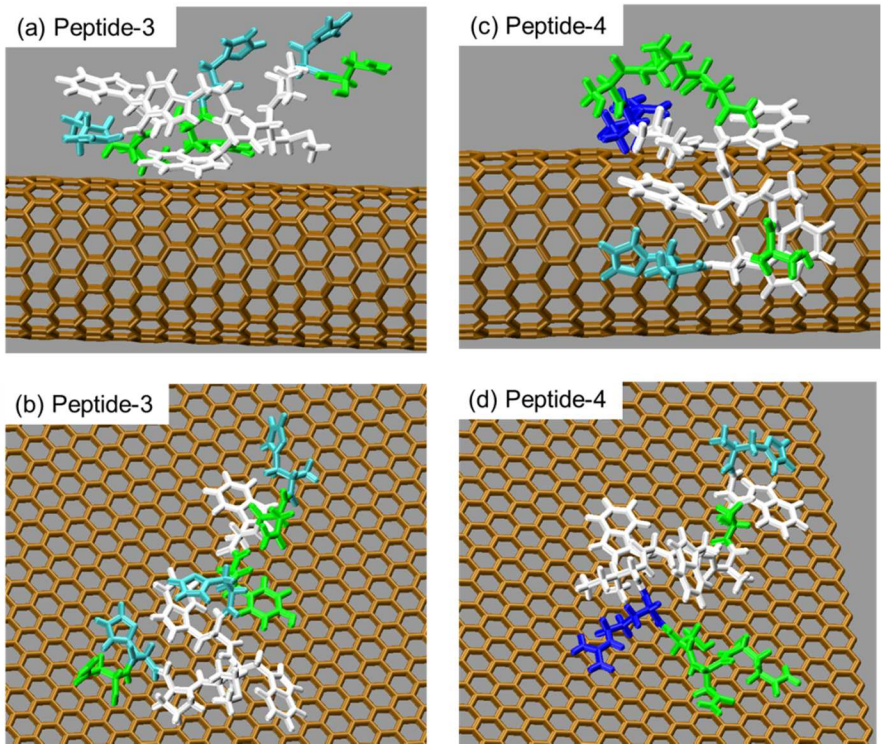

Fig. 3: Snapshots of peptide-3 and peptide-4 after 35 ns of simulation: (a) peptide-3 in SWCNT-peptide-water system, (b) peptide-3 in graphene-peptide-water system, (c) peptide-4 in the SWCNT-peptide-water system, and (d) peptide-4 in the graphene-peptide-water system. The residues are colored based on residue type with non-polar residues shown in white, basic residues are blue, acidic residues are red, polar residues are green, and histidine is shown in cyan. Histidine was protonated on the epsilon nitrogen.

3.5.2 Adsorption – distance between peptide and SWCNT

Fig. 4(a-j) shows the minimum distance between the aa-residues of the peptide and the SWCNT surface as averaged over the last 10 ns of the simulation. In all cases except that of peptide-1, the peptides adsorbed to the SWCNT within ~10 ns. The minimum distance was calculated as the smallest distance between the heavy atoms (C, N, O, and S) of the side chain of a given residue and the carbon atoms of the SWCNT. We consider the peptide to be in contact with the SWCNT when the distance between the heavy atoms of the side chain of a given residue was less than 0.4 nm. The distance of 0.4 nm was chosen because the first minimum of methane-methane potential of mean force in water occurs around this distance.(Ghosh, García et al. 2001)

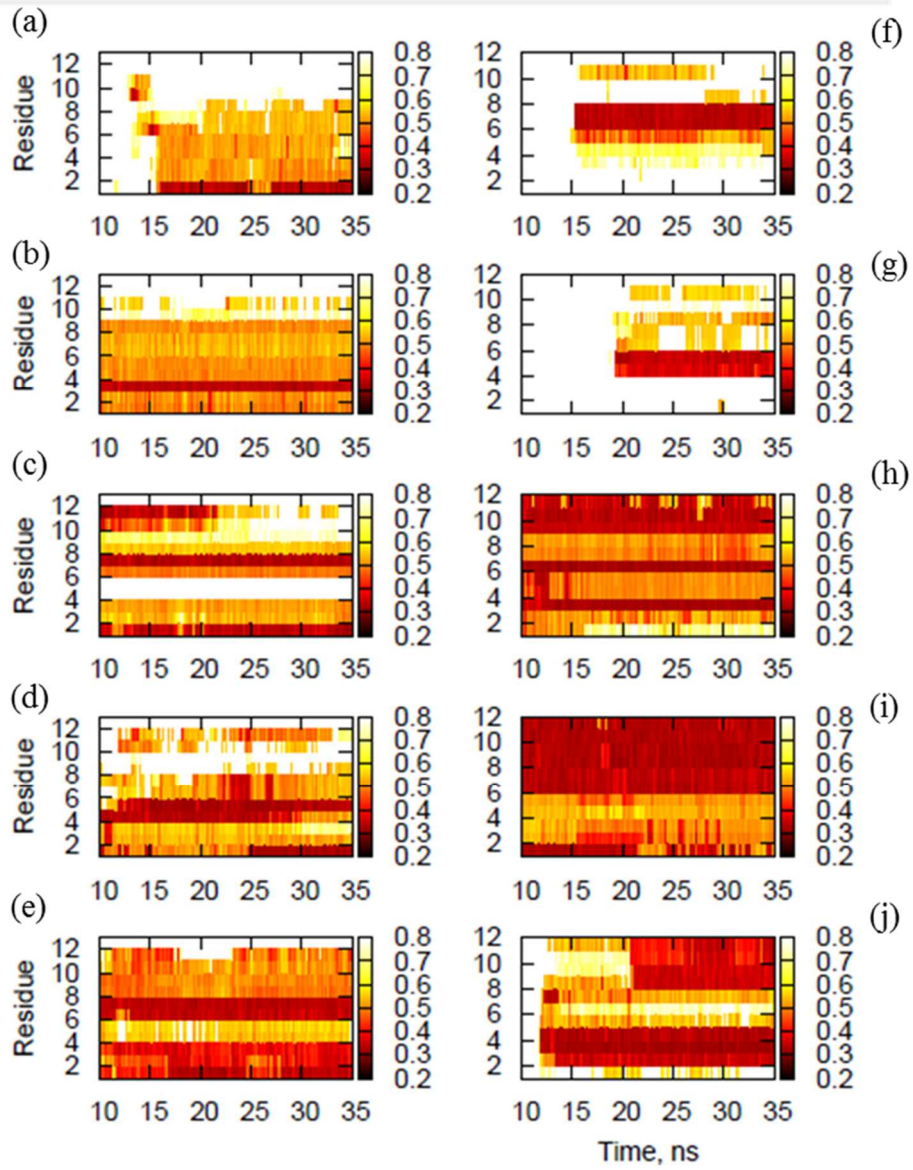

Fig. 4: Residue contact (in nm) for peptides 1 (a) through 5 (e) with SWCNT and for peptides 1 (f) through 5 (j) with graphene. The figure shows the minimum distance between the residue of the peptide and carbon atoms of the SWCNT or graphene (y-axis) as a function of time up to 35 ns. Any distance greater than 0.7 nm will be white.

3.5.3 Adsorption – interactions of specific residues

It is expected that hydrophobic residues will drive the binding of the peptides to the SWCNTs. Indeed in the case of peptide-1, the residues closest to the SWCNT (i.e. distance < 0.4 nm) include 2TRP, 4HIS and 6TRP (**Fig. 4 and 6(a)**). In contrast, in peptide-2, which differs from peptide-1 in only the sixth residue, the residues closest to the SWCNT are 1HIS, 3LYS, 4HIS, 6SER, and 9TRP. Thus, a single residue change at position 6 has a profound influence on the pattern of adsorptive interaction. It is however, worth noting that although the adsorption pattern for peptide-1 and 2 differ, their R_g distributions overlap significantly. For peptide-3, the residues 1HIS, 2ASN, 4TYR, 7TRP and 8MET are in contact with the carbon nanotube. Residues 1HIS, 2 TRP, 5TRP, 6TRP and 8ARG of peptide-4; and residues 1HIS, 2HIS, 4HIS, 6TRP, 7CYS, 8MET, 10HIS, and 12THR of peptide-5 are in contact with the SWCNT. In the latter case, the distances of the residues 2HIS and 10HIS from SWCNT are approximately equal to our contact cut-off distance, 0.4 nm. In all cases, except for peptide-1, we find that the N-terminal binds to the SWCNT, while the C-terminal remains essentially unbound.

3.5.4 Comparison with graphene

MD simulations were also performed on the interactions of the five peptides with graphene sheet in explicit water in order to evaluate the effect of curvature of the carbonaceous nanostructures on the peptide-nanomaterial interactions. In addition, we also performed simulations of the peptides in explicit water in the absence of any carbonaceous nanostructure. As seen in the case of SWCNT, we find that all peptides adsorb to the

graphene sheet. Similar to the observation in case of SWCNT, we find that the R_g distribution of the peptides adsorbed on the graphene sheet varies with the peptide sequence **(Fig. 5)**. In the case of graphene, peptide-3 displays the most extended conformation, while peptide-2 is the most compact. This is in contrast with SWCNT where peptide-4 is the most extended and peptides-1 and 2 are similarly the most compact.

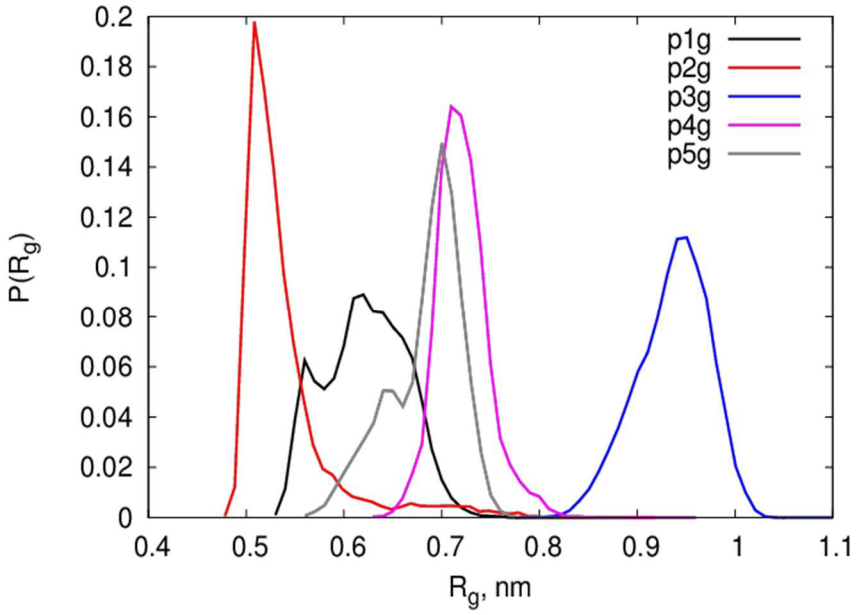

Fig. 5: Distribution of the radius of gyration, R_g, of peptides calculated over the last 10 ns of the simulations of graphene-peptide-water system. Clearly, while all the peptides adsorbed to the surface of graphene, their configurations on the graphene sheet were quite varied. Peptides 1 and 2 were more compact, while peptide 3 was the most extended on the graphene surface. Color scheme is the same as in Fig. 2.

Differences between the adsorption of peptides can be observed from the residue-nanostructure contact distance (**Figs. 3, 4 and 6**). Residues 6TRP, 8ALA, 9TRP and

12LEU of peptide-1; and residues 5PRO, 6SER, 9TRP and 12LEU of peptide-2 are in contact with the graphene sheet. In peptides 3, 4 and 5 most residues are in contact with the graphene sheet. This indicates that the peptides approach a two-dimensional flat structures on the graphene sheet and are correspondingly larger in their sizes (R_g-values) than in bulk or near the SWCNTs. In the case of peptide-2, the only peptide to become more compact near the graphene sheet, the number of residues in contact with graphene relative to the SWCNT decreases. Peptide-2 seems to be adsorbed to the graphene sheet primarily through the contact of residues 5PRO and 6SER.

Since these five peptide sequences were obtained from phage display and SMD experiments, their sequences do not follow systematic differences. However, some features can be described. In all peptides except peptide-5 there is at least one pair of neighboring hydrophobic residues. Peptide-4 has the largest sequence of consecutive hydrophobic residues (4ALA-5TRP-6TRP-7ILE). Peptide-3 has two smaller consecutive hydrophobic residues (3TRP-4TYR and 6TRP-7TRP-8MET) separated by one residue (5HIS). Peptide conformations are governed by intrapeptide, peptide-water, peptide-nanomaterial, water-nanomaterial and water-water interactions, which are challenging to elucidate and beyond the scope of the presented work. The precise reason for the differences in the conformations of the peptides at these surfaces is not yet known.

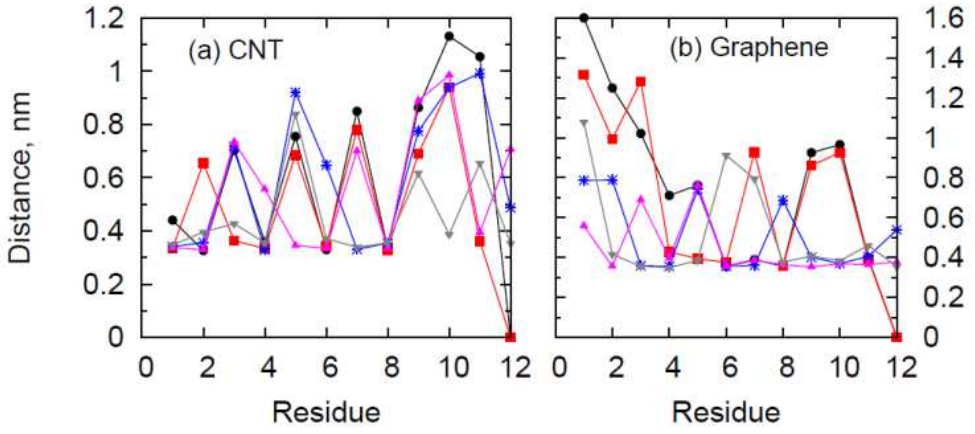

Fig. 6: Average of minimum distance between residue and SWCNT (left) and graphene (right). Color scheme is the same as in Fig. 2. Note that in peptides 1 and 2, since residue-7 is GLY, which has no side chain, the distance between the residue and carbon surface was not calculated. In the figures, residues 7-11 therefore, correspond to residues 8-12 for peptides 1 and 2.

Fig. 7(a) shows the distribution of the R_g values of the five peptides in bulk water, in the absence of any nanostructure. Unlike the cases of the R_g values of the individual peptides on SWCNT and graphene (**Fig. 7(b-f)**), the distribution of R_g values for all peptides overlap considerably, indicating that the peptides are similarly compact in bulk water irrespective of the peptide sequence. **Fig. 7(b-f)** compares the distribution of the R_g values for each peptide in bulk, near SWCNT and in the vicinity of the graphene sheet. We find that the peptides, which in bulk tended to be relatively extended, are compact near the nanostructures. In all cases, the distribution on SWCNT is placed somewhere between that in bulk and near the graphene sheet. For example, the R_g distribution of peptide-1 in bulk water is skewed towards larger values. This distribution becomes peaked towards the larger

values of R_g when the peptide is adsorbed on the SWCNT and graphene sheet. Similar effects are observed in the case of peptides 3, 4 and 5. In contrast, peptide-2 becomes more compact relative to bulk in the vicinity of the nanostructures. Interestingly, peptide-2 is the only peptide to have a hydrophilic group (SER) at residue 6, which is hydrophobic (TRP) in all other peptides. Peptide-3 undergoes significantly more extension on graphene than on (16,0) SWCNT. **Fig. 3(a) and (b)** indicate that near the graphene sheet peptide-3 can structure such that the non-polar residues are close to graphene and the polar residues are oriented towards water. On the other hand, near the SWCNT several non-polar residues are oriented towards water. Peptide-4 structures such that most non-polar residues are in contact with the nanostructure, in case of both SWCNT and graphene (**Fig. 3(c) and (d)**).

Recent studies have indicated that water fluctuations near hydrophobic surfaces provide a measure of the hydrophobicity of surfaces at the molecular level.(Godawat, Jamadagni et al. 2009; Sarupria and Garde 2009) In a previous study, we showed that water fluctuations, and therefore hydrophobicity, increased as the curvature of the surface was reduced (Sarupria and Garde 2009). That is, in this case, the SWCNT is expected to be less hydrophobic than the graphene sheet by virtue of its curvature. This suggests that there is a correlation between the hydrophobicity of the surface and the deviation in the peptide structure near the surface relative to that in bulk water, as seen in **Fig. 7(b-f)**.

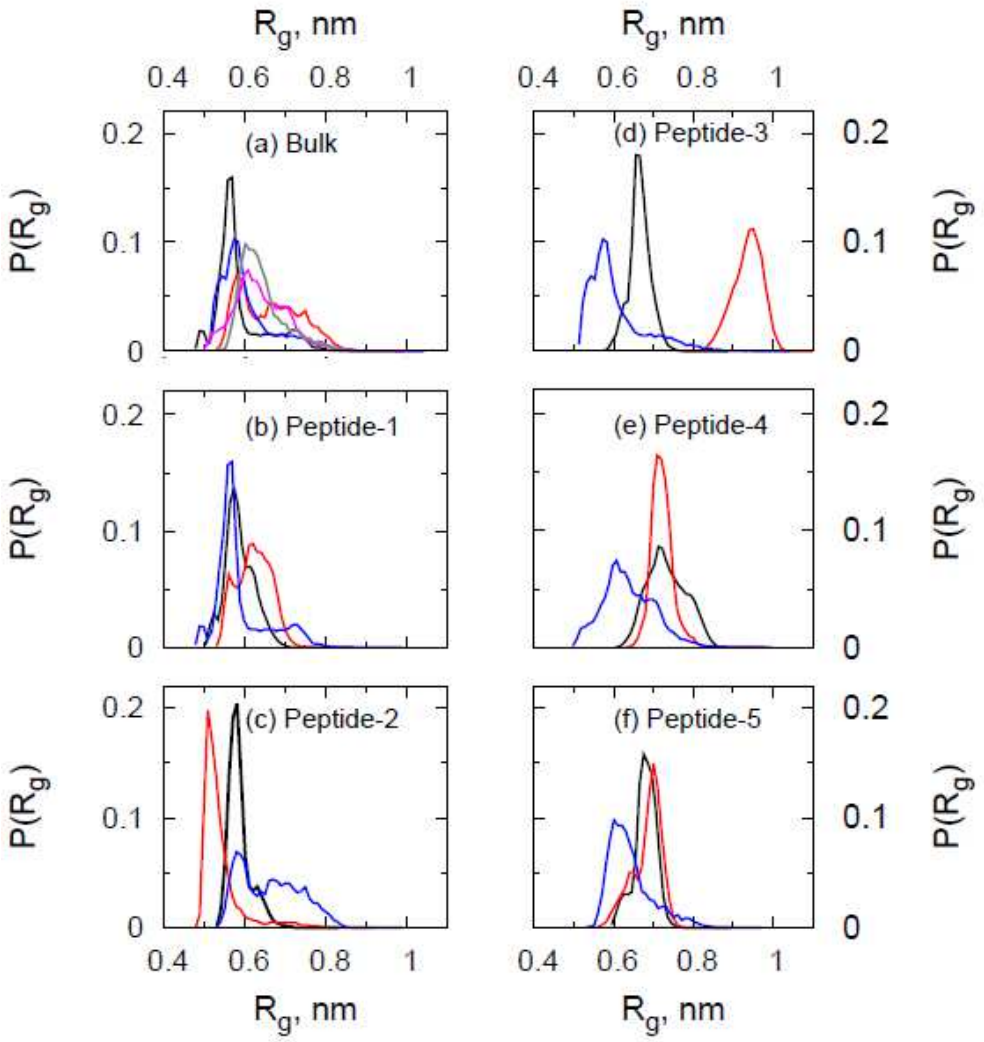

Fig. 7: (a) Comparison of radius of gyration, Rg, of the five peptides in bulk and (b-f) comparison of the radius of gyration, Rg, of the individual peptides in bulk (blue), SWCNT (black) and on graphene sheet (red). Color scheme in panel (a) is the same as that in Fig. 2.

3.6 Discussion

The peptides studied (from phage display) are important for their acknowledged strong interaction with SWCNTs. The relative importance of the peptide sequences is to serve as a rational starting point to investigate corresponding sequences within enzymes of interest (glucose oxidase, lactate oxidase and laccase) so that we may form non-covalent, supramolecular conjugates for generation-3 biosensors and advanced enzyme biofuel cells. We are interested to know if similar sequences occur within the subject enzymes, if they do occur where are they located within the enzyme (close to the binding site, cofactor or some other location).

Table 3. Summary of the calculated physicochemical attributes of the five peptides studied. (See text for details of calculations)

					‡Hydrophobicity				***Solubility Parameter (δ)**	**†R_g,Mean over 10 ns (nm)**	
						CCS scale, 180°			$(J/cm^3)^{½}$	SW CNT	Graphene
Peptide	MW	IP	Net Charge	Attribute	(Nh/N)* 100	mH	mHm	mHrel	Mean		
HWKHPWGAWDTL	1533.7	7.72	2	Basic	41.67	0.45	2.19	0.21	25.9	0.59	0.62
HWKHPSGAWDTL	1434.6	7.72	2	Basic	33.33	-0.70	1.02	0.10	26.4	0.59	0.54
HNWYHWWMPHNT	1708.9	7.80	3	Basic	41.67	0.55	0.20	0.02	27.2	0.66	0.94
HWSAWWIRSNQS	1557.7	10.55	2	Basic	41.67	-0.25	0.25	0.02	27.5	0.73	0.72
HHWHHWCMPHKT	1636.9	8.58	6	Basic	33.00	-0.93	0.78	0.07	26.4	0.68	0.68
SWCNT	-	-	-	-	-	-		-	15.5[18]	-	-
Graphene	-	-	-	-	-	-		-	23.0[36]	-	-

‡ See Section 3.5.1;*See Section 3.3; †See Section 3.4.1

3.6.1 The solubility parameter and hydrophobicity for each peptide and SWCNT

Table 4. Pearson Correlation Coefficient among the various attributes			
R_g *vs.* Solubility Parameter, δ	R_g *vs.* Mean Hydrophobicity Index, mH.	R_g *vs.* Mean Hydrophobic moment, mHm	R_g *vs.* Relative Hydrophobic moment, mHrel.
0.7979	-0.1706	-0.7548	-0.0998

The solubility parameter of SWCNT has been reported to vary inversely with the diameter of the SWCNTs, being 19.7 $(J/cm^3)^{½}$ for the (6,0) SWCNT-5 ($\phi = 0.47$), 18.07 $(J/cm^3)^{½}$ for the (10,0) SWCNT-5 ($\phi = 0.78$), and 15.95 $(J/cm^3)^{½}$ for the (15,0) SWCNT-5 ($\phi = 1.17$) (Lee, Lim et al. 2013). By extrapolation, the (16,0) SWCNT ($\phi = 1.25$) studied in this work has a solubility parameter of 15.53 $(J/cm^3)^{½}$. The solubility parameters of the five peptides were calculated (as described in the Methods section), and are presented in **Table 3**. There is clearly a considerable difference in the solubility parameter between the (16,0) SWCNT ($\phi = 1.270$) of 15.53 $(J/cm^3)^{½}$ and that of the peptides, which range from 25.9 - 27.5 $(J/cm^3)^{½}$. This suggests little or no compatibility between the peptides and the SWCNTs.

The hydrophobicity of a peptide may be expressed using parameters such as the percentage of hydrophobic residues (FLYWAVIMC) within the peptide (**Col. 6, Table 3**),**mean hydrophobicity index**, **mH** (**Col. 7, Table 3**) **mean hydrophobic moment (mHm)** (the vector sum of individual hydrophobicity indices divided by the number of residues) (**Col. 8, Table 3**), and the **relative hydrophobic moment (mHrel)** (the mean hydrophobic moment relative to that of a reference amphipathic peptide) (**Col. 8, Table 3**).

The **mH and mHrel** values depend upon the selected scale and conformation, in this case the CSS and 180°.

The Pearson correlation among the final radius of gyration, $R_{g,}$, of the peptides as revealed by MD simulations and the hydrophobicity indices and solubility parameter attributes is summarized in **Table 4.** The radius of gyration is seen to strongly correlate with the solubility parameter (0.80) and to equally strongly anti-correlate with the mean hydrophobicity moment (-0.76). Correlation with the mean hydrophobic index is weak (-0.17) and is essentially non-existent with the relative hydrophobic index (-0.10). The strong correlation between the radius of gyration (a measure of the compactness of the peptide upon its adsorptive interaction with the SWCNT) and the solubility parameter (a measure of its chemical compatibility with the SWCNT) suggests that the solubility parameter may in fact be a suitable initial screening criterion for the selection of peptides for the debundling and individualization of SWCNTs. Interestingly, we find that the solubility parameter is very strongly anti-correlated with the relative hydrophobic index (-0.90).

Table 5. Summary of some of the homologous sequences for Peptide 1 (**HWKHPWGAWDTL**). The Universal Protein Resource database was consulted and Peptide 1 (row [A]) mapped to specific enzymes of interest; glucose oxidase (1GPE, 1CF3), lactate oxidase (2J6X), and laccase (1GYC). The analogous positions (row [B]) and sequences (row [C]) within these enzymes are also included. An alignment will display the following symbols ("*", "**:**", or "**.**") denoting the degree of conservation (row [D]) observed in each column:

- An "*" (asterisk) indicates positions which have a single, fully conserved residue.
- A ":" (colon) indicates conservation between groups of strongly similar properties - scoring > 0.5 in the Gonnet PAM 250 matrix.
- A "." (period) indicates conservation between groups of weakly similar properties - scoring =< 0.5 in the Gonnet PAM 250 matrix.

Selective affinity for SWCNT (**HWKHPWGAWDTL**)

GOx (1GPE) [GOx125 – GOx131, GOx136 – GOx140]	[A]	**H**	**W**	**K**	**H**	**P**	**W**	**G**	**A**	**W**	**D**	**T**	**L**
	[B]	125	126	127	128	129	130	131	136	137	138	139	140
	[C]	S	W	E	K	V	F	G	N	W	D	N	M
	[D]		*	:	:		:	*		*	*	.	:
GOx (1CF3) [GOx110 – GOx115, GOx120 – GOx125]	[A]	**H**	**W**	**K**	**H**	**P**	**W**	**G**	**A**	**W**	**D**	**T**	**L**
	[B]	110	111	112	113	114	115	120	121	122	123	124	125
	[C]	T	W	T	R	P	H	D	S	W	E	T	V
	[D]		*	.	:	*			:	*	:	*	:
LOx (2J6X) [LOx330 – 341]	[A]	**H**	**W**	**K**	**H**	**P**	**W**	**G**	**A**	**W**	**D**	**T**	**L**
	[B]	330	331	332	333	334	335	336	337	338	339	340	341
	[C]	G	W	Q	G	A	Y	S	V	L	D	Y	F
	[D]	*	:				:	.	.		*		:
Lac (1GYC) [Lac64 – Lac69, Lac489 – Lac494]	[A]	**H**	**W**	**K**	**H**	**P**	**W**	**G**	**A**	**W**	**D**	**T**	**L**
	[B]	64	65	66	67	68	69	489	490	491	492	493	494
	[C]	H	W	H	G	F	F	P	I	Y	D	G	L
	[D]	*	*	:			:			:	*		*

This is suggestive of the fact that peptides isolated via phage display using SWCNTs as substrates are expected to be amphiphilic rather than hydrophobic, reflecting the need to serve as interfacial molecules set between the hydrophobic carbonaceous material and the aqueous milieu from within which they were derived.

3.6.2 Homology with relevant enzymes

In the design of advanced biosensors and biofuel cells we are interested in the use of enzymes such a glucose oxidase (1GPE, 1CF3 for the amperometric measurement of glucose and for service as the anodic catalysts in enzyme biofuel cells), lactate oxidase (2J6X for the amperometric detection of lactate) and

laccase (1GYC for service as the cathode catalysts in enzyme fuel cells). Each of these enzymes may be fashioned into supramolecular complexes by physical or chemical conjugation with SWCNTs. The goal in the fashioning of such complexes is to achieve strategic placement of the SWCNT within tunneling distance of the redox cofactor of the enzyme and so achieve rapid charge transfer and ballistic conduction along the SWCNT towards discharge at the electrode. It is therefore of interest to learn if the peptides identified by phage display and studied by adsorptive interaction using MD simulations in this paper also exist within the above referenced enzymes. To obtain this sequence homology certain online resources were used.(Cui, Lee et al. 2001; Kim, Abidian et al. 2004) To evaluate this, the Universal Protein Resource data base was consulted (UniProt Consortium http://www.uniprot.org/)(Consortium 2013) and the FASTA amino acid sequence for each of the above enzymes was obtained. The principal peptide sequence

(Peptide-1 HWKHPWGAWDTL) was then mapped to the enzyme sequence. Analogous sequences and their positions are displayed in **Table 5**.

For GOx (1GPE), it is evident that an almost perfect match exists in the form of an almost contiguous sequence that occurs between GOx125–140 with a 4-residue interruption between GOx132-135. Similarly, for GOx (1CF3), an almost perfect match exists between GOx110–125 with a 4-residue interruption between GOx116-119. For LOx (2J6X), there exists a perfect match with peptide-1 sequence found to reside at LOx330–341. For Lac (1GYC), the sequence is found in two vastly different parts of the protein. A partial match was found between Lac64–69 and the remains of the match found at Lac489–494. It is anticipated that these sequences, having been identified by phage display as being strongly interacting with SWCNT should, like the SWCNTs, be hydrophobic and as such should be buried(Meirovitch, Rackovsky et al. 1980; Silverman 2001) deep within the structure of fully folded proteins, much like the redox-active prosthetic groups of the oxidoreductases of interest.

3.6.3 Location of homologous sequences within relevant enzymes

It is unclear if SWCNTs that are interacting with these homologous sequences will in fact disturb the native 3D structure of the protein. The early functional evidence suggests not, as conjugates are being formed with high residual enzyme activity.(Owino, Arotiba et al. 2008; Karunwi and Guiseppi-Elie 2013) **Fig. 8** shows the structure of the four enzymes (glucose oxidase - 1GPE, glucose oxidase - 1CF3, lactate oxidase - 2J6X, laccase - 1GYC) and the location of the four analogous peptide-1 sequences (HWKHPWGAWDTL) in the 3D structure. Contrary to expectation these analogous sequences occur on the surface of

the enzyme or the sub-unit. Interestingly, for glucose oxidase and lactate oxidase, although the affinity sequence is interrupted, the affinity residues are quite close to each other in the folded enzyme. Laccase shows one portion deeply embedded and the other on the surface.

An interesting secondary question is where are these analogous affinity sequences located relative to the enzyme's prosthetic groups? In **Fig. 8**, the residues that bind the cofactors (FAD in glucose oxidase, FMN in lactate oxidase and copper in laccase) are shown in yellow. For 1GPE they are separate but proximal. In 1CF3 they are quite close to each other with T110 (GOx95 to GOx109 that bind to FAD) being very close to the affinity peptide sequence. Finally, in 2J6X, there is overlap (H64 and H66) between binding site for copper and the analogous affinity sequence. The close proximity of these analogous binding peptides to prosthetic groups portend well for the creation of supramolecular conjugates that place the SWCNT within tunneling distance (ca. 10 Å) of the cofactor. The high aspect ratio of tubes will similarly suggest that some part of the tube will likely achieve such proximal placement. The enzyme *pseudoazurin,* the blue copper protein that shares some homology/analogy with laccase,(Stevens 2008) has been shown to participate in direct electron transfer with SWCNTs.(Guiseppi-Elie, Brahim et al. 2005) However, it is tubes ends that appear to have the highest electrocatalytic activity(Hao, Dong et al. 2012; Yuan, Zhou et al. 2013) and their placement within tunneling distance of redox active prosthetic groups will be far more challenging.

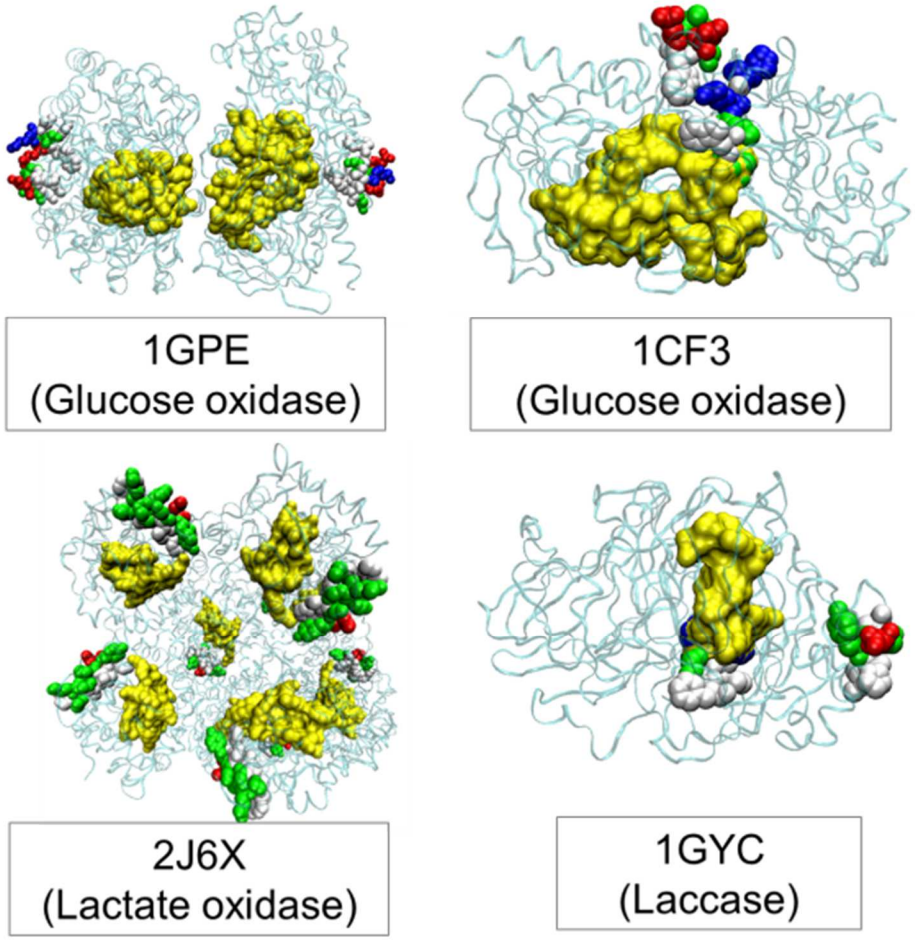

Fig. 8: Structure of the enzymes 1GPE, 1CF3, 2J6X and 1GYC showing the location of the analogous peptides [non-polar residues (white), basic residues (blue), acidic residues (red), polar residues (green)] and binding sites for cofactors (yellow).

The peptide sequences obtained from phage display are usually not present as a contiguous sequence in proteins. The MD simulations presented here highlight that based on the peptide affinity sequence identified by phage display, the protein can have different structure while retaining its propensity to bind/adsorb to the SWCNTs. One can expect however that they may occur spatially close to each other in the enzyme structures. We don't see, within the protein structures, sequentially contiguous residues matching the high

affinity peptides, however, we find sections. These sections appear spatially "contiguous". Hence, a combination of the sequence analogy and spatial arrangement could result in absorption without appreciable change in global protein structure. The MD simulations suggest that the high affinity binding peptide do not bind fully to the SWCNT. Some residues meet the criterion for contact while others do not. Therefore, R_g values, reflective of the physicochemical embrace of the surface (SWCNT or graphene) have a strong positive correlation with the solubility parameter but do not correlate with the usual global indicators of hydrophobicity of the peptides.

3.7 Conclusions

Using MD simulations we have followed the progression of the radius of gyration, measured the final radius of gyration, and the final residue proximity of five 12-residue peptides derived from phage display as they interact with (16,0) SWCNT and graphene sheets. We have found that the peptides were concertedly adsorbed and that the adsorption behavior was governed by peptide segments as evidenced by the strong correlation between the solubility parameter and the final radius of gyration and the equally strong anti-correlation with the mean hydrophobicity moment. Single residue changes, such as that at position 6 had profound influence on the pattern of adsorptive interaction. The end residue appears to dominate the progression to adsorption. Curvature is confirmed as a major factor in the adsorptive interaction of peptides with SWCNTs where SWCNTs of smaller diameter appear less hydrophobic. Consensus sequences identified by phage display share analogy with important enzymes used in biosensors and enzyme-based biofuel cells. These sequences appear to be proximal to the sites of association with the redox-active prosthetic

groups. There is the potential to extend this study to investigate analogous sequences present in other enzymes and proteins. Further confirmation of adsorptive behavior could be confirmed by running the entire enzyme or protein system with the various carbonaceous surfaces.

3.8 Acknowledgments

This work was supported by the US Department of Defense (DoDPRMRP) grant PR023081/DAMD17-03-1-0172, by the Calhoun Honors College at Clemson University, by the Consortium of the Clemson University Center for Bioelectronics, Biosensors and Biochips (C3B) and by ABTECH Scientific, Inc. Computations were performed on Palmetto supercomputer maintained by Clemson Computing and Information Technology at Clemson University.

3.9 References

1. Guiseppi-Elie, A., C. Lei, and R.H. Baughman, *Direct electron transfer of glucose oxidase on carbon nanotubes.* Nanotechnology, 2002. **13**(5): p. 559.

2. Zhu, Z., L. Garcia-Gancedo, A.J. Flewitt, H. Xie, F. Moussy, and W.I. Milne, *A Critical Review of Glucose Biosensors Based on Carbon Nanomaterials: Carbon Nanotubes and Graphene.* Sensors, 2012. **12**(5): p. 5996-6022.

3. Saifuddin, N., A.Z. Raziah, and A.R. Junizah, *Carbon Nanotubes: A Review on Structure and Their Interaction with Proteins.* Journal of Chemistry, 2013. **2013**: p. 18.

4. Guiseppi-Elie, A., A.R.A. Rahman, and N.K. Shukla, *SAM-modified microdisc electrode arrays (MDEAs) with functionalized carbon nanotubes.* Electrochimica Acta, 2010. **55**(14): p. 4247-4255.

5. Banks, C.E. and R.G. Compton, *New electrodes for old: from carbon nanotubes to edge plane pyrolytic graphite.* Analyst, 2005. **131**(1): p. 15-21.

6. Banks, C.E., T.J. Davies, G.G. Wildgoose, and R.G. Compton, *Electrocatalysis at graphite and carbon nanotube modified electrodes: edge-plane sites and tube ends are the reactive sites.* Chemical communications, 2005(7): p. 829-841.

7. Banks, C.E. and R.G. Compton, *Exploring the electrocatalytic sites of carbon nanotubes for NADH detection: an edge plane pyrolytic graphite electrode study.* Analyst, 2005. **130**(9): p. 1232-1239.

8. Owino, J.H.O., O.A. Arotiba, P.G.L. Baker, A. Guiseppi-Elie, and E.I. Iwuoha, *Synthesis and characterization of poly (2-hydroxyethyl methacrylate)-polyaniline based hydrogel composites.* Reactive and Functional Polymers, 2008. **68**(8): p. 1239-1244.

9. Karunwi, O. and A. Guiseppi-Elie, *Supramolecular glucose oxidase-SWNT conjugates formed by ultrasonication: effect of tube length, functionalization and processing time.* Journal of Nanobiotechnology, 2013. **11**(1): p. 6.

10. Kotanen, C.N., F.G. Moussy, S. Carrara, and A. Guiseppi-Elie, *Implantable enzyme amperometric biosensors.* Biosensors and Bioelectronics, 2012. **35**(1): p. 14-26.

11. Neto, S.A., J.C. Forti, and A.R. Andrade, *An Overview of Enzymatic Biofuel Cells.* Electrocatalysis, 2010. **1**(1): p. 87-94.

12. Jia, W., C. Jin, W. Xia, M. Muhler, W. Schuhmann, and L. Stoica, *Glucose Oxidase/Horseradish Peroxidase Co-immobilized at a CNT-Modified Graphite Electrode: Towards Potentially Implantable Biocathodes.* Chemistry – A European Journal, 2012. **18**(10): p. 2783-2786.

13. Kim, J. and K.-H. Yoo, *Glucose oxidase nanotube-based enzymatic biofuel cells with improved laccase biocathodes.* Physical Chemistry Chemical Physics, 2013. **15**(10): p. 3510-3517.

14. Willats, W.T., *Phage display: practicalities and prospects.* Plant Molecular Biology, 2002. **50**(6): p. 837-854.

15. Wang, S., E.S. Humphreys, S.-Y. Chung, D.F. Delduco, S.R. Lustig, H. Wang, K.N. Parker, N.W. Rizzo, S. Subramoney, Y.-M. Chiang, and A. Jagota, *Peptides with selective affinity for carbon nanotubes.* Nat Mater, 2003. **2**(3): p. 196-200.

16. Yu, T., Y. Gong, T. Lu, L. Wei, Y. Li, Y. Mu, Y. Chen, and K. Liao, *Recognition of carbon nanotube chirality by phage display.* RSC Advances, 2012. **2**(4): p. 1466-1476.

17. Raut, V.P., M.A. Agashe, S.J. Stuart, and R.A. Latour, *Molecular Dynamics Simulations of Peptide−Surface Interactions.* Langmuir, 2005. **21**(4): p. 1629-1639.

18. Lee, K., H.J. Lim, S.J. Yang, Y.S. Kim, and C.R. Park, *Determination of solubility parameters of single-walled and double-walled carbon nanotubes using a finite-length model.* RSC Advances, 2013. **3**(14): p. 4814-4820.

19. Duan, Y., C. Wu, S. Chowdhury, M.C. Lee, G. Xiong, W. Zhang, R. Yang, P. Cieplak, R. Luo, T. Lee, J. Caldwell, J. Wang, and P. Kollman, *A point-charge force field for molecular mechanics simulations of proteins based on condensed-phase quantum*

mechanical calculations. Journal of computational chemistry, 2003. **24**(16): p. 1999-2012.

20. Jorgensen, W.L., D.S. Maxwell, and J. Tirado-Rives, *Development and testing of the OPLS all-atom force field on conformational energetics and properties of organic liquids.* Journal of the American Chemical Society, 1996. **118**(45): p. 11225-11236.

21. Jorgensen, W.L., J. Chandrasekhar, J.D. Madura, R.W. Impey, and M.L. Klein, *Comparison of simple potential functions for simulating liquid water.* The Journal of chemical physics, 1983. **79**(2): p. 926-935.

22. Hess, B., C. Kutzner, D. Van Der Spoel, and E. Lindahl, *GROMACS 4: Algorithms for highly efficient, load-balanced, and scalable molecular simulation.* Journal of chemical theory and computation, 2008. **4**(3): p. 435-447.

23. Darden, T., D. York, and L. Pedersen, *Particle mesh Ewald: An N [center-dot] log(N) method for Ewald sums in large systems.* The Journal of chemical physics, 1993. **98**(12): p. 10089-10092.

24. Bussi, G., D. Donadio, and M. Parrinello, *Canonical sampling through velocity rescaling.* The Journal of chemical physics, 2007. **126**(1): p. 014101-7.

25. Berendsen, H.J.C., J.P.M. Postma, W.F. van Gunsteren, A. DiNola, and J.R. Haak, *Molecular dynamics with coupling to an external bath.* The Journal of chemical physics, 1984. **81**(8): p. 3684-3690.

26. Hess, B., H. Bekker, H.J.C. Berendsen, and J.G.E.M. Fraaije, *LINCS: A linear constraint solver for molecular simulations.* Journal of computational chemistry, 1997. **18**(12): p. 1463-1472.

27. Hildebrand, J.H. and R.L. Scott, *The Solubility of Nonelectrolytes*. 3rd ed1950: Reinhold, New York. 488.

28. Fried, J.R., *Conformations, Solutions and Molecular Weight*, in *Polymer Science and Technology*2003, Prentice Hall: Upper Saddle River, NJ. p. 582.

29. Hansen, C.M., *Hansen solubility parameters: a user's handbook*. 2nd ed2007: CRC Press, 2007. 544.

30. Kyte, J. and R.F. Doolittle, *A simple method for displaying the hydropathic character of a protein.* Journal of Molecular Biology, 1982. **157**(1): p. 105-132.

31. Eisenberg, D., R.M. Weiss, T.C. Terwilliger, and W. Wilcox, *Hydrophobic moments and protein structure.* Faraday Symposia of the Chemical Society, 1982. **17**(0): p. 109-120.

32. Lobanov, M.Y., N.S. Bogatyreva, and O.V. Galzitskaya, *Radius of gyration as an indicator of protein structure compactness.* Molecular Biology, 2008. **42**(4): p. 623-628.

33. Ghosh, T., A.E. García, and S. Garde, *Molecular dynamics simulations of pressure effects on hydrophobic interactions.* Journal of the American Chemical Society, 2001. **123**(44): p. 10997-11003.

34. Sarupria, S. and S. Garde, *Quantifying water density fluctuations and compressibility of hydration shells of hydrophobic solutes and proteins.* Physical review letters, 2009. **103**(3): p. 037803.

35. Godawat, R., S.N. Jamadagni, and S. Garde, *Characterizing hydrophobicity of interfaces by using cavity formation, solute binding, and water correlations.* Proceedings of the National Academy of Sciences, 2009. **106**(36): p. 15119-15124.

36. Hernandez, Y., M. Lotya, D. Rickard, S.D. Bergin, and J.N. Coleman, *Measurement of multicomponent solubility parameters for graphene facilitates solvent discovery.* Langmuir, 2009. **26**(5): p. 3208-3213.

37. Kim, D.-H., M. Abidian, and D.C. Martin, *Conducting polymers grown in hydrogel scaffolds coated on neural prosthetic devices.* Journal of Biomedical Materials Research Part A, 2004. **71A**(4): p. 577-585.

38. Cui, X., V.A. Lee, Y. Raphael, J.A. Wiler, J.F. Hetke, D.J. Anderson, and D.C. Martin, *Surface modification of neural recording electrodes with conducting polymer/biomolecule blends.* Journal of Biomedical Materials Research, 2001. **56**(2): p. 261-272.

39. Consortium, T.U., *Update on activities at the Universal Protein Resource (UniProt) in 2013.* Nucleic Acids Research, 2013. **41**(D1): p. D43-D47.

40. Silverman, B.D., *Hydrophobic moments of protein structures: Spatially profiling the distribution.* Proceedings of the National Academy of Sciences, 2001. **98**(9): p. 4996-5001.

41. Meirovitch, H., S. Rackovsky, and H.A. Scheraga, *Empirical Studies of Hydrophobicity. 1. Effect of Protein Size on the Hydrophobic Behavior of Amino Acids.* Macromolecules, 1980. **13**(6): p. 1398-1405.

42. Stevens, F.J., *Homology versus analogy: possible evolutionary relationship of immunoglobulins, cupredoxins, and Cu,Zn-superoxide dismutase.* J Mol Recognit, 2008. **21**(1): p. 20-9.

43. Guiseppi-Elie, A., S. Brahim, G. Wnek, and R. Baughman, *Carbon-nanotube-modified electrodes for the direct bioelectrochemistry of pseudoazurin.* NanoBiotechnology, 2005. **1**(1): p. 83-92.

44. Hao, F., P. Dong, J. Zhang, Y. Zhang, P.E. Loya, R.H. Hauge, J. Li, J. Lou, and H. Lin, *High Electrocatalytic Activity of Vertically Aligned Single-Walled Carbon Nanotubes towards Sulfide Redox Shuttles.* Sci. Rep., 2012. **2**.

45. Yuan, W., Y. Zhou, Y. Li, C. Li, H. Peng, J. Zhang, Z. Liu, L. Dai, and G. Shi, *The edge- and basal-plane-specific electrochemistry of a single-layer graphene sheet.* Sci. Rep., 2013. **3**.

CHAPTER FOUR

BIOFABRICATION, IN VITRO AND IN VIVO PERFORMANCE OF DUAL RESPONSIVE LACTATE AND GLUCOSE BIOSENSORS IN A PIGLET TRAUMA MODEL

1.1. *Introduction*

The fabrication of multi-analyte biotransducers remains a major technical challenge especially when the length scales of the individual transducer elements are on the order of microns (Zimmermann, Fienbork et al. 2004,Park, Kim et al. 2006,Kotanen and Guiseppi-Elie 2013). Such biotransducers are critical for *in vivo* (intramuscular) wireless biosensor systems (Endo, Yonemori et al. 2009) that allow for immediate and continual pre-hospital and Intensive Care Unit (ICU) monitoring of lactate and glucose to inform patient specific interventions that will improve survivability from trauma-associated or postoperative hemorrhage (Endo, Yonemori et al. 2009,Kotanen and Guiseppi-Elie 2013). Continued examination of interstitial compartments using biosensors will aid in understanding the temporal relationships among biomarkers of physiological stress in these environments and how they relate to hemorrhagic shock states (Uyehara and Sarkar 2013).

Electropolymerization of certain conductive electroactive polymers (CEPs) such as polypyrrole (Bartlett and Whitaker 1987,Bartlett and Whitaker 1987,Sadki, Schottland et al. 2000), polythiophenes (Rahman, Kwon et al. 2005,Rahman, Kothalam et al. 2012) and polyanilines (Yehezkeli, Yan et al. 2009,Bai, Beyer et al. 2011) as well as electropolymerization of non-conductive polymers, such as poly(o-phenylenediamine)

(Palmisano, Centonze et al. 1994), poly(m-phenylenediamine) (Badea, Curulli et al. 2003,Zhou, Chen et al. 2004) and poly(phenylene oxide) (Bartlett and Caruana 1992,Bartlett and Caruana 1994), have been well studied and is one of the emerging additive methods of biofabrication that may be used to guide and deposit biological entities such as enzymes, antibodies, nucleic acids, sub-cellular fragments, and even whole cells to metallic or semi-conducting electrode sites of more complex devices (Apetrei, Rodríguez-Méndez et al. 2011,Karunwi, Wilson et al. 2013,Tseng, Yao et al. 2013). Biofabrication techniques using conducting electroactive polymers have been previously described for use in the design and fabrication of the biological recognition membranes of biotransducers (Palmisano, Zambonin et al. 2000,Karunwi, Wilson et al. 2013). Polypyrrole is a conductive electroactive polymer electropolymerized from its monomer pyrrole, which, because of its facility to direct the deposition of dopant and entrained macromolecules onto electrode surfaces, has been previously described and reviewed for the fabrication of amperometric, voltammetric, and impedimetric biotransducers (Guiseppi-Elie 1998,Cosnier 1999,Guiseppi-Elie, Brahim et al. 2006). It is particularly useful in that it may be readily overoxidized to yield a polyelectrolyte membrane (Hsueh and Brajter-Toth 1994,Qi, Rees et al. 1996,Debiemme-Chouvy and Tran 2008) well suited for hosting biological recognition molecules (Kotanen, Tlili et al. 2013).

Biorecognition membranes of precisely controlled thickness may be fabricated through judicious control of electropolymerization charge density (Valaski, Ayoub et al. 2002). In so doing, a wide range of copolymers may be electrosynthesized and a wide range of biorecognition molecules can serve as monomeric and polymeric dopants and so may be

incorporated through judicious control of the materials and solvent composition of the electropolymerization bath (Lee, Yang et al. 1999,Lee, Yang et al. 2002). In addition, post-processing of biorecognition membrane layers, such as overoxidation or chemical derivatization may be used to enhance or stabilize performance of the fabricated biorecognition layer. Most importantly, all these processing steps may be performed in batch or continuous mode, in bio-benign aqueous environments at pH values close to 7.0 and with the use of modest electrode potentials under conditions that are close to ambient; conditions that are compatible with biological recognition entities and that prevent denaturation. Thus, conducting electroactive polymers (CEPs) have many attractive features such as selectivity of enzyme entrapment to electrode surfaces (Kotanen and Guiseppi-Elie 2010,Tseng and Monbouquette 2012), reduction of interfacial impedance, thickness control via charge density (Holdcroft and Funt 1988), enzyme stability, biocompatibility (Wang, Gu et al. 2004,George, Lyckman et al. 2005,Ramanaviciene, Kausaite et al. 2007), and adjustment of biosensor enzyme kinetic properties. Polypyrrole, along with other electroactive polymers, once formed, can be surface modified and used for various chemical coupling reactions (Kang, Neoh et al. 1996,Goddard and Hotchkiss 2007). During electropolymerization, the biological molecule may serve as the dopant anion (most enzymes possess a net negative charge). Hence, biomolecules, such as enzymes, can be used to dope polypyrrole during electropolymerization when fabricating biosensors (Kotanen and Guiseppi-Elie 2010,Kotanen and Guiseppi-Elie 2012,Kotanen, Tlili et al. 2012,Karunwi, Wilson et al. 2013).

Biosensors fabricated with polypyrrole-based electroconductive hydrogels have shown no loss of sensitivity in vitro over an 18-day period when stored in PBS buffer at 4 °C (Kotanen, Tlili et al. 2013). Glucose biosensors fabricated with overoxidized polypyrrole were observed to limit the response to ascorbic acid to no more than 5% of the total response to glucose, reduce signal response to other negatively charged endogenous interferents by 92% and have an interferent rejection ratio of 12:1 (Kotanen, Tlili et al. 2012,Kotanen, Tlili et al. 2013). Nonspecific adsorption of enzymes companion sites during the biofabrication process has been shown to be insignificant and to have little to no influence on biosensor response (Kotanen and Guiseppi-Elie 2013). Dual analyte electrochemical biotransducers for the amperometric detection of glucose and lactate have been developed for use in thin layer flow cells that employ flow injection analysis (Palmisano, Rizzi et al. 2000).

In the meantime, amperometric oxidoreductase enzyme biotransducers that depend upon the electrochemical discharge of hydrogen peroxide have benefitted from the development and use of electrodeposited solid-state mediator layers of Fe, Ni or Fe/Ni hexacyanoferrate (Karyakin and Karyakina 1999,Krylov and Lisdat 2007,Sitnikova, Borisova et al. 2011,Chen, Chen et al. 2012). The mediator, which may be deposited potentiodynamically, potentiostalically or galvanostatically forms as a discontinuous layer of nanocrystals of iron(II,III) hexacyanoferrate ([Fe(II,III)HCFe] Prussian Blue) or nickel(II) hexacyanoferrate [Ni(II)HCFe] on metallic, semiconducting or carbonaceous surfaces and serves to enhance the low concentration detection of enzymatically generated peroxide.

Additionally, external hydrogel layers are often used to coat in-dwelling devices (Karunwi, Wilson et al.) as a means to control analyte diffusion (Peppas, Bures et al. ,Wilson, Salas et al.), mitigate interferences and proteases, and confer cytocompatibility (Slaughter, Khurshid et al. ,Nakamura, Matsumoto et al. ,Guiseppi-Elie, Dong et al. 2012). Particularly relevant are hydrogels containing zwitterionic phosphorylcholine (PC) units and ethylene glycol units as these confer cytocompatibility and high hydration, respectively, and the resulting hydrogel may be molecularly engineered with precise architectures for control of transport properties (Aucoin, Wilson et al. 2013).

In this chapter we employ pyrrole electropolymerization as an additive technique for the biofabrication of side-by-side biotransducers for glucose and lactate with minimum cross-talk. Here, a layer-by-layer technique based on alternation of PPy-PSSA and PPy-Enzymes of different charge densities were evaluated for their contributions to the biosensor's bioanalytical performance. The MDEA 5037-Pt biotransducers, developed in conjunction with ABTECH Scientific, Inc. were microlithographically fabricated, modified with an electrodeposited layer of Fe/Ni hexacyanoferrate to serve as peroxide mediator, decorated with the electropolymerized PPy-Enzyme biorecognition layer, characterized *in vitro*, and implanted into the trapezius muscle of a piglet (*Sus scrofa*) hemorrhage model. Additionally, a UV cross-linked biomimetic poly(2-hydroxyethyl methacrylate) (pHEMA)-based hydrogels containing tetraethylene glycol (TEGDA 3 mol%), MPC units (1 mol %) and oligo(ethylene glycol) (400) monomethacrylate (OEG(400)MA) (5 mol%) was used to coat the device prior to implantation. Internal

calibration, response under controlled hemorrhage conditions, and post–resection re-characterization were used to evaluate biotransducer performance.

1.2. *Experimental Section*

1.2.1. *Chemicals and Reagents*

The polymeric dopant, poly(styrene sulfonic acid) (PSSA 30%, MW = 70,000, 6–10% sulfonation, ρ = 1.10 g/mL), was purchased from Polysciences, Inc. The reagents pyrrole (reagent grade 98+%), 4-(3-pyrrolyl)butyric acid (PyBA), glucose oxidase (GOx, E.C. 1.1.3.4 from *Aspergillus niger*), lactate oxidase (LOx, E.C. 1.13.12.4 from *Pediococcus sp*), β-D(+)-glucose, lithium lactate (reagent grade 95%), 1-ethyl-3-[3-dimethylaminopropyl] carbodiimide (EDC), sodium *N*-hydroxysulfosuccinimide (Sulfo-NHS), N-hydroxysuccinimide (NHS), (3-aminopropyl)triethoxysilane (reagent grade 99%), 2-Aminoethyl methacrylate hydrochloride (reagent grade 90%), ferrocene monocarboxylic acid (FcCOOH), hydrogen peroxide (30 w/w % solution) and all other common solvents were purchased from Sigma Aldrich Co. (St. Louis, MO, USA). Pyrrole monomer was purified by double passage through an alumina silicate column (Supelclean ™, LC-Alumina-A SPE, 570*2-U, 1 g). Hydrogels used to coat the biotransducer were formulated from the following components; HEMA, OEG(400)MA, the divalent cross linker, TEGDA, and the photoinitiator, 2,2-dimethoxy-2-phenylacetophenone (DMPA, 99%) and were purchased from Sigma Aldrich, USA. The biomimetic reagent 2-methacryloyloxyethyl phosphorylcholine (MPC) was prepared elsewhere as previously described (Ishihara, Ueda et al.). The polymerization inhibitors hydroquinone and

monomethyl ether hydroquinone were removed from the individual cocktail components by passing the liquid monomers over an inhibitor removal column. Aqueous solutions were prepared in deionized water that was purified by passing distilled water through a Milli-Q® plus (Millipore Inc.) ultrapure water system. A mixed substrate stock solution was prepared to contain glucose at 100 mM and a lithium lactate at 50 mM. This stock was allowed to mutarotate overnight at 4 °C before use.

1.2.2. *Electropolymerization and Electrochemical Characterization*

Electropolymerization of pyrroles and electrochemical characterization of polypyrrole thin and composite films were performed using a PAR 283 Potentiostat/Galvanostat (Princeton Applied Research) equipped with PowerSuite® software or a BAS-100B/W Electrochemical Analyzer with a BAS PA-1 preamplifier module used to amplify the current and to filter out noise (BASi, West Lafayette, Indiana, USA). All experiments used the three-electrode setup with platinum microelectrodes (BASi, φ = 100μm; West Lafayette, Indiana, USA), the microdisc array of the ECC MDEA 5037-Pt (ABTECH Scientific, Inc., Richmond, Virginia, USA) serving as the working electrode, an external Ag/AgCl (3 M KCl) reference electrode (RE803; ABTECH Scientific, Inc., Richmond, Virginia, USA) and a large area platinum mesh counter electrode. Electrochemical impedance spectroscopy (EIS) was performed using a Solartron 1260 Frequency Response Analyzer (Solartron Analytical) interfaced to the Princeton Applied Research Potentiostat/Galvanostat Model 283 (Princeton Applied Research). Fabricated transducers and biotransducers were studied in freshly prepared 0.1X working concentration of PBS of pH = 7.2 at room temperature (22 °C) except where noted. EIS used non-perturbing 20

mV peak-to-peak interrogating amplitude with zero offset over the frequency range 10^{-1} – 10^{6} Hz.

1.2.3. *Transducer Cleaning and Surface Modification with a Mediator Layer*

Two types of electrochemical transducers were used; platinum microelectrodes (μE) for the *in vitro* characterization of polymer films and mediator layers and microlithographically fabricated micro disc electrode arrays (MDEA) for *in vitro* characterization and *in vivo* animal implantation. The platinum microelectrode was mechanically polished for 1 min using 1.0 μm diamond slurry and then washed with methanol. This was followed by further polishing for 1 min using 0.05 μm alumina and rinsed with DI-water in order to expose a fresh platinum surface. Electrodes were subsequently ultrasonicated for 3 min each in DI-water, propanol, DI-water; cleaned in a UV-ozone Cleaner (Boekel Industries, Philadelphia, USA) and cathodically cleaned by repeated cycling over the range 0.0 to −1.2 V in PBS *vs.* Ag/AgCl (Guiseppi-Elie, Wilson et al. 1995). The ECC MDEA 5037-Pt is a microlithographically fabricated dual analyte electrochemical transducer intended for amperometric and voltammetric biosensor application. Developed for simultaneous monitoring of interstitial glucose and lactate (Kotanen, Karunwi et al. 2014) the transducer possesses two complete electrochemical cells. The working electrode of each cell comprises 37 recessed (0.5 microns) microdiscs arranged in a hexagonal array. Each disc has φ = 50 microns for a total working electrode area, WEA = 7.3×10^{-4} cm^2 (Guiseppi-Elie, Brahim et al. 2005). The microlithographic fabrication and geometric patterning of the three-electrode electrochemical biotransducers have been previously described (Guiseppi-Elie, Brahim et al. 2005) and the assembly and

packaging of the chip in a manner suitable for implantation into small vertebrate animals has similarly been described (Rahman, Justin et al. 2009). In summary, the electrochemical transducers (0.2 cm × 0.4 cm × 0.05 cm) were microfabricated from e-gun deposited platinum (100 nm) on an adhesion promoting titanium/tungsten (Ti/W) layer (10 nm) onto a 0.5 mm thick electronics grade borosilicate glass (Schott D263). The photoresist patterning and lift off process served to reveal two separate three-electrode electrochemical cells and the metallization was subsequently fully passivated with 0.5 micron thick silicon nitride (Si_3N_4). The nitride layer was eventually itself photolitographically patterned and fluoro-plasma etched to reveal the array of multiple microdiscs of the working electrode (7.3×10^{-4} cm^2), the large area counter electrode (7.3×10^{-3} cm^2) and the shared reference electrode (each = 7.3×10^{-5} cm^2) that were connected to the five individually addressable bonding pads. The epoxy packaged MDEA 5037-Pt transducer was first ultrasonicated for 3 min in each of DI-water, IPA and DI-water. Next, the transducer was placed in a UV-ozone cleaner (Boekel Industries) under irradiated ozone generation for 10 min followed by 1 min of ultrasonication in IPA. This was followed by plasma surface modification of the transducer to generate a controlled density of surface hydroxyl groups on the silicon nitride surface (Harrick Plasma Cleaner). The transducer was then immersed in PBS, made the working electrode of a three electrode electrochemical cell and was cathodically cleaned by sweeping the potential between 0 to −1.2 V (*vs.* Ag/AgCl, 3 M KCl) at 100 mV/s for 40 cycles. The Fe/Ni hexacyanoferrate redox mediator layer was applied to the Pt uE or the MDEA W.E. via 3-electrode potentiodynamic electrodeposition using cyclic voltammetry in a freshly prepared deposition solution containing a mixture of 0.5 mM

$NiCl_2$ and 0.5 mM $K_3Fe(CN)_6$ in 0.1 M KCl + 0.01 M HCl. A potential sweep from 0.1 to 1.1 V at a scan rate of 100 mV/s for 30 cycles was used and the modified device rinsed with DI water. In one construct, one MDEA W.E. had a catalytic layer applied while the other, with no catalytic layer, served as a control and the same biorecognition receptor layer subsequently applied. In yet another construct, the catalytic layer was applied to both MDEA W.E. and different biorecognition receptor layers subsequently applied.

1.2.4. *Conferring Biospecificity to Transducers*

In general, biospecificity was conferred to each Pt μE or array working electrode of the MDEA 5037-Pt device by immobilizing a different bioreceptor to each working electrode of the same chip by the process of potentiostatic electropolymerization at +850 mV *vs.* Ag/AgCl (3M KCl). To achieve this, PyBA was first conjugated to AEMA using the well characterized EDC-NHS coupling (**Scheme 1**).

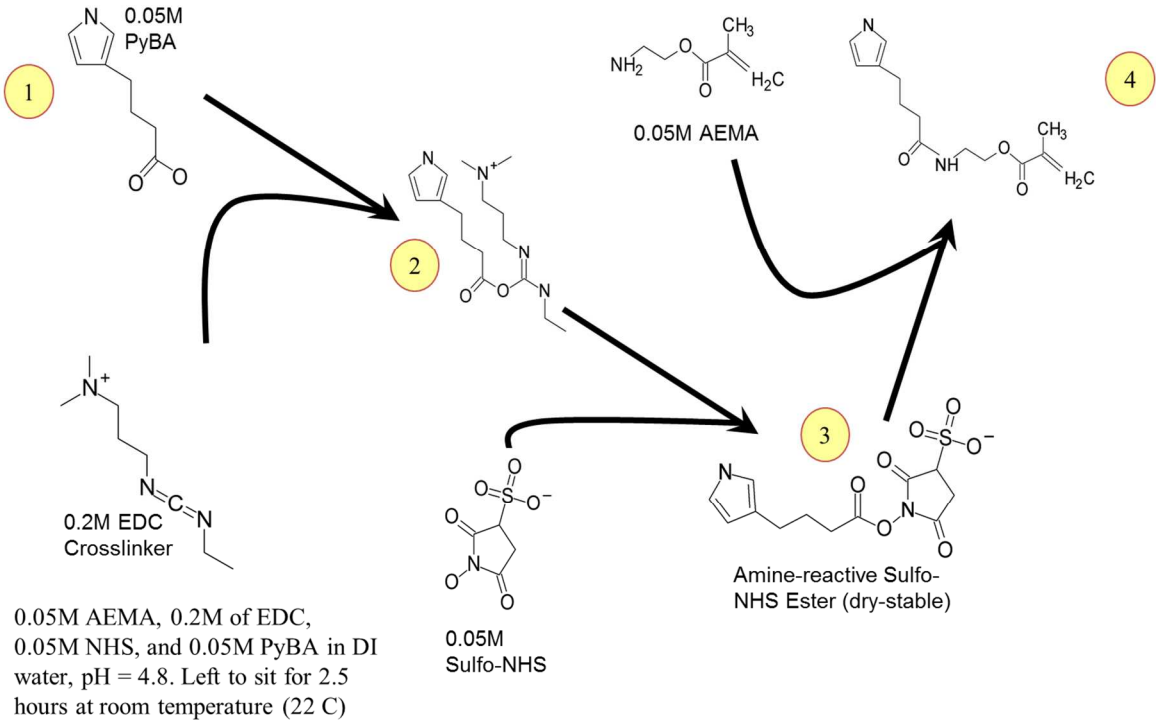

Scheme 1: Conjugation of pyrrole butyric acid to amino ethyl methacrylate using the well characterized EDC-NHS coupling chemistry

Briefly, under UV-free conditions, a solution was prepared to contain 0.2 M Py, 0.05 M PyBA, 0.05 M AEMA, 0.2 M EDC and 0.05 M NHS and allowed to incubate at room temperature for 2.5 hours under acidic conditions (pH=4.7). The pH was then adjusted to pH=5.2 using drop-wise addition of 1.0 M and 0.1 M NaOH with monitoring. The required amount of enzyme (GOx or LOx) was then added to achieve the desired concentration of 0.1 mg/mL. The resulting final solution was degased by bubbling with argon and gently stirred under anaerobic conditions. To this was added 2 mM glucose (or lactate) to occupy and block the enzyme's active site during electropolymerization. This helps protect the active sites during further biofabrication processes.

The potentiostatic electropolymerization proceeded via a multi-layer approach. The first layer was formed from the above solution to which no dopant anions were specifically added. The next layer was formed from a similarly prepared solution that contained 0.05 M PSSA rather than enzyme. In creating the multilayer structures the enzyme layer (GOx or LOx) was electropolymerized at various charge densities (Q = 5 mC/cm^2, 10 mC/cm^2, 100 mC/cm^2) followed by a PSSA layer of the same charge density until a total charge densities (Q_T) of 50 or 100 mC/cm^2 was achieved. This was done by applying 800 mV *vs.* Ag/AgCl for the specified total charge density. Following fabrication, biotransducers were placed in PBS (pH = 7.2) and refrigerated at 4 °C overnight. Before use, enzyme-modified microelectrodes were over-oxidized (OO-PPy) by repeatedly cycling the electrode in PBS between −200 to +1,300 mV *vs.* Ag/AgCl (3M KCl) for 40 cycles at 100 mV/s. In a further construct, a previously described polyHEMA-based biomimetic hydrogel layer (Karunwi, Wilson et al. 2013,Kotanen, Wilson et al. 2013) was applied by dip-coating and UV cross-linked to form an outer layer for the complete device.

1.2.5. *Hydrogel cocktail preparation*

The pre-polymer hydrogel cocktail was prepared by mixing monomer constitutes with the following composition; HEMA=90 mol%, the divalent cross linker TEGDA=3 mol%, OEG(400)MA=5 mol % (calculated on the basis of the repeat unit molecular weight), MPC=1 mol% and DMPA=1 mol%. Ethylene glycol and water were added to the mixture in a 1:1 (v/v) ratio such that the two species combined comprised 20 volume % of the formulation (see **Table 1** for formulation details). After combining the various constituents, the mixture was ultrasonicated for 5 minutes and sparged with ultra high pure (UHP)

nitrogen to remove dissolved oxygen. The biotransducer was dip-coated and immediately placed in a UV-crosslinker (CX-2000, UVP, Upland, CA, USA) and UV irradiated at 366 nm for 10 min to initiate polymerization. The transducers were then removed, hydrated in 1xPBS (pH=7.2) at 4°C until use.

Table 1. Monomer components and composition of the hydrogel cocktail formulated to coat and protect the implantable dual responsive amperometric biotransducer.

Mole Percent of Hydrogel (%)	Hydrogel Constituent
90.0	HEMA
3.0	TEGDA
5.0*	OEG(400)MA
1.0	MPC
1.0	DMPA
*Mole % calculated on the basis of the repeat unit.	

1.2.6. *In Vitro Biosensor Calibration Prior to in Vivo Implantation*

To interrogate the biotransducer, the 8100-K1 fixed frequency wireless dual potentiostat system was used (Pinnacle Technology, Lawrence, KS, USA). The kit contained the Pinnacle 8151 wireless dual potentiostat, the voltage programmer, and a receiver base station (Model 8106) with USB cables. Software for data acquisition (PAL) was also included in the kit. Biotransducers were interfaced with the 8151 wireless potentiostat via

a custom connector specifically designed to interface with the MDEA 5037 devices (see Fig. 1).. Two-electrode amperometric measurements of glucose and lactate was enabled, with the on-board working microelectrode array serving as the working electrode and the shorted on-board counter and reference electrodes serving as the counter electrode. A bias potential of 0.65 V was programmed into the wireless potentiostat and applied to the working electrode array of the MDEA 5037 with respect to the onboard counter electrode.

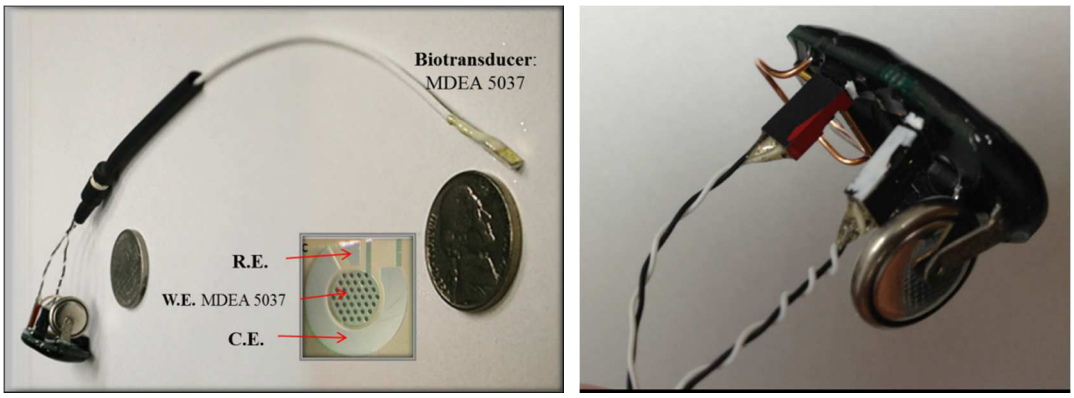

Fig. 1: MDEA 5037 device (showing its relative size) connected to the wireless potentiostat via a custom made connector (see close up shot)

To ensure functionality prior to implantation, *in vitro* calibration of MDEA 5037s was performed at 37 °C at least 8 h prior to. Steady state amperometric current produced was measured and the bioanalytical parameters of the device were determined. *In vitro* calibrated sensitivity (S_o) was determined by the ratio of the resulting change in current density (based on electrode geometric area) to change in concentration of analyte in buffer (G_o for glucose, L_o for lactate) in units of $\mu A \cdot cm^{-2} \cdot mM^{-1}$. Time dependent estimations of intramuscular glucose, $G_o(t)$ or lactate, $L_o(t)$ were made based on this reference sensitivity

after implantation of the device. The kinetic parameters were determined using Lineweaver-Burk (LWB) analysis of biosensor amperometric response (Kotanen, Tlili et al. 2013). The apparent Michaelis–Menten constant K_{Mapp} and the maximum current response, I_{max}, were calculated from the slope and the intercept of the Lineweaver–Burk plots [20,21]. Limits of detection were calculated by dividing 3*STDev (three times the standard deviation) of the steady-state, blank solution current response by the calculated sensitivity.

1.2.7. *Implantation of Biotransducers into the Trapezius Muscles of Piglets*

In accordance with IACUC Protocol at the Tripler Army Medical Center (TAMC) entitled "Maintaining Tissue Viability after Acute Hemodynanic Stabilization in *Sus scrofa* Models of Shock; Amendment #7 piglets (*Sus scrofa*) weighing between 100 and 120 lbs were shaved, sterilized and placed under anesthesia on an operating table. Catheters were put into place to get accurate blood readings on vitals and to allow for controlled hemorrhage. An incision was made above the bicep muscle on the foreleg to expose the fascia and muscle (see **Fig. 2**). Fascia was spread apart using blunt-tipped scissors to expose the muscle. A small pocket was formed by spreading the muscle tissue apart using forceps. The MDEA 5037-Pt was carefully inserted into the pocket by hand. The muscle tissue was closed over the working region of the biotransducer and secured with a suture. Fascia was secured over the muscle tissue with a suture and the wound was closed with sutures as well. After implantation, the MDEA 5037 biotransducer was coupled to the Pinnacle 8151 dual potentiostat and allowed to reach steady state for an hour. Baseline measurements were collected from the pig at this time.

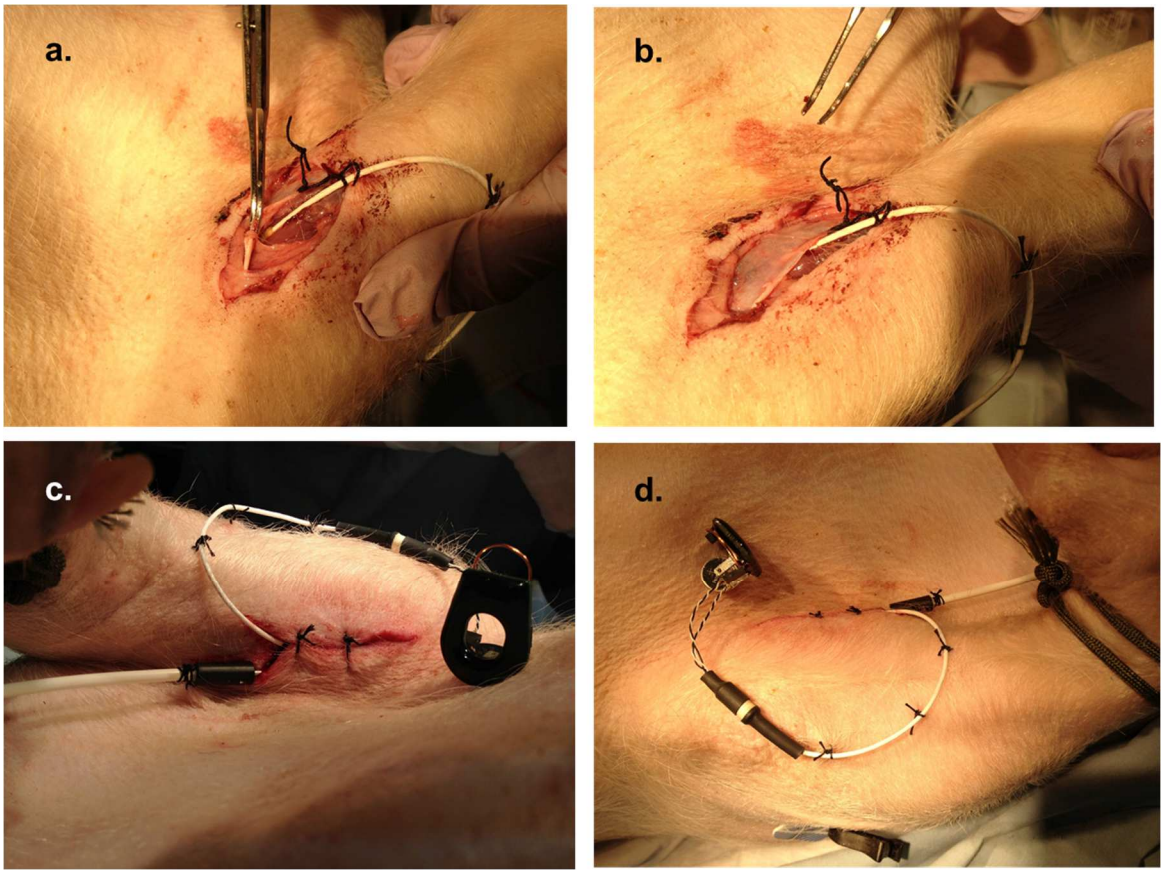

Fig. 2: Surgical implantation of biotransduction device in the trapezius muscle of the piglet (a, b). c and d show the entire biosensor system (including the wireless dual potentiostat) post surgery

1.2.8. *In Vivo Biosensor Sensitivity and Response Time to Bolus Infusion of Analytes*

After biosensor response reached a steady baseline value of intramuscular analytes, measurements of blood analytes from the femoral artery were made. All measurements were made by drawing blood, and running it through the ABL 800 blood gas analyzer. Procedures for measurement of interstitial analytes lasted for up to 12 hours. One hour was used to allow the biosensors to reach a steady state, and to take baseline readings from the

pig prior to procedures. Hemorrhage was started about 39 minutes to 1 hour after the baseline reading (P1). Estimated interstitial analyte responses measured by biosensors calibrated *in vitro* were compared to analyte concentrations in the blood measured using the ABL 800. Interstitial concentrations of glucose in non-diabetic rats have been shown to have a good 1:1 correlation to plasma glucose concentration at the basal state (Aussedat, Dupire-Angel et al. 2000). Hemorrhage lasted for 1 hour, from which a 3-6 hour recovery period followed. Pigs were subsequently euthanized following procedures. A necropsy was performed and muscle surrounding the biotransducer was resected in order to safely recover the devices. Resected biotransducers were re-characterized *in vitro* to assess the functionality and lifetime of the device *in vivo*. Upon explantation, the base current, sensitivity and response time of biosensors were once again evaluated in 1× PBS at 37 °C. Resected biotransducers were considered functional if sensitivity and maximum current were maintained, being not significantly different from freshly prepared sensors, can detect the physiologically relevant range of glucose or lactate, and have a response time within 5% of their original response time. A summary table of the biosensor performance can be seen in **Table 2**.

1.3. *Results and Discussion*

1.3.1. *Biofabrication Using Pyrrole Electropolymerization*

The method of biotransducer fabrication using pyrrole electropolymerization to guide and direct the immobilization of bioreceptors onto microelectrodes is well documented in the

literature. Typically, a potentiostatic, potentiodynamic, or galvanostatic method is used. This work employed a potentiostatic method but explored the use of multi-layered structures created by alternating an enzyme rich layer with a PPy-PSS layer and compared these multi-layered structures with single layer constructs (**Scheme 2**).

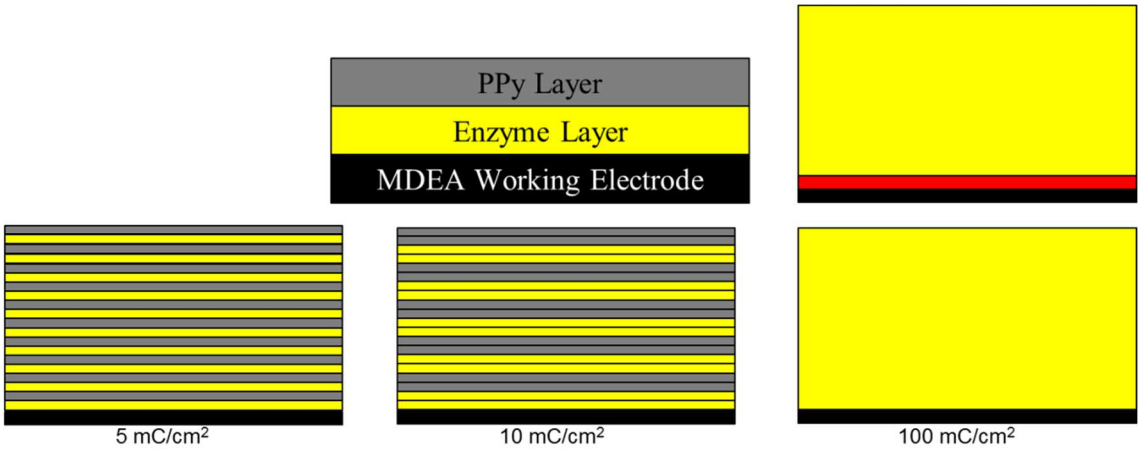

Scheme 2: Layer by layer cartoon representation of the electrodeposition step of alternating layers of polypyrrole and enzymes at 3 different charge densities per layer.

The layer by layer (LBL) approach was chosen due to its versatility and its various advantages (Rodrigo M. Iost 2012). Diverse materials can be employed in film fabrication such as polyelectrolytes (polypyrrole, polyaniline). The versatility of this technique permits the porosity, roughness, and thickness of the film to be controlled by adjusting the pH, temperature, ionic strength of the media, polyelectrolyte concentration and even the ratio between multiple polyelectrolytes in use. One important use of the LBL method is to improve electron hopping in multilayer films.

1.3.2. *Electropolymerization Kinetics of Covalently Conjugated Systems*

The kinetics of electropolymerization, defined as the time to reach the total target charge density (Q_T = 100 mC/cm^2 or 50 mC/cm^2) were compared for all systems studied. During electrodeposition of single and multiple layers, there was some variation in the overall time taken to reach a specified charge density (Q = 100 mC/cm^2) for both GOx and LOx based devices (see **Fig. 3(a – c)**). For the single layered system (Q = 100 mC/cm^2/layer) both GOx and LOx took ca. the same time (3854 s vs. 3754 s) while the multi-layered (Q = 5 mC/cm^2/layer and 10 mC/cm^2/layer) showed that GOx based systems (6440 s and 4120 s) took longer than the LOx systems (3750 s and 3060 s). Even within the GOx and LOx systems, the 5 mC/cm^2/layer (6440 s and 3750 s) took longer overall than the 10 mC/cm^2/layer systems (4120 s and 3060 s).

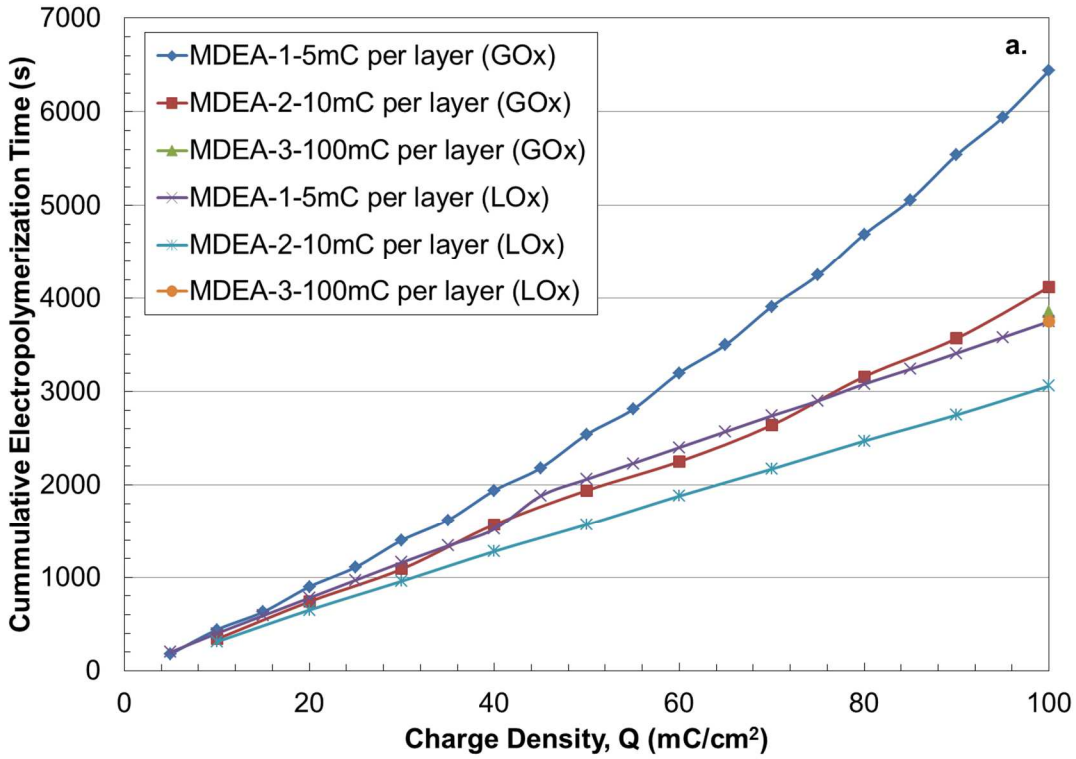

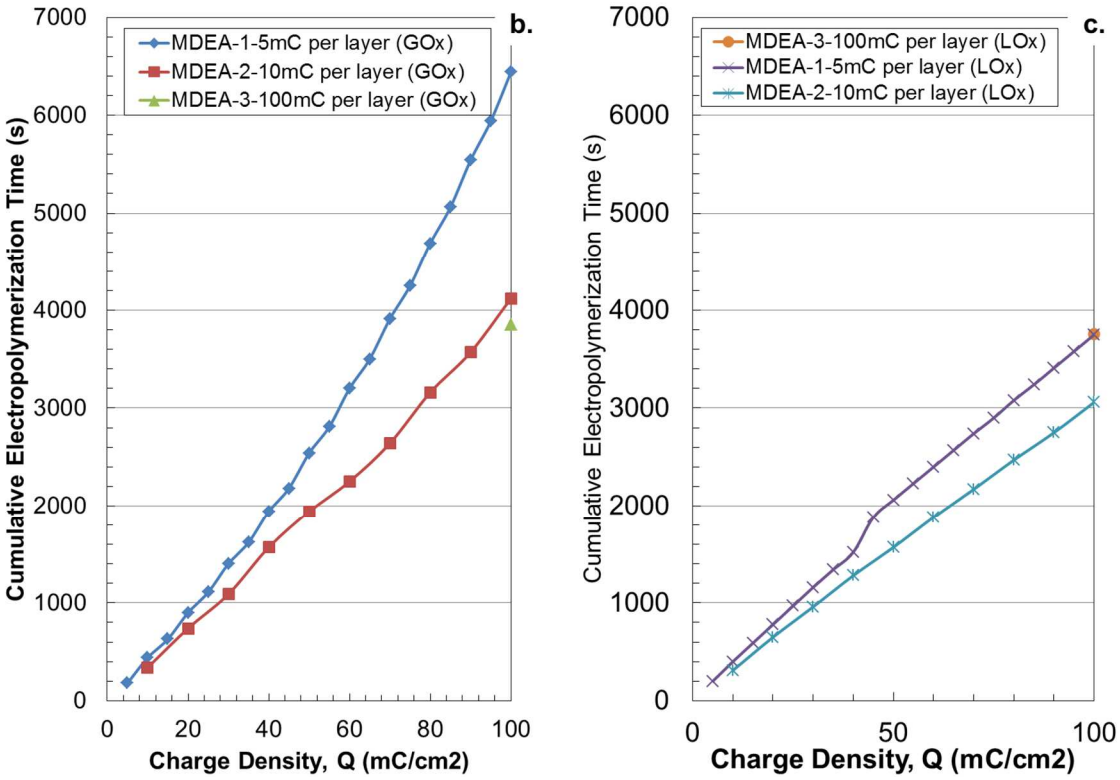

Fig. 3 (a): Cumulative electropolymerization time vs. cumulative charge density for 3 different layered systems. (b), (c): Cumulative electropolymerization time vs. cumulative charge density for 3 different layered systems for glucose oxidase based systems (b) and lactate oxidase based systems (c)

During electrodeposition of multiple layers, the elapsed time was measured at varying charge densities. Electrodeposition performed on the bare devices took the shortest overall time compared to the catalytic layered devices. The catalytic layered devices on the other hand exhibited a more consistent deposition kinetics compared with the bare devices.

1.3.3. *Effects of a Layer-by-Layer Approach on Bioanalytical Performance of Biotransducers*

The dose response curves of biotransducers fabricated using a single layer compared to multi layers are shown in Fig. 3 and biosensor performance parameters for all systems are summarized in Table 2

Table 2: *In-vitro* sensitivity characterization of dual-responsive biotransducers prior to implantation into porcine hemorrhage model.

Device	Sensitivity (nA/mM) - Glucose	Sensitivity (nA/mM) - Lactate	Response Time
MDEA 5037-Pt|[PPy-GOx(100mC cm^{-2})]	2.19	1.05	12 minutes (no hydrogel layer)
MDEA-Pt|[PPy-GOx(10mC cm^{-2}) |PPy-PSSA(10mC cm^{-2})]5|gel	N/A	0.70	18-20 minutes

MDEA-Pt|[PPy-GOx(5mC cm^{-2}) |PPy-PSSA(5mC cm^{-2})]10|gel	N/A	0.07	18-20 minutes
MDEA 5037-Pt|[PPy-GOx(100mC cm^{-2})]|gel	3.05	1.95	10-14 minutes (thinner hydrogel layer)
MDEA 5037-Pt|**Med**|[PPy-GOx(100mC cm^{-2})]|gel	0.67	0.57	10-14 minutes (thinner hydrogel layer)

The single layered systems (Pt|[PPy-GOx(100mC/cm^2)]) appeared to be the most consistent and stable during fabrication compared to the multi-layered systems. The layer-by-layer approach was employed to increase the loading of enzymes per device and this was not the result seen. The single layered enzyme systems performed much better than the multi-layered devices. Three different single layered enzyme systems were tested; one without a hydrogel layer, one encapsulated with a hydrogel layer and one with a mediator layer and encapsulated with a hydrogel layer. The mediator modified device underperformed compared to the other devices. While the device without any hydrogel performed well and had a quicker response time, the device sensitivity dropped within minutes due to biofouling of the device surface. The hydrogel covered devices were all

reusable following implantation and explantation while the non hydrogel covered devices were compromised and non usuable following implantation.

1.3.4. *Effects of a Mediator Layer on Performance of Biotransducers*

The role of the mediator layer was investigated in varying concentrations of hydrogen peroxide. There was a ca. 5 fold increase in sensitivity (**Fig. 4**) of mediator layer modified device over the unmodified (1.99 nA/mM *vs.* 0.40 nA/mM) with a 20 fold increase in current seen at low concentrations (< 0.01 mM)

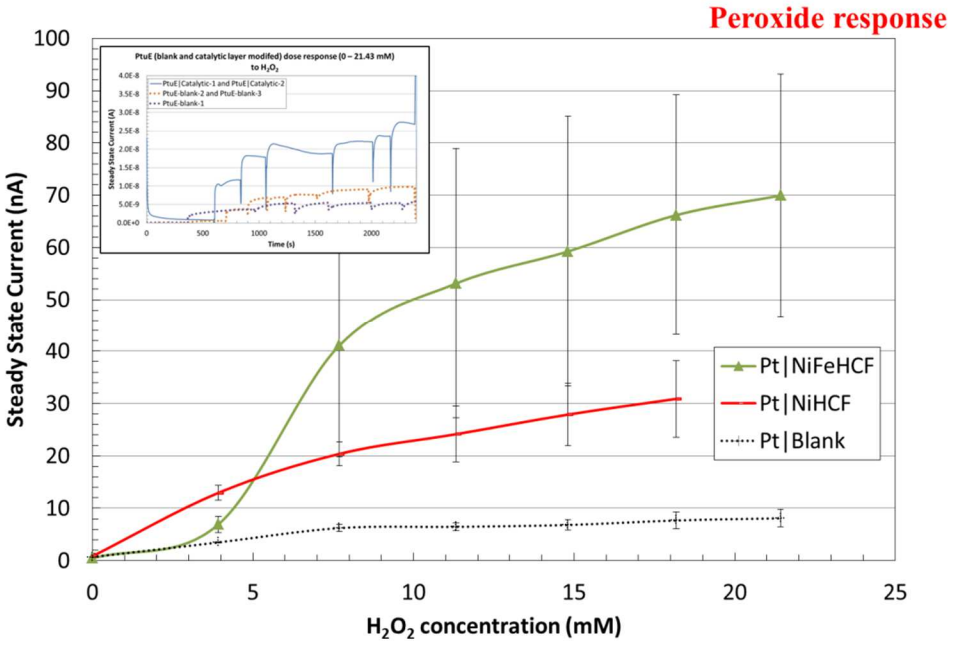

Fig. 4: Role of NiHFe (mediator) layer and NiFeHCF (mediator) layer. Sensor response to varying H_2O_2 concentration. Insert showing sample dose response steps performed at 650 mV *vs.* Ag/AgCl in buffered H_2O_2.

Electrochemical Impedance Spectroscopy (EIS) data showed that the measured impedance for both bare and mediator-modified devices were the same in PBS. This showed that the mediator layer did not adversely affect the electrical impedance properties of the abio interface of the biotransducer. As alternate layers of enzymes and polypyrrole were added, the impedance of the mediator-modified devices showed an increase in |Z| compared to the bare devices (see **Fig 5**). This indicated that the process of electrodeposition of the polypyrrole, either the bath or the potentiodynamic process, had a deleterious influence on the overall impedance of the interface. Once the final layer was deposited, the entire device was overoxidized (OOx) so that the background current contribution from the polypyrrole was eliminated and the EIS taken. The impedance of the OOPPy coated devices (both bare and mediator modified devices) showed considerable similarity. This confirms that by the end of the electrodeposition process, the presence of the mediator had no influence on the impedance characteristics of the interface.

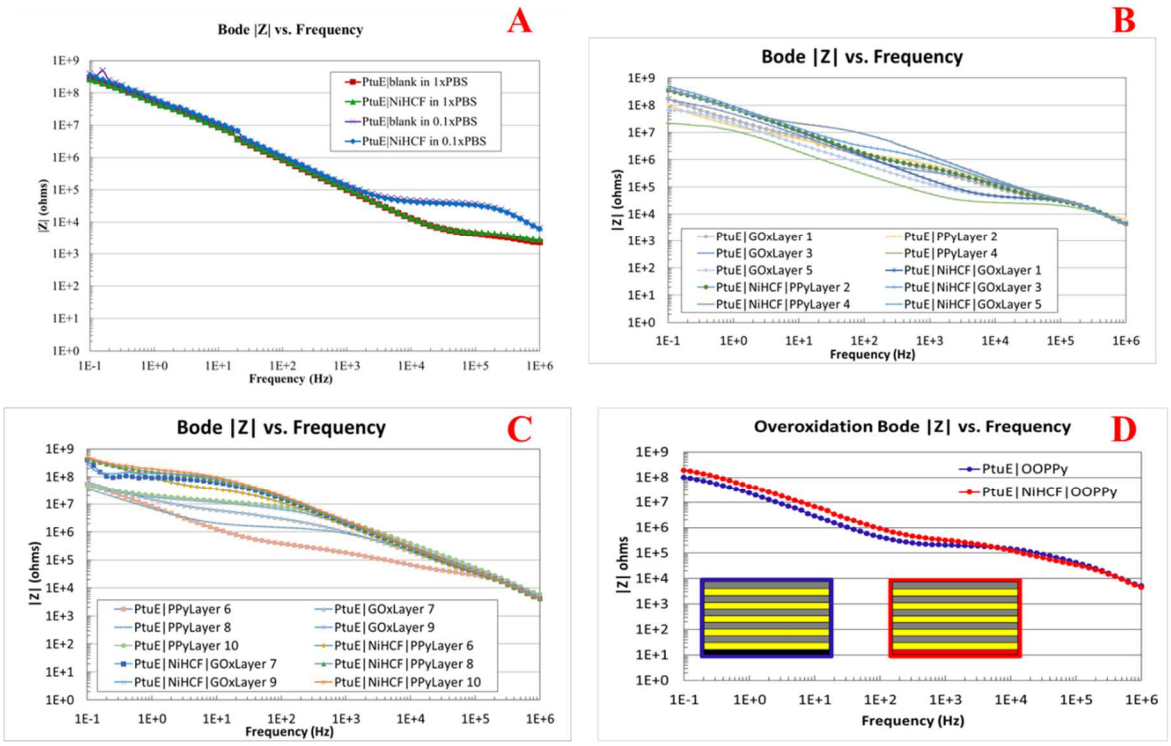

Fig. 5: Bode plots of impedance magnitude, |Z|, vs. frequency of bare and mediator-modified PtuEs tested in PBS at RT. (A) Variation in |Z| due to the difference in buffer concentration (1.0x and 0.1x pH 7.2 PBS). (B) and (C) show variation in |Z| for successive alternate layers of PPy and PPy-GOx on the blank and mediator-modified devices. (D) **Both** the blank and mediator-modified devices appear **similar** following overoxidation and do not show any variation in |Z|.

Once the enzyme layers were applied, the dose response curves showed the bare devices displaying a higher sensitivity (0.9354 nA/mM) compared to the mediator-modified devices (0.3208 nA/mM). This was surprising considering that the mediator layer

had a higher sensitivity (higher current response for small change in concentration) to pure hydrogen peroxide doses.

1.3.5. *In Vivo Response of MDEA 5037 Biotransducers to Feeding and Hemorrhage*

The devices showed response to both glucose and lactate changes simultaneously. However, in our pig model, the tissues behaved opposite to the blood. As shown in Figure 6 (A), the control porcine model (non-trauma induced) showed that the lactate sensing domain of the biotransducer measured a higher current for lactate levels compared to the blood lactate while the glucose sensing domain had similar measurements (except for 2 concentrations in the middle of the experiment). After the control experiment was performed, trauma was induced and the responsive measurements taken (Fig. 6(B)).

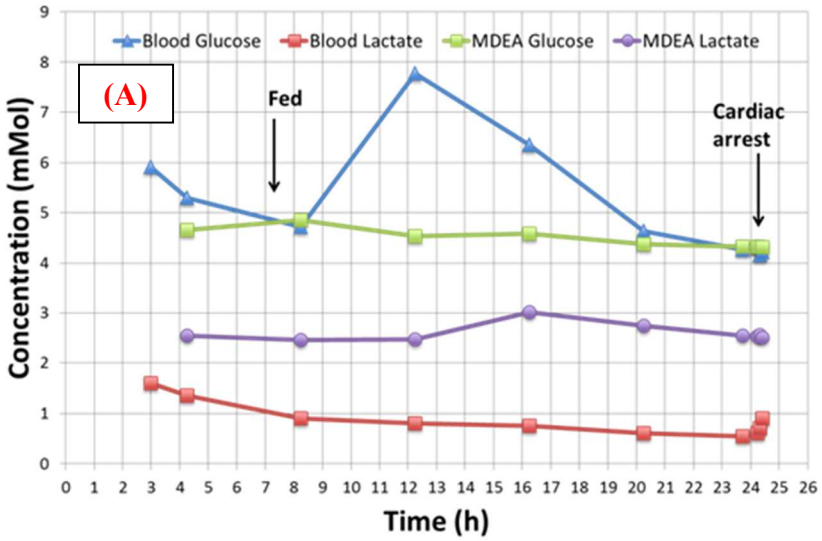

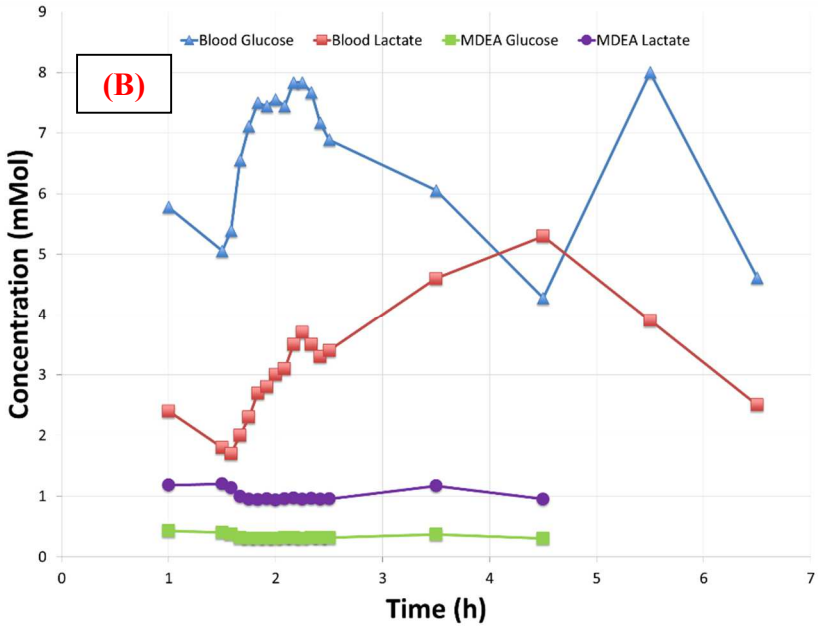

Figure 6. *In vivo* amperometric performance of the implanted PSMBioChip during surgical preparation of a *Sus scrofa* porcine control (A) and a *Sus scrofa* porcine hemorrhage (B) model.

In the trauma induced porcine model, the biotransducer devices were not sensitive enough to the variation in glucose and lactate concentrations in the tissue although the blood glucose and lactate showed these concentration changes. Although there was simultaneous measurement of glucose and lactate in the tissue, the measurements did not correspond to the blood glucose and blood lactate measurements.

1.4. *Conclusions*

A dual glucose and lactate responsive biotransducer has been demonstrated for use *in vivo*. The increase of the charge density does not appear to change the biotransduction characteristics significantly as shown in the deposition kinetics although the single layered 100 mC/cm^2 device showed a higher sensitivity compared to the multi layered devices.

The inclusion of a nickel hexacyanoferrate (NiHCF) mediative layer showed consistency in electrodeposition compared to unmodified devices. Electrochemical Impedance Spectroscopy (EIS) data showed that the mediative layer did not change the impedance of the Pt electrode compared to a bare Pt electrode and each successive layer reduced the impedance of the blank device compare to the mediative layer modified device. More importantly, the overoxidation data showed that the impedance of both devices are similar regardless of mediative layer. Thus showing that the inclusion of the mediative layer did not modify the final impedance profile of the completed device compared to the non mediative layer modified device.

In vitro dose response to glucose, showed that the non mediator modified device has a higher sensitivity (0.94 nA/mM) than the mediator modified device (0.32 nA/mM) while the *in vivo* response to glucose and lactate showed that the device with no mediator layer had ~5x (3.05 nA/mM vs. 0.67 nA/mM) the sensitivity to glucose and ~4x (1.95 nA/mM vs. 0.57 nA/mM) the sensitivity to lactate. The hydrogel coated device showed a greater sensitivity to glucose and lactate over the non hydrogel coated device due to the quick adsorption of proteins and other biofoulants to the surface of the non coated biotransducers.

Future studies will refine the biofabrication process to include enzyme-carbon nanotube supramolecular conjugates for a more sensitive and stable dual responsive device and will seek to understand the interaction between the pyrrole based enzyme layer and the catalytic layer.

1.5. *Acknowledgments*

This work was conducted under Cooperative Research and Development Agreement (CRADA) MRMC W81XWH-13-0409 between Tripler Army Medical Center (TAMC) (Uyehara) and Clemson C3B (Guiseppi-Elie). Support was received from the US Department of Defense (DoD PRMRP) grant PR023081/DAMD17-03-1-0172 to Clemson University, by the Consortium of the Clemson University Center for Bioelectronics, Biosensors and Biochips (C3B) and by ABTECH Scientific, Inc.

1.6. *References*

References

Apetrei, C., et al. (2011). "Amperometric tyrosinase based biosensor using an electropolymerized phosphate-doped polypyrrole film as an immobilization support. Application for detection of phenolic compounds." Electrochimica Acta**56**(24): 8919-8925.

Aucoin, H., et al. (2013). "Release of Potassium Ion and Calcium Ion from Phosphorylcholine Group Bearing Hydrogels." Polymers**5**(4): 1241-1257.

Aussedat, B., et al. (2000). "Interstitial glucose concentration and glycemia: implications for continuous subcutaneous glucose monitoring." American Journal of Physiology - Endocrinology and Metabolism**278**(4): E716-E728.

Badea, M., et al. (2003). "Oxidase enzyme immobilisation through electropolymerised films to assemble biosensors for batch and flow injection analysis." Biosensors and Bioelectronics**18**(5): 689-698.

Bai, J., et al. (2011). 3.331. Conjugated polymers for biosensor devices, Elsevier: Oxford, UK**:** 529-556.

Bartlett, P. and R. Whitaker (1987). "Electrochemical immobilisation of enzymes: Part I. Theory." Journal of electroanalytical chemistry and interfacial electrochemistry**224**(1): 27-35.

Bartlett, P. and R. Whitaker (1987). "Electrochemical immobilisation of enzymes: Part II. Glucose oxidase immobilised in poly-N-methylpyrrole." Journal of electroanalytical chemistry and interfacial electrochemistry**224**(1): 37-48.

Bartlett, P. N. and D. J. Caruana (1992). "Electrochemical immobilization of enzymes. Part V. Microelectrodes for the detection of glucose based on glucose oxidase immobilized in a poly (phenol) film." Analyst**117**(8): 1287-1292.

Bartlett, P. N. and D. J. Caruana (1994). "Electrochemical immobilization of enzymes. Part VI. Microelectrodes for the detection of L-lactate based on flavocytochrome b2 immobilized in a poly (phenol) film." Analyst**119**(2): 175-180.

Chen, X., et al. (2012). "Glucose biosensor based on three dimensional ordered macroporous self-doped polyaniline/Prussian blue bicomponent film." Analytica chimica acta**723**: 94-100.

Cosnier, S. (1999). "Biomolecule immobilization on electrode surfaces by entrapment or attachment to electrochemically polymerized films. A review." Biosensors and Bioelectronics**14**(5): 443-456.

Debiemme-Chouvy, C. and T. T. M. Tran (2008). "An insight into the overoxidation of polypyrrole materials." Electrochemistry Communications**10**(6): 947-950.

Endo, H., et al. (2009). "Wireless enzyme sensor system for real-time monitoring of blood glucose levels in fish." Biosensors and Bioelectronics**24**(5): 1417-1423.

George, P. M., et al. (2005). "Fabrication and biocompatibility of polypyrrole implants suitable for neural prosthetics." Biomaterials**26**(17): 3511-3519.

Goddard, J. M. and J. Hotchkiss (2007). "Polymer surface modification for the attachment of bioactive compounds." Progress in polymer science**32**(7): 698-725.

Guiseppi-Elie, A. (1998). Chemical and biological sensors having electroactive polymer thin films attached to microfabricated devices and possessing immobilized indicator moieties, U.S. Patent No. 5,766,934.

Guiseppi-Elie, A. (2010). "Electroconductive hydrogels: synthesis, characterization and biomedical applications." Biomaterials**31**(10): 2701-2716.

Guiseppi-Elie, A., et al. (2005). "Design of a subcutaneous implantable biochip for monitoring of glucose and lactate." IEEE Sensors Journal**5**(3): 345-355.

Guiseppi-Elie, A., et al. (2006). "Biosensors based on electrically conducting polymers." Handbook of conducting polymers: conjugated polymer processing and applications**3**: 435-479.

Guiseppi-Elie, A., et al. (2012). "Crosslink density of a biomimetic poly(HEMA)-based hydrogel influences growth and proliferation of attachment dependent RMS 13 cells." Journal of Materials Chemistry**22**(37): 19529-19539.

Guiseppi-Elie, A., et al. (1995). "Specific immobilization of electropolymerized polypyrrole thin films onto interdigitated microsensor electrode arrays." Langmuir**11**(5): 1768-1776.

Holdcroft, S. and B. L. Funt (1988). "Preparation and electrocatalytic properties of conducting films of polypyrrole containing platinum microparticulates." Journal of electroanalytical chemistry and interfacial electrochemistry**240**(1): 89-103.

Hsueh, C. and A. Brajter-Toth (1994). "Electrochemical Preparation and Analytical Applications of Ultrathin Overoxidized Polypyrrole Films." Analytical Chemistry**66**(15): 2458-2464.

Ishihara, K., et al. (1990). "Preparation of phospholipid polymers and their properties as polymer hydrogel membranes." Polym J**22**(5): 355-360.

Jongwon, P., et al. (2006). "Oxidase-coupled amperometric glucose and lactate sensors with integrated electrochemical actuation system." Instrumentation and Measurement, IEEE Transactions on**55**(4): 1348-1355.

Kang, E., et al. (1996). "Surface modification of electroactive polymer films by ozone treatment." Surface and interface analysis**24**(1): 51-58.

Karunwi, O., et al. (2013). "Engineering the abio-bio interface to enable more than moore in functional bioelectronics." Journal of The Electrochemical Society**160**(4): B60-B65.

Karunwi, O., et al. (2013). "Engineering the Abio-Bio Interface to Enable More than Moore in Functional Bioelectronics." Journal of The Electrochemical Society**160**(4): B60-B65.

Karunwi, O., et al. (2013). "Engineering the Abio-Bio Interface to Enable More than Moore in Functional Bioelectronics." Journal of The Electrochemical Society**160**(4): B60-B65.

Karyakin, A. A. and E. E. Karyakina (1999). "Prussian Blue-based `artificial peroxidase' as a transducer for hydrogen peroxide detection. Application to biosensors." Sensors and Actuators B: Chemical**57**(1–3): 268-273.

Kotanen, C. and A. Guiseppi-Elie (2010). "Development of an implantable biosensor system for physiological status monitoring during long duration space flights." Gravitational and Space Biology**23**(2): 55-63.

Kotanen, C. and A. Guiseppi-Elie (2013). "Characterization of a wireless potentiostat for integration with a novel implantable biotransducer."

Kotanen, C., et al. (2014). "Biofabrication Using Pyrrole Electropolymerization for the Immobilization of Glucose Oxidase and Lactate Oxidase on Implanted Microfabricated Biotransducers." Bioengineering**1**(1): 85-110.

Kotanen, C. N. and A. Guiseppi-Elie (2012). "Bioactive Electroconductive Hydrogels Yield Novel Biotransducers for Glucose." Macromolecular Symposia**317-318**(1): 187-197.

Kotanen, C. N., et al. (2012). "Implantable enzyme amperometric biosensors." Biosensors and Bioelectronics**35**(1): 14-26.

Kotanen, C. N., et al. (2012). "Bioactive electroconductive hydrogels: the effects of electropolymerization charge density on the storage stability of an enzyme-based biosensor." Applied biochemistry and biotechnology**166**(4): 878-888.

Kotanen, C. N., et al. (2013). "Amperometric glucose biosensor based on electroconductive hydrogels." Talanta**103**: 228-235.

Kotanen, C. N., et al. (2013). "Amperometric glucose biosensor based on electroconductive hydrogels." Talanta**103**(0): 228-235.

Kotanen, C. N., et al. (2013). "The effect of the physicochemical properties of bioactive electroconductive hydrogels on the growth and proliferation of attachment dependent cells." Biomaterials**34**(27): 6318-6327.

Krylov, A. V. and F. Lisdat (2007). "Nickel Hexacyanoferrate-Based Sensor Electrode for the Detection of Nitric Oxide at Low Potentials." Electroanalysis**19**(1): 23-29.

Lee, H., et al. (1999). "Dependence of the electrochemical behavior of poly (N-phenylpyrrole) films on the type of anion and solvent used in the electropolymerization." The Journal of Physical Chemistry B**103**(29): 6030-6035.

Lee, H., et al. (2002). "Effects of dopant anions and< i> N</i>-substituents on the electrochemical behavior of polypyrrole films in propylene carbonate solution." Electrochemistry Communications**4**(2): 128-133.

Nakamura, S., et al. (2010). "Effect of Calcium Ion Concentrations on Osteogenic Differentiation and Hematopoietic Stem Cell Niche-Related Protein Expression in Osteoblasts." Tissue Engineering Part A**16**(8): 2467-2473.

Palmisano, F., et al. (1994). "An< i> in situ</i> electrosynthesized amperometric biosensor based on lactate oxidase immobilized in a poly-o-phenylenediamine film: determination of lactate in serum by flow injection analysis." Biosensors and Bioelectronics**9**(7): 471-479.

Palmisano, F., et al. (2000). "Simultaneous monitoring of glucose and lactate by an interference and cross-talk free dual electrode amperometric biosensor based on electropolymerized thin films." Biosensors and Bioelectronics**15**(9): 531-539.

Palmisano, F., et al. (2000). "Amperometric biosensors based on electrosynthesised polymeric films." Fresenius' journal of analytical chemistry**366**(6-7): 586-601.

Park, J., et al. (2006). "Oxidase-coupled amperometric glucose and lactate sensors with integrated electrochemical actuation system." Instrumentation and Measurement, IEEE Transactions on**55**(4): 1348-1355.

Peppas, N., et al. (2000). "Hydrogels in pharmaceutical formulations." European journal of pharmaceutics and biopharmaceutics**50**(1): 27-46.

Qi, Z., et al. (1996). "Electrochemically Induced Substitution of Polythiophenes and Polypyrrole." Chemistry of Materials**8**(3): 701-707.

Rahman, A. R. A., et al. (2009). "Towards an implantable biochip for glucose and lactate monitoring using micro-disc electrode arrays (MDEAs)." Biomedical Microdevices**11**(1): 75-85.

Rahman, M. A., et al. (2012). "Stability and Sensitivity Enhanced Electrochemical In Vivo Superoxide Microbiosensor Based on Covalently Co-immobilized Lipid and Cytochrome c." Analytical Chemistry**84**(15): 6654-6660.

Rahman, M. A., et al. (2005). "Functionalized Conducting Polymer as an Enzyme-Immobilizing Substrate: An Amperometric Glutamate Microbiosensor for in Vivo Measurements." Analytical Chemistry**77**(15): 4854-4860.

Ramanaviciene, A., et al. (2007). "Biocompatibility of polypyrrole particles: an in-vivo study in mice." Journal of pharmacy and pharmacology**59**(2): 311-315.

Rodrigo M. Iost, F. N. C. (2012). "Layer-by-layer self-assembly and electrochemistry: Applications in biosensing and bioelectronics." Biosensors and Bioelectronics**31**(1): 10.

Sadki, S., et al. (2000). "The mechanisms of pyrrole electropolymerization." Chemical Society Reviews**29**(5): 283-293.

Sitnikova, N. A., et al. (2011). "Superstable Advanced Hydrogen Peroxide Transducer Based on Transition Metal Hexacyanoferrates." Analytical Chemistry**83**(6): 2359-2363.

Slaughter, B. V., et al. (2009). "Hydrogels in regenerative medicine." Advanced Materials**21**(32-33): 3307-3329.

Tseng, T. T.-C. and H. G. Monbouquette (2012). "Implantable microprobe with arrayed microsensors for combined amperometric monitoring of the neurotransmitters, glutamate and dopamine." Journal of Electroanalytical Chemistry**682**: 141-146.

Tseng, T. T.-C., et al. (2013). "Selective enzyme immobilization on arrayed microelectrodes for the application of sensing neurotransmitters." Biochemical Engineering Journal**78**: 146-153.

Uyehara, C. F. and J. Sarkar (2013). "Role of vasopressin in maintenance of potassium homeostasis in severe hemorrhage." American Journal of Physiology-Regulatory, Integrative and Comparative Physiology**305**(2): R101-R103.

Valaski, R., et al. (2002). "Influence of film thickness on charge transport of electrodeposited polypyrrole thin films." Thin Solid Films**415**(1): 206-210.

Wang, X., et al. (2004). "Evaluation of biocompatibility of polypyrrole in vitro and in vivo." Journal of Biomedical Materials Research Part A**68**(3): 411-422.

Wilson, A. N., et al. (2012). "Bioactive hydrogels demonstrate mediated release of a chromophore by chymotrypsin." Journal of Controlled Release**160**(1): 41-47.

Yehezkeli, O., et al. (2009). "Integrated Oligoaniline-Cross-Linked Composites of Au Nanoparticles/Glucose Oxidase Electrodes: A Generic Paradigm for Electrically Contacted Enzyme Systems." Chemistry-a European Journal**15**(11): 2674-2679.

Zhou, H., et al. (2004). "Preparation and bioelectrochemical responses of the poly (< i> m</i>-phenylenediamine) glucose oxidase electrode." Sensors and Actuators B: Chemical**101**(1): 224-230.

Zimmermann, S., et al. (2004). "In-device enzyme immobilization: wafer-level fabrication of an integrated glucose sensor." Sensors and Actuators B: Chemical**99**(1): 163-173.

CHAPTER FIVE

FURTHER WORK

The work of this thesis may be extended in multiple directions. In view of the motivation to address the development and deployment of an advanced generation-3 biotransducer with integrated wireless reporting, the following considerations arise.

Generation 3 system: The fabrication of physico-chemical conjugates of enzymes and SWNTs was shown in the previous work of Choi to be feasible and in the work of Chapter 2 that the application of cavitation energy associated with ultrasonication was effective in creating the conjugates without loss of enzyme bioactivity. However, there was no direct evidence of conjugate formation. For example, Raman Spectroscopy could have been used to elucidate any interactions between the enzyme and SWNT. By studying the G and B bands of the SWNT one may be able to discern any shifts in these band structures arising from the interactions of the enzyme and the SWNT. Similarly, IR spectroscopy could have been used to study the corresponding shifts in the enzyme. Furthermore, by also conducting these Raman and IR spectroscopies with the peptides of Chapter 3, there could be further elucidation of these interactions. A study of these interactions would therefore serve to tie the findings of Chapters 2 and 3 more closely together. Similarly, a study of the percent incorporation of the SWNT by the enzyme could be gleaned for a study by Energy Dispersive X-tray Analysis (EDAX). EDAX will allow a comparison of the carbon to nitrogen ratio (C:N) of the pristine enzyme and the enzyme-SWNT conjugate. In this way, the amount of SWNT entrained by the enzyme could be determined.

Energetics: The fundamental nature of the interaction between the enzyme co-factor, FAD, and the SWNT has not been addressed. Hence, it is unclear as to whether this is thermodynamically feasible. The energetics of the redox process involving FAD and the SWNT will be governed by the band structures of the components. Accordingly, the band energies of SWNT and the redox potential of FAD must be reconciled so that there is clear appreciation of the thermodynamic feasibility of the direct electron transfer.

Electrical properties: The physico-chemical enzyme-SWNT conjugates were to be fully characterized for their electrical and electrochemical properties. Preliminary work performed by a summer intern (Jorge Hernandez) that involved casting of the enzyme-SWNT conjugates onto chemically modified interdigitated microsensor electrodes of gold and platinum allowed the study of AC Electrical Impedance Spectroscopy (EIS) as well as IV (DC) characterization. **I-V Characterization** was performed in air (-1.0 to +1.0 V) using a Keithley 4200 Semiconductor Characterization System connected to a probe station via a switching matrix and was run using the Keithley Interactive Test Environment (KITE) software. **Electrical Impedance Spectroscopy (EIS)** (20 mV p-t-p, 10^{-1} – 10^{6} Hz, RT) was performed in air, in freshly prepared 1X PBS, and in 1X PBS containing 50 mM $[Fe(CN)_6]^{3-/4-}$) (EIS-2E) using a Solartron 1260 Frequency Response Analyzer equipped with ZView and ZPlot software. Preliminary indications are that entirely ohmic behavior was observed across 10 micron channel widths. I-V characterization (**Fig. 1**) shows that bioconjugate samples containing SWNTs to be conductive compared to their controls. De-bundling of SWNTs by BSA appears more efficient than GOx, producing larger conductivity.

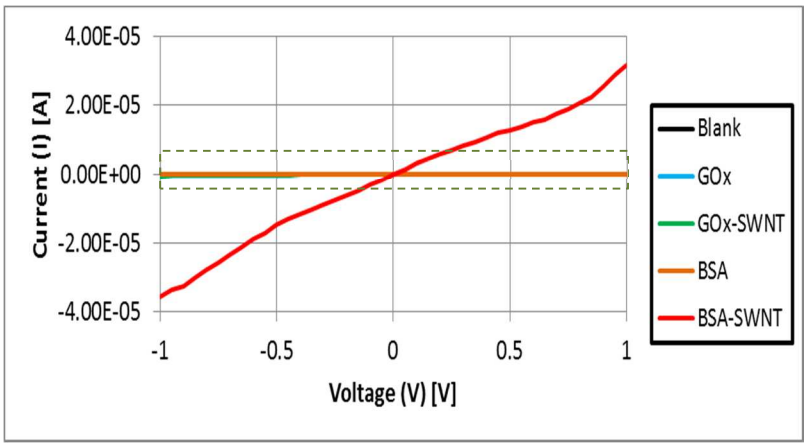

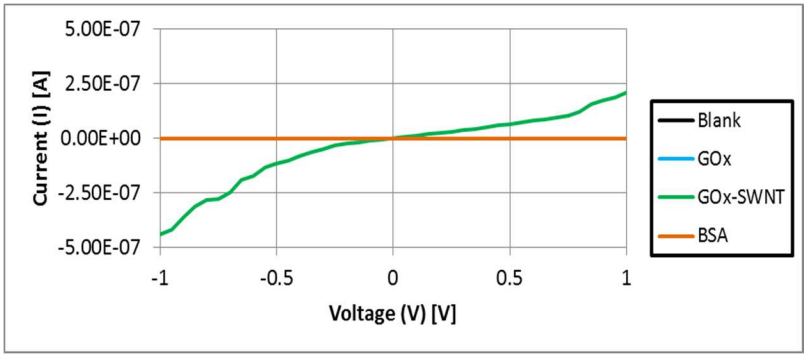

Figure 1. IV characterization curves of OTS modified IME-co-IAME 2-1-Pt chips, in air; left plot displays all chips, right plot excludes BSA-SWNT chip to make the rest visible.

Optical characterization: Full TEM and AFM characterization were to be performed on these conjugates. Conjugates isolated from the supernatant following centrifugation should be cast onto TEM grids and analyzed using both environmental TEM and standard TEM.

Fabrication of biotransducers: Bioactive membrane layers should be evaluated at 10, 30, 70, 100, 150, 200 mC/cm^2. In previous work, seeding layers of varying thicknesses (electropolymerization charge density) was investigated. The conclusion was to use a particular seeding layer thickness which did not adversely impact the device sensitive but greatly accelerated the electropolymerization of the bioactive layer. Further work is needed to optimize the thickness of the bioactive layer. Hence, bioactive membrane layers fabricated from electropolymerization charge densities corresponding to 10, 30, 70, 100, 150, 200 mC/cm^2 should be evaluated.

Performance of the mediator layers: In this work, two different mediator layers were fabricated and studied – NiHCFe and/or FeHCFe. Both there mediators have demonstrated the expected mediator performance in the presence of hydrogen peroxide (H_2O_2) and so confirmed previously reported literature findings. However, when the bioactive layers were electrodeposited onto these mediators, there was no corresponding mediator enhancement of the peroxide response. There are several possibilities 1) that the mediator layer is unstable in the electropolymerizing medium. That is, that the medium (pH, ionic strength

or chemical composition) may be inappropriate for maintaining the stability of the mediator layer. This may be tested by simply immersing the electrodeposited mediator layer into the electropolymerization bath for a time corresponding to the time it takes to electropolymerize the bioactive layer and then returning the electrode to the peroxide dose response test. 2) That the potentiodynamic voltage sweep that corresponds to the electrodeposition of the bioactive layer eliminates or inactivates the mediator layer. This may be tested by placing the mediator layer into a similarly composted test solution (minus the pyrrole components), conducting the "dummy" electropolymerization and then returning it the electrode to the peroxide dose response test. 3) That the extreme conditions associated with over-oxidation eliminates or renders the mediator layer in active. This may be tested by employing an electrodeposition process that results in the formation of an insulating membrane layer. Electrodeposition of enzyme-loaded membranes has generated as much as 102 mA/cm^2, [1] which is three orders of magnitude higher than the values obtained in this work.

Use of alternative mediator layers: Mediator layers, such as NiHCFe or FeHCFe, have been thoroughly investigated in the literature. However, the novelty of an electrodeposited bioactive layer formed by electropolymerization of pyrrole was an attractive option. In view of the challenges found in the use of these layers, alternative layers should be explored. Among these are; i) Enzyme layers such as peroxidases, ii) under-potential deposited platinum, iii) platinum black and iv) tethered osmium layers.

Peroxidases are enzymes that catalyze the conversion of hydrogen peroxide to water and molecular oxygen ($2\ H_2O_2 = O_2 + 2\ H_2O$). This allows the amperometric monitoring of oxygen (E_{app} = 650 mV *vs.* Ag/AgCl, 3M Cl-) and thus an indirect measurement of catalytic bioactivity of the immobilized oxidoreductase. They generally occur in close association with oxidoreductases such as glucose oxidase, lactate oxidase and laccase and possess very high catalytic turnover rates that serve to rapidly remove and so protect the surrounding milieu, include the enzyme that generated it, from the deleterious effects of H_2O_2 and the formation of perodixe radicals. Among these are catalase (EC 1.11.1.6; MW = 240,000, k_{cat} = ($3.8 \times 10^7\ M^{-1}\ s^{-1}$; heme NADP(+) binding) the kinetic coupling of glucose oxidase

with catalase has been studied and shown to offer a best fit of [O_2] to a kinetic model is obtained with the rate constants for glucose oxidation and peroxide decomposition equal to 0.116 s^{-1} and 0.090 s^{-1} respectively [2].

In addition to peroxidases, molecules based on the heme prosthetic group, such as deuteroferrihaem, mesoferrihaem, coproferrihaem and haematoferrihaem have also been shown to the catalytic for hydrogen peroxide [3].

Toxicity studies: While SWNT conjugated to enzymes have not shown any adverse effect on enzyme bioactivity or structure over a period of months, there is still concern about these conjugated SWNTs eluting from the hydrogel covered biosensors and triggering adverse effects similar to asbestos fibers due to their high aspect ratio.

References

1. Tan, Y., et al., *Immobilization of enzymes at high load/activity by aqueous electrodeposition of enzyme-tethered chitosan for highly sensitive amperometric biosensing.* Biosens Bioelectron, 2010. **25**(12): p. 2644-50.
2. Tao, Z., et al., *Kinetic Studies on Enzyme-Catalyzed Reactions: Oxidation of Glucose, Decomposition of Hydrogen Peroxide and Their Combination.* Biophysical Journal, 2009. **96**(7): p. 2977-2988.
3. Hatzikonstantinou, H. and S.B. Brown, *Catalase model systems. Decomposition of hydrogen peroxide catalysed by mesoferrihaem, deuteroferrihaem, coproferrihaem and haematoferrihaem.* Biochemical Journal, 1978. **174**(3): p. 893-900.

APPENDICES

Appendix A

Standard Operating Procedures

Subject: MDEA 5037 Bio-transducer Preparation and *In vitro* Characterization			
GOAL: Prepare the transducer device for the simultaneous in vitro and in vivo detection of glucose and lactate			
Equipment: UV_Clean Boekel Model, Temperature controlled water bath, Ultrasonic cleaner, Convection oven, EG&G PAR M283 for Biofabrication, BAS 100B/W for Bioanalysis, PA-I low module current.			
Material: MDEA-Pt 5037 devices, 3-aminopropyl-trimethoxysilane (APTES), trichloroethylene, 2-propanol, acetone, toluene, DI water, ethanol			
Prepared by:	Christian Kotanen, Kayode Karunwi, Chaker Tlili, Ph.D., Prof. Anthony Guiseppi-Elie December 24, 2013 (modified January 4, 2014)		
Approved by:			
Laboratory Director	Date	Laboratory Manager	Date
Prof. Anthony Guiseppi-Elie	12/6/2013	Kayode Karunwi	12/9/2013

There are four principal steps in the preparation and characterization of **MDEA 5037-M (M= Pt of Au) Biotransducers**. These steps are:

1. *Packaging of the transducer*
2. *Surface cleaning of MDEAs 5037-Pt*
3. *Surface Modification and Functionalization*
4. *Amperometric characterization of enzymatic response*

MDEA 5037	1 ea. MDEA W.E.	2 ea. R.E.	1 ea. C.E.

Area (cm^2)	7.27×10^{-4}	14.54×10^{-5}	7.27×10^{-3}

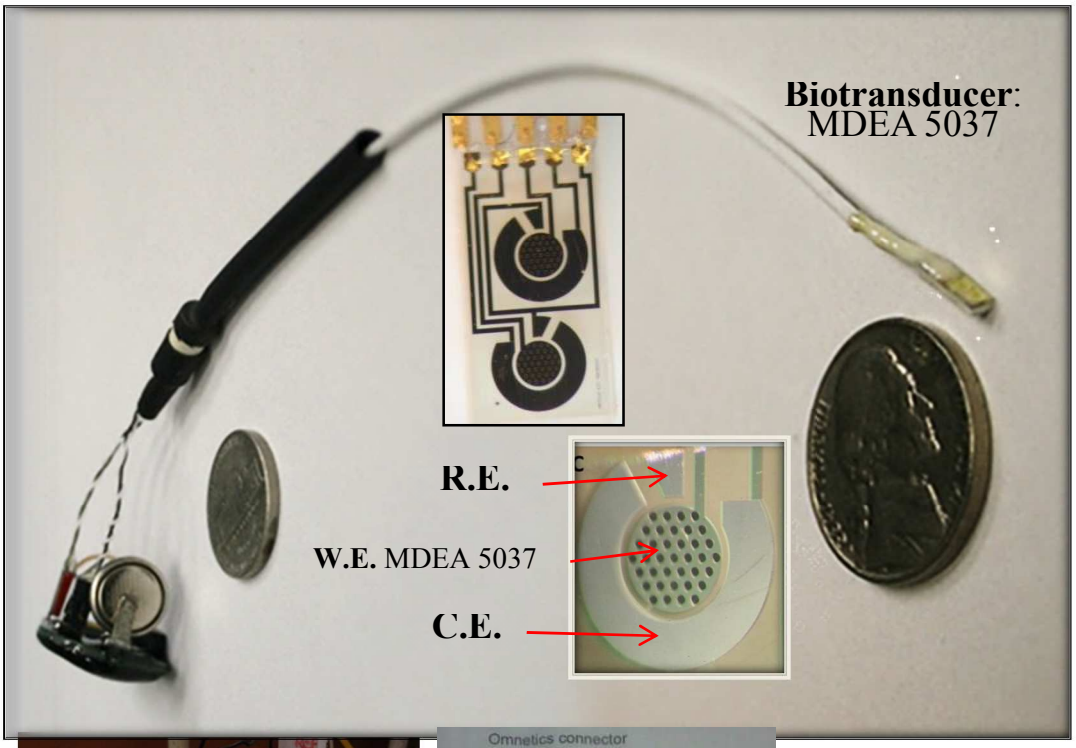

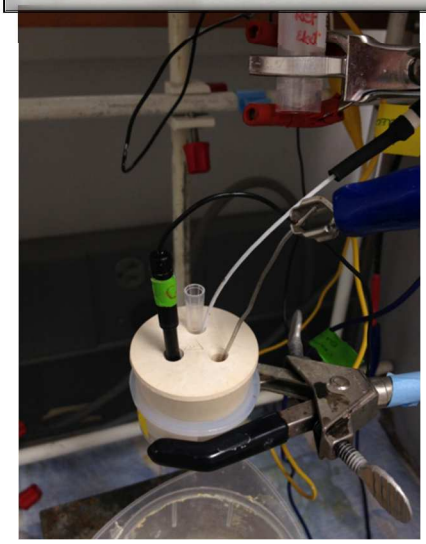

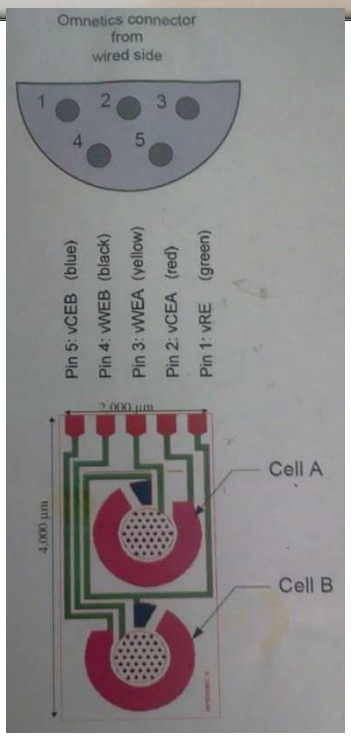

Yellow-A (Ch1)

Black-B (Ch2)

2. Packaging of the MDEA-5037-M Chip

Transducers are provided as partly packaged devices (Figure 1). However, there is need to protect the adhesive layer that sits between the chip and its ceramic substrate. To achieve this, a layer of biocompatible epoxy is applied around the perimeter of the chip.
Using a brush pick, apply a thin layer of one-component epoxy around the perimeter of the chip and cure it at 150°C for 90 minutes.

3. Surface cleaning of MDEAs 5037-Pt:

Glass: If glass containers are used, it is often necessary to clean them extensively to prevent solution contamination with other organic or inorganic compounds. Piranha solution (30:70 v/v solution of 30% of hydrogen peroxide (H_2O_2) and concentrated sulfuric acid (H_2SO_4) can be used to clean the glass containers. **Caution:** ***extremely aggressive, please take care by wearing safety goggles and protective clothes***. After one hour, take out the glass containers and wash extensively with ultrapure (DI) water.

3.1. *Degreasing cleaning steps:*

*Packaged MDEA 5037s must **not** be immersed in boiling solvents or the chip will dis-bond from its ceramic carrier.*

- The clear polymer coating, if used to protect the platinum or gold surface of the chip, should be removed mechanically using a sharp tipped pair of forceps and inspected under the optical inspection microscope.
- Immerse the *MDEA-Pt 5037* into the following cleaning solvents that are placed within suitable glass containers and the containers placed in a water bath:
- Ultrasonicate in DI water for 3 min.
- Ultrasonicate in 100% IPA for 3 min.
- Ultrasonicate in DI-water for 3 min.
- Blow dry with UHP Nitrogen

3.2. *II.2- UV-Ozone Clean steps:*

- Clean the tray of the UV-Clean™ ozone cleaner (Boekel Industries) by wiping with and isopropyl alcohol (2-propanol) lint-free, wet wipe.
- Place the MDEA-Pt 5037 with the electrode side facing upwards in the tray of the UV-Clean™ ozone cleaner, close the door and clean for 10 minutes. This step removes adventitious adsorbed organics and tenaciously adsorbed organic thin films. This is not suitable for thick organic films.

- Wash the UV-cleaned devices by ultrasonic washing for 1 min in 2-propanol in a beaker.

3.3. *Plasma Cleaning and Surface Activation Steps:*

Air/water vapor Plasma Treatment – 10 min - maintaining as good and stable a vacuum as possible. Apply brief vacuum to water container to fill chamber with water vapor, seal off chamber and evacuate for 5 minutes. Turn on plasma, DO NOT BLEED IN AIR – Plasma should be blue not purple – **wear UV protection glasses.**

This step cleans and introduces a controlled abundance of surface -OH functional groups to the Si_3N_4 layer of the device.

4. Surface Modification and Functionalization:

4.1. *Organosilane Surface Modification:*

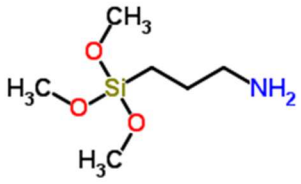

- Freshly prepare a 3-aminopropyl trimethoxysilane (Y-APS) solution using 4.33 µL γ-APS (0.1 wt%) and 5 mL in anhydrous ethanol (stored over molecular sieves).
- Place the transducer into the solution and incubate in a convection oven at 40 ºC for 45 minutes. (*Keep covered to limit evaporation*)
- Remove transducer from organosilane and ultrasonicate in IPA for 3 minutes.
- Cure in (preferably a 0.22 micron filtered) convection oven at 40°C for 20 min, 110°C for 20 min then 40°C for 20 min.

This step introduces surface $–NH_2$ functional groups by depositing and coupling the γ-APS **silanol to the –OH groups of the Si_3N_4 layer of the device. It also deposits an uncoupled layer** γ-APS **silanol on the Pt or Au of the device.**

4.2. *Further PEG Surface* Derivatization*:*

The ACLT-PEG-NHS ester is a light sensitive compound and will cross-link upon exposure to ultraviolet light. HANDLE UNDER UV-FREE CONDITONS ONLY. ACLT-PEG-NHS has a substitution of 90% or greater at the acrylate end and 95% or greater at the NHS ester end.

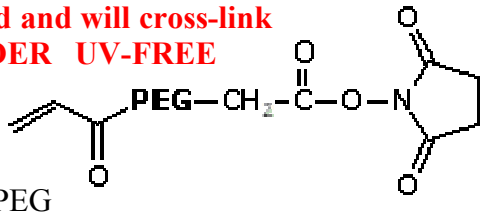

(An alternative is M-PEG(5000)-ALD-5000 Methoxy PEG Propionaldehyde, MW 5000)

- Freshly prepare a derivatizing solution of ACLT–PEG(3500) -NHS (MW 3500) to 0.1 wt% in 3 mL of slightly alkaline DI water (pH 7.2-8.5).
- Place the γ-APS-modified transducer into the derivatizing solution and incubate at RT for 30 min with gentle stirring. (*Keep covered to limit evaporation*)
- Remove transducer from the derivatizing solution and ultrasonicate in IPA for 1 min.
- s to yield stable amide bonds. The reaction.

This step introduces oligomeric chains of ethylene oxide to mitigate physical adsorption of enzymes onto the Pt or Au electrodes orother parts of the device. The NHS ester reacts with the primary amine of the γ-APS on the surface to form a stable amide bond and releases *N*-hydroxysuccinimide (MW 115) which is removed by washing.

4.3. *Electrochemical Cleaning to Remove Adsorbed Silanol from Working Electrodes to be Immediately Modified:*

Clean ONLY the working electrode that is to be modified and complete the enzyme entrapment step BEFORE cleaning the other working electrode and entrapping the next enzyme system.

For Anodic cleaning:

- For MDEA5037-Pt (platinum) electrodes: Prepare a solution of 0.5M H_2SO_4: Carefully add 5.5 ml H_2SO_4 (98%) in 194.5 ml of ultrapure (DI) water.
- For MDEA 5037-Au (gold) electrodes: Prepare solution as stated above, then dilute to 0.05 M H_2SO_4 and use this for the following electrochemical cleaning.
- Use a three-electrode electrochemical configuration (Working electrode (W.E.), counter electrode (C.E.), and a reference electrode (R.E.); (usually Ag/AgCl,3M Cl^-) in 0.5M (or 0.05M) of H_2SO_4 at RT.
- Using the Cyclic Voltammetric mode of the potentiostat, cycle the potential of the working electrode of the MDEA between -0.2 and +1.5 V vs. Ag/AgCl (3M KCl) at **100 mV/s** for 8 minutes or until stable, non-varying CVs are obtained.
- Rinse the electrode with ultrapure (DI) water and dry by blowing 0.22 micron filtered compressed air or pure nitrogen (N_2).

This step removes the adsorbed, uncoupled γ-APS silanol layer from the Pt or Au of the device. This procedure has been shown to be effective by coupling a fluorophore to the $-NH_2$ and following its removal from the surface.

For Cathodic cleaning:

- Prepare an electrochemical cell with PBS buffer (pH=7.2) at room temperature.

- Cycle between 0 to -1200 mV vs. Ag/AgCl (3 M KCl) at 100 mV/s for 8 minutes or until stable non-varying CVs are obtained.
- Rinse the electrode with ultrapure (DI) water and dry by blowing 0.22 micron filtered compressed air or pure nitrogen (N2). γ-APS silanol layer from the Pt or Au of the device.

This step removes the adsorbed, uncoupled γ-APS silanol layer from the Pt or Au of the device. This procedure has been shown to be effective by coupling a fluorophore to the $-NH_2$ and following its removal from the surface.

4.4. *Deposit a Flash of Polypyrrole on the W.E. for Adhesion Promotion:*

- Prepare the following electropolymerization solution: 5.0 ml in DI-Water - 0.2 M Py, 0.05 M polystyrene sulfonic acid (PSSA 30%, 70,000 MW, ρ=1.10 g/ml). (Using the basis of 4 pyrroles to 1 sulfonate, calculate the PSSA concentration to establish a 4:1 mol ratio of pyrrole monomer to sulfonate repeat units in the solution)
    - 4 mL DI water
    - 42 uL of 30% PSSA, pH = 1.68
    - About 10 uL 1.0 M NaOH and 10 uL 0.1 M NaOH, pH = 4.5-5.0 (you may need to do 100, then gradually add increments of 1-5 µL with stirring until you get to the right pH)
    - 70 uL Py (previously passed over an activated alumina column)
    - 788 uL of DI-Water (Or however much is still needed to achieve 5.0 mL)
    - pH = Check using pH FET meter, anywhere from 4.5 – 5.0 is acceptable.
- Electropolymerize pyrrole using the EG&G PAR M283:
    - Apply 750 mV vs. Ag/AgCl to achieve a targeted for 1 - 10 mC/cm^2.
    - Note that electropolymerization timescale is FAST; on the order of 0.1 to 10.0 seconds.
    - Record and retain the electropolymerization curve
    - IF ADDING HYDROGEL LAYER - Rinse with 0.1 M HCl and blow dry with UHP-Nitrogen – Proceed directly to 4.2.
    - IF ADDING ELECTROPOLYMERIZAED ENZYME LAYER – Proceed directly to 4.

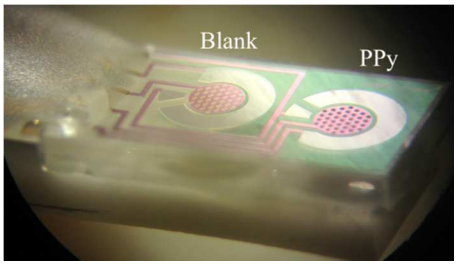

Targeted Charge Density (7.27×10^{-4} cm^2)	**Total Charge To Be Deposited (mC)**
1 mC/cm^2	**7.27×10^{-4}**
5 mC/cm^2	**3.64×10^{-3}**
10 mC/cm^2	**7.27×10^{-3}**

This step introduces a thin, adherent layer of polypyrrole onto the exposed metal of the working electrode (Pt or Au). This layer, along with the APS layer will serve for attachment of the hydrogel membrane

5. METHOD 1. Direct Electrodeposition of Enzyme Layer:

This method adds the enzyme rich layer via electropolymerization within PPy and then places a biocompatible hydrogel coating on the outside.

5.1. ***METHOD 1. Electropolymerization of PPy to Entrap Enzyme***

- Prepare the following electropolymerization solution A: 5.0 ml in DI-Water; 0.2 M Py, 0.05 M PyBA (Using the basis of 4 pyrroles to 1 PyBA, calculate the PyBA concentration to establish a 4:1 mol ratio of pyrrole monomer to carboxylate repeat units in the solution)
    - 3.0 mL DI water
    - 70 uL Py (previously passed over an activated alumina column)
    - 38.30 mg of PyBA
- Use pH FET meter to check and adjust to pH 5.0 – 5.5 by the addition of 0.1 M NaOH
- Prepare an enzyme solution B of GOx or LOx to achieve 100 ug/ml GOx or 100 ug/ml LOx
    - 1 mL DI water
    - 1 mg of GOx (LOx is in solution form. Read the concentration on the stock solution bottle and measure accordingly)
- Add 500 uL of Sol B to Sol A
- Degas by bubbling with argon and maintain gently stirred under anaerobic conditions
- Prepare muta-rotated stock solution C of 100 mM glucose or 100 mM lactate to achieve 2 mM Glucose or 2 mM Lactate
    - 100 mL DI water
    - 1.802 g of glucose or 0.901 g of lactate
- Add 20 uL of Sol C to Sol A + B

The hydrogen peroxide produced by the enzyme activity (and trace oxygen) will immediately initiate oxidative polymerization of Py to P(Py-co-PyBA) and may produce some observable darkening of the solution.

- Using the EG&G PAR M283 , immediately initiate electropolymerization of pyrrole by applying 800 mV vs. Ag/AgCl for 1 - 100 mC/cm^2 or to whatever charge density is required.

Note that electropolymerization timescale is SLOW because of low electrolyte background; on the order of 0.1 to 10.0 hours

- Record and retain the electropolymerization curve
- IMMEDIATELY RINSE PROFUSELY with flowing 1xPBS
- Transfer to 0.1 M PBS pH=7.2 buffer.

This step coats the MDEA W.E. with a further layer of PPy-co-PyBA that entraps the oxidoreductase enzyme.

5.2. *METHOD 1. Overoxidize the polypyrrole to reduce background current (Is not necessary in electro-actuation or biomolecule actuation applications)*

- Overoxidize the PPy or P(Py-*co*-PyBA) in 0.1 M PBS 7.2 Buffer.
- Prepare an electrochemical cell with PBS buffer (pH=7.2) at room temperature.
- Cycle between 0 to +1200 mV vs. Ag/AgCl (3 M KCl) at **100 mV/s** for 8 minutes, or for 40 cycles, or until stable non-varying CVs are obtained. This produces over-oxidized polypyrole (OO-PPy)
- Retain cyclic voltammograms for review.
- Rinse the electrode with ultrapure (DI) water and dry by blowing 0.22 micron filtered compressed air or pure nitrogen (N_2).

This step overoxidizes the PPy and creates a non-conductive polymer film by promoting reactions at the 3 position of polypyrrole. This reduces the amperometric background current and establishes an additive process of an electrochemically directed film capable of host the enzyme of interest.

5.3. *METHOD 1. Benzophenone for Hydrogel Adhesion Promotion*

DO NOT USE ETHANOL AS SOLVENT IF THE PPY LAYER CONTAINS ENZYMES OR OTHER SOLVENT-VULNERABLE BIOMOLECULES

- Prepare a benzophenone solution (0.01 M) in 40% EtOH/H_2O

- Dip the device into the solution or apply a single drop of the solution to working device surface
- Allow the solvent to evaporate completely.
- UV-Irradiate both sides of the device for 5 min on each side.
- Rinse with flowing 1xPBS for 10 seconds.
- Blow dry with UHP-Nitrogen.

This step creates benzaphenone free radicals that abstract hydrogen atoms from the carbonaceous surfaces, both silanol and polypyrrole layers, and results in the uniform covalent attachment of the photoinitiator benzophenone to the surface of the device.

5.4. *METHOD 1. Application of The Hydrogel Layer:*

Anneal at 37 ^{o}C for 1 h if the PPy layer or the hydrogel layer contains enzymes or other active biomolecules.

- In the BioClean Room
- Prepare a biocompatible hydrogel cocktail according to the prevailing composition and method. (Typically 3 mol% TEGDA, 5 mol% MPC and 5 mol% OEG(400)MA)
- Dip-coat the device into the viscosity-adjusted hydrogel cocktail.
- Allow to drain and remove excess from sides by gently touching by a Kimwipe®.
- UV-irradiate both sides for 5 min to crosslink the hydrogel.
- Anneal the hydrogel coated device in a convection oven at 60 ^{o}C for 1 h, except as noted above.

This step coats the device with your formulated hydrogel, establishes photoinitiation of polymerization from the surface confined benzophenone on the surface resulting in uniform attachment of the hydrogel to the organic layers on the device and anneals the hydrogel (very important). Anneal at 37 ^{o}C for 1 h if the hydrogel contains enzymes or other biomolecules.

5.5. *Go to Step 7 – In vitro Characterization*

6. METHOD 2 - Electropolymerize Py-*co*-PyBA into the Hydrogel Layer

This method adds the enzyme rich layer via electropolymerization within or through or into the attached hydrogel coating. The hydrogel layer of this method may be different than of Method 1. Here the hydrogel must possess highly swellable and open architecture with high void volume to accommodate the enzymes and conductive polymer.

6.1. *METHOD 2 - Electropolymerize Py-co-PyBA into the Hydrogel Layer*

- Starting from the flash or seeding layer of 3.3 above, apply the hydrogel layer directly to the benzophenone-modified seed layer.
- Prepare a benzophenone solution (0.01 M) in HPLC grade Ethanol (b.p. 78.4 °C)
- Dip the device into the solution or apply a single drop of the solution to working device surface
- Allow the ethanol solvent to evaporate completely (a few minutes).
- UV-Irradiate both sides of the device for 5 min on each side.
- Rinse with flowing ethanol for 10 seconds.
- Blow dry with UHP-Nitrogen.
- Prepare the following solution: DI-Water, 0.4 M Py, 0.1 M PyBA (Using the basis of 4 pyrrole to 1 carboxylate, calculate the PyBA concentration to establish a 4:1 mol ratio of pyrrole monomer to carboxylate units in the solution).
- Immerse the benzophenone-attached, hydrogel-coated transducer into the electropolymerization solution and soak for 1 h.
- Electropolymerize Py-*co*-PyBA by applying 800 mV vs. Ag/AgCl for 1 mC/cm^2
- Note that the experiment timescale is on the order of 1 to 10 seconds.
- Rinse with DI-water and blow dry with UHP-Nitrogen.

This step electropolymerizes an additional thin layer of pyrrole co-polymer within voids of the hydrogel and builds an intertwining layer between the seeding PPy layer and the hydrogel layer at the Polypyrrole|Hydrogel interface.

6.2. *METHOD 2 – Electropolymerization of Pyrrole to Deposit and Entrap Biomolecule within the Hydrogel Layer*

- Prepare the following electropolymerization solution: DI-Water, 0.2 M Py, 0.05 M PyBA (Using the basis of 4 pyrroles to 1 PyBA, calculate the PyBA concentration to establish a 4:1 mol ratio of pyrrole monomer to carboxylate repeat units in the solution)
- Use pH FET meter to check and adjust to pH 5.0 – 5.5 by the addition of 0.1 M NaOH
- Immerse and soak the hydrogel-coated transducer for 1 h in the electropolymerization solution.
- Add solution of GOx or LOx to achieve 100 ug/ml GOx or 100 ug/ml LOx
- Degas by bubbling with argon and maintain gently stirred under anaerobic conditions
- Add muta-rotated glucose or lactate to achieve 2 mM Glucose or 2 mM Lactate
- *The hydrogen peroxide produced by the enzyme activity (trace oxygen) will immediately initiate polymerization of Py to P(Py-co-PyBA) and may produce some observable darkening of the solution.*

- Immediately initiate electropolymerization of pyrrole by applying 800 mV vs. Ag/AgCl for 1 - 100 mC/cm^2 or to whatever charge density you require.
- Note that electropolymerization timescale is SLOW because of low electrolyte background; on the order of 0.1 to 10.0 hours
- Record and retain the electropolymerization curve
- IMMEDIATELY RINSE PROFUSELY with flowing 1xPBS
- Transfer to 0.1 M PBS 7.2 Buffer.

This step electropolymerizes the pyrrole within the hydrogel and entraps the enzyme within the hydrogel layer.
This step occupies and protects the enzyme's active site with its substrate glucose or lactate during electropolymerization and entrapment with the goal of maintaining enzymatic activity; it initiates polymerization of pyrrole by H_2O_2 but also simultaneously electropolymerizes the pyrrole (P(Py-*co*-PyBA) within the hydrogel and entraps the enzyme within the hydrogel.

7. Overoxidize the polypyrrole to reduce background current (Is not necessary in electro-actuation or biomolecule actuation applications)

- Overoxidize the PPY of P(Py-co-PyBA) in 0.1 M PBS 7.2 Buffer.
- Prepare an electrochemical cell with PBS buffer (pH=7.2) at room temperature.
- Cycle between 0 to -1200 mV vs. Ag/AgCl (3 M KCl) at **100 mV/s** for 8 minutes or until stable non-varying CVs are obtained.
- Retain cyclic voltammograms for review.
- Rinse the electrode with ultrapure (DI) water and dry by blowing 0.22 micron filtered compressed air or pure nitrogen (N_2).

This step overoxidizes the PPy and creates a non-conductive polymer film by promoting reactions at the 3 position of polypyrrole. This reduces the amperometric background current and establishes an additive process of an electrochemically directed film capable of host the enzyme of interest.

8. Amperometric Characterization of the Biotransducer

1) Prepare a stock solution of muta-rotated glucose in 0.1 M PBS buffer (for general testing) or in protein amended Plasma Lite® or RPMI 1640 supplemented with rat/human serum (for simulating *in vivo* testing) and store it at 4°C when not in use.

2) Amperometric response of the enzyme electrodes to glucose or lactate are to be measured in gently stirred 5.0 ml of 0.1 M PBS (pH 7.2) by applying a potential of +0.70 V vs. Ag/AgCl reference electrode to the enzyme electrodes at RT or 37°C.

3) Before starting injection of glucose in the electrochemical cell, the background current should be allowed decay to a stable, steady-state value.

4) Start by adding the glucose in electrochemical cell to get a concentration range between 0 to 100mM.

MDEA 5037 Calibration Protocol before Implanting in Piglet

I. Preparation

1. Obtain one 500 µL and one 20 µL mico pipetter
2. Calibrate them on a scale using DI water.
3. Record the amount of DI water each one obtains.
4. Enter the data into the grey cells on the spreadsheet. This will automatically calculate concentrations of your "steps"

II.

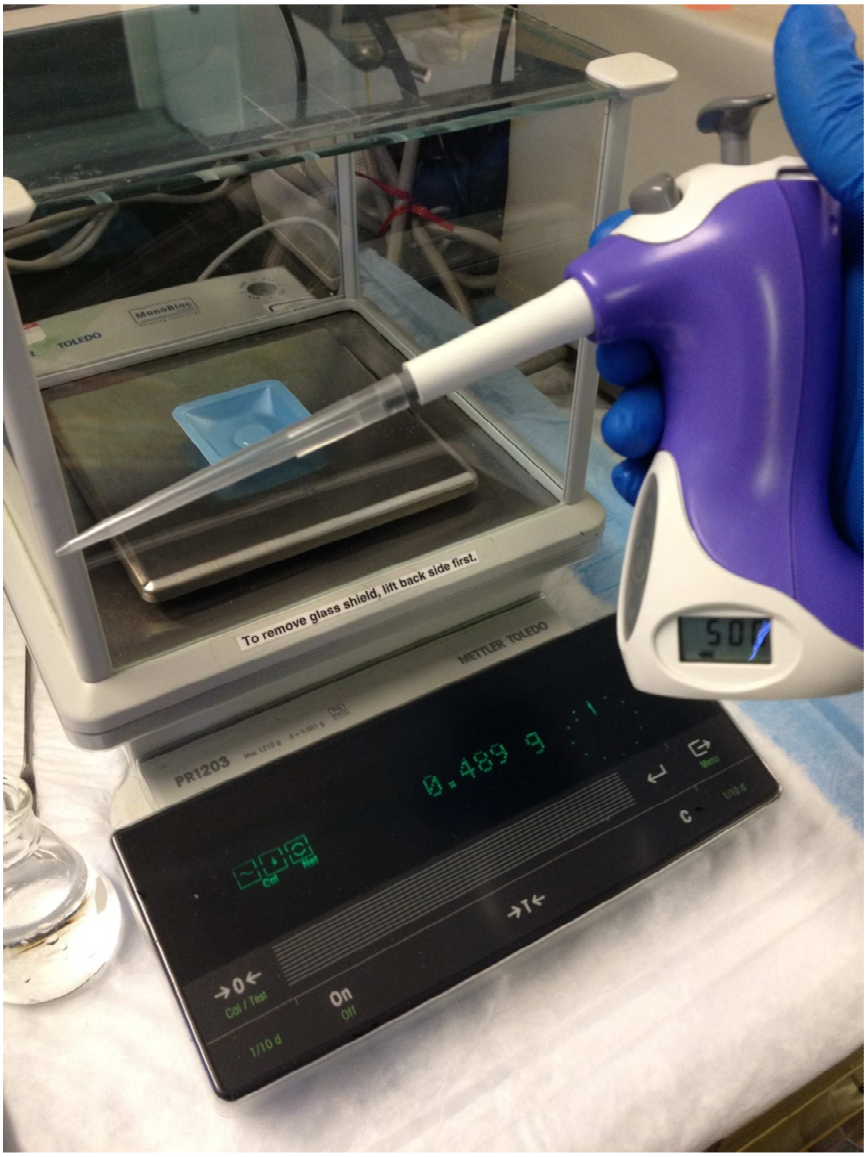

Positioning the sensor

1. Put sensor in fresh 0.1x PBS solution (Dilute 1x with DI water, if necessary) a 5mL solution will suffice (alternatively, 10 squirts of your pipetting device, with 1 squirt of 1.0x PBS and 9 squirts of DI water)
2. Prepare a 0.1x PBS solution with 100 mMol Glucose and 50 mMol Lithium Lactate concentration. (We are using the lithium salt in order to NOT change the pH!) Prepare about 10 mL, as this will last you through several calibrations.

3. Place the sensor to be calibrated into the calibration solution. Use a paper clip to secure the sensor in place, so that it doesn't shake around.

III. Connecting the Sensor

1. Start up the laptop. Once it turns on and logs in, you should plug in the wireless receiver to the laptop, and wall outlet. Only one light should be blinking on the receiver at this time
2. Add a battery to the wireless transmitter. Use a fresh battery! :) **Be sure to have the (+) side of the battery facing the hole inside the transmitter!!!**

3. Now, all 3 lights on the transmitter should start blinking. Once this occurs, start up the pinnacle software on the computer. It should connect to the base station, and points should start appearing on screen.
4. Now, plug up the transmitter to the sensor head prepared in the previous section. In the Pinnacle Software, Click *File > Log > Start logging.*
5. WAIT at least 30 minutes. The transmitter takes about 30 minutes to warm up and present a level signal. Zero the signal every 10 minutes while you wait, so you can see if it's drifting downwards. **DO NOT SKIP THIS STEP, as it will throw off your calibration**

IV. Calibrating

1. Once the signals are level, zero again. They should stay at zero. Now, we are ready to calibrate. **WARNING: From this point on, if the sensor shakes, you may have to RESTART from the previous section!!!**

2. Wait 5 minutes to establish a baseline reading. This is your ZERO mMol Glu/Lac concentration.
3. Add a 20 µL squirt of the 100 mMol Glucose/ 50 mMol Lactate calibration solution. Add a comment to the graph at the time at which you squirt this into the sensor's 0.1x PBS solution. Wait at least 20 minutes to ensure that the sensor signal is level again. *Warning, DO NOT SHAKE THE SENSOR*
4. When the signal levels off, add another squirt of 20 µL. Be sure to add a comment to the graph about when it was added. Wait at least 20 minutes to ensure that the sensor signal is level again. (Sometimes, analytes will take up to 10-15 minutes to diffuse through the solution and into the gel layers on the sensor.) *DO NOT SHAKE THE SENSOR.*
5. Repeat step 4 six or seven times.
6. Finish logging the data. *File > Log > Stop* and click *yes*.
7. Disconnect the sensor, remove the battery from the transmitter (short the poles when you remove the battery)

V. Cleanup

1. Remove holding clip, and swirl sensor head in a clean DI water solution for 60 seconds before storing in a fresh 0.1x PBS solution.
2. Remove battery, using tweezers to short the circuit before pulling the cell out of its clamp
3. Place the potentiostat in an anti-static bag, and place both the receiver and potentiostat in the large carrying bag. Coil all cables, and place them in the carrying bag.